NUMERICAL MODELLING OF THE INTERAC-TION BETWEEN OAT PLANTS AND REALISTIC WIND LOADING

YINGYAO CHENG

BEng., MEng

A thesis submitted to The University of Birmingham

for the degree of

MASTER OF PHILOSOPHY

School of Civil Engineering

The University of Birmingham

June 2013

ABSTRACT

Wind, one of the important influences that plants experience, is a major factor contributing to economic losses in oat production, which can reduce yields by up to 40% (Fischer & Quail, 1990). Aiming to provide a deeper understanding of the dynamic behaviours of oat plants under wind conditions, this thesis gives an insight into the factors that affect oat plant damage. Four objectives of this research are addressed:

1) To generate an appropriately correlated wind field over a series of oats containing the appropriate energy-frequency relationship.

2) To construct an idealised plant model, capable of modelling the dynamic movements of oat plants subject to a time varying loading.

3) To use the outcomes from objectives (1) and (2) examine the behaviour of oats in winds and model the likelihood of lodging.

4) To examine the interaction of the oat with its neighbours and how this affects lodging in oat.

With the aid of the Weighted Amplitude Wave Superposition (WAWS) method and Finite Element (FE) technique, these objectives are achieved.

The effect of the coherent natural wind field containing the appropriate energy-frequency relationship is simulated using the WAWS method. The comparison of this simulated wind with the theoretical (Von Karman) power spectrum, theoretical correlations, and measured wind data above the oat canopy is presented.

Two three-dimensional oat plant models corresponding to an isolated oat plant at two growth stages, capable of modelling the dynamic movements of oats subjected to a time varying loading, are constructed. The natural frequencies and bending moment transfer functions of these two models are examined. It is found that the natural frequencies of oat plants play a key role in the plant's damage. Therefore, a parametric investigation of this natural frequency to changes in the properties of an oat plant, i.e., the plant height, the cross sectional radius, the wall width, the tapered parameter of the stem, the material density, the Young's Modulus, the Poisson's ratio, the parameters of oat branches, and the total grain weight, is undertaken. The natural frequency is most sensitive to variations in the plant height. This finding agrees with the measurement using free vibration test.

Applying the simulated wind fluctuations to the idealised oat model, the behaviour of oats in winds is studied. The underlying mechanism of an isolated oat plant subjected to realistic wind loading is explored. When the mean wind speed is less than 6m/s, the relationship between the square of the wind speed and the response of an isolated oat plant is linear. However, during high winds (i.e., the mean wind speed is higher than 6m/s, where the failure wind speed occurs), the influence of the geometric non-linearity of an oat plant is significant. These results suggest that this new analysis method is more accurate than previous models, which are based on the linear assumption. A parametric investigation into the sensitivity of the plant's response to changes in the parameters of the wind and the parameters of the plant itself is undertaken. It is found that variations in the drag coefficient, the projected area, the plant height and the section radius of an oat plant produce a large change in the movement of an oat plant.

Finally, the interactions of oat plants with its neighbours are modelled. A case study of

five oat plants in a line is examined and validated against the experimental data. It is found that the motions between the individual plant and its nearby neighbours are correlated in real wind conditions.

The main contribution of this research is to offer a new method to assess lodging in oats. The method, which is more accurate than previous alternatives, developed is not only limited to oat crops but could be extended to other plants subjected to wind such as trees and other cereal crops.

KEY WORDS: Weighted amplitude wave superposition method (WAWS), Finite Element method (FEM), Numerical simulation, Oat lodging, Plants interaction, Wind

ACKNOWLEDGEMENTS

First and foremost, I sincerely thank my supervisor Prof. Mark Sterling, for his constant encouragement and guidance on my research, and also for being a role model in my daily life. I greatly appreciate all the time and ideas that he has contributed.

Thanks also go to my cooperating supervisors Prof. Chris Baker and Prof. Chan for their far-sighted guidance, kind help, patient advice, as well as encouraging support during the period of my studies.

Appreciation is also expressed to all the people in room F59B for their input and help with my research; the School of Civil Engineering for providing a good environment of my research; and BlueBEAR Committee for their efficient technical support throughout the course of this thesis.

Special gratitude also goes to Dr Sarah Clark for her technical expertise and advice which was essential in order to construct the oat models, Ms Helen Booth for her kind support and sweet smiles, and Mr Mike Vanderstam, Mr James Guest, and Mr David Cope for their supports about constructing the apparatus.

I wish to extend my thanks to the people from St. Stephen's Church for helping me learn about the meaning of my life. The fear of the LORD is indeed the beginning of wisdom.

Last but not least, my thanks also go to my parents and husband for their love throughout the past three years.

CONTENTS

LIST OF TABLES

LIST OF FIGURES

TABLE OF SYMBOLS

Symbol	Definition
B_M	Bending moment
c	Damping
c_c	Critical damping
$c_{ii}(\tau)\quad i=u,v\ \ or\ w$	Auto-covariance coefficient
C_D	Drag coefficient
d	Distance, diameter
d_0	Zero plane displacement
d_R	The root cone diameter
Δ	Change of a quantity
E	Young's modulus (also called Modulus of elasticity)

f, n	Frequency
f_n	Natural frequency
Δf	Frequency interval
$f_k (k = 1, 2, \ldots, N)$	The central frequency of frequency interval
$f_k^{'}$	A sum of central frequency f_k in interval Δf
F	Force
$G(f_k)$	the two-side PSD matrix
h	Height of canopy/plant
h_m	Height from base of a tree to point of force application
$H_{ik}(f_k)(k = 1, 2, \ldots, N)$	the set of N lower-triangle matrixes of dimension $M \times M$
I	2nd Moment of area (moment of inertia)
I_t	Turbulent intensity

k	Spring constant
L	Length
M	Moment
$\overline{M}$	Mean moment
N_w	The number of spectrum internals
s_R	The soil shear strength
$T^2(f)$	Transfer function
$\overline{u}$	Mean (time-averaged) velocity
$u*$	The friction velocity
u'	Fluctuating velocity
$u_i^{'}(t)$	The velocity time series of point i (i=1,2,…,M)
$\overline{U}(z)$	The mean horizontal wind speed at height z above the ground

t	Time
z_0	Roughness length
X	Longitudebody force
Y	Lateral body force
Z	Vertical body force
ζ	Damping ratio
θ	Angle
κ	The von Karman constant
μ	The dynamic viscosity
ρ_a	The density of air
σ	Standard deviation
τ	Time lag
τ_b	the surface shear stress

φ_e	The latitude
Φ_k	The set of N random values of phase shift angles taken from the range 0, 2π
$\chi_a^2(f)$	Aerodynamic admittance function
$w(z,t)$	Assumed displacement functions
ω	Circular frequency
ω_e	The angular velocity of the earth
ω_d	Natural damped frequency
ω_n	Natural circular frequency

1 INTRODUCTION

1.1 Motivation and problems

Wind damage to plants, for example forest trees and cereal crops, is a worldwide problem contributing to economic losses (Peltola e*t al*., 1999; Zeng *et al*., 2007; Gardiner *et al*., 2000, 2008). In the US, Hurricane Katrina damaged 5.3 billion square meters of forest, and the economic loss was estimated to be 0.8 billion pounds (Meeker, 2005). In Europe, 7 million m^3 of timber, worth roughly 0.5 billion pounds, was damaged in Finland during 2001, and 70 million m^3 of timber, worth 5 billion pounds, was lost in Sweden in 2004 due to wind damage (Zeng *et al.*, 2007). In particular, in the case of the cultivation of oats, it has been reported that *lodging*, the permanent displacement of a plant from its vertical axis (Pinthus, 1973), can reduce yields by up to 40% (Fischer & Quail, 1990).

In the UK, approximately 735,000 tonnes of oats were produced in 2010 and demand is increasing (Ingver, 2010). At the same time, the effect of wind damage on oats is expected to increase because climate change and warmer weather patterns predicted for the future are likely to reduce oat plant anchorage due to a decrease in the strength of the soil which holds the plant root (Peltola et al., 1999). This decrease results from more rainfall produced in the warmer weather patterns wets the soil to reduce its strength. Thus, understanding the effect of winds on oat plants is likely to be even more prominent in the

UK as these effects increase.

However, there is no tool to adequately assess oat lodging induced by wind. Previous research has successfully studied a variety of crops, such as wheat (Baker, 1995; Sterling *et al*., 2003; Berry *et al*., 2003), and has developed appropriate aero-mechanical models that are capable of predicting plant lodging. However, using such models to assess oat lodging is not always appropriate.

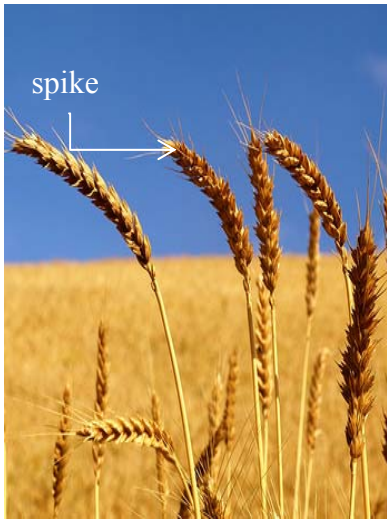

Figure 1.1 Shape of a wheat or barley plant (http://www.lightstalking.com/wheat [Accessed 19th Jan 2013])

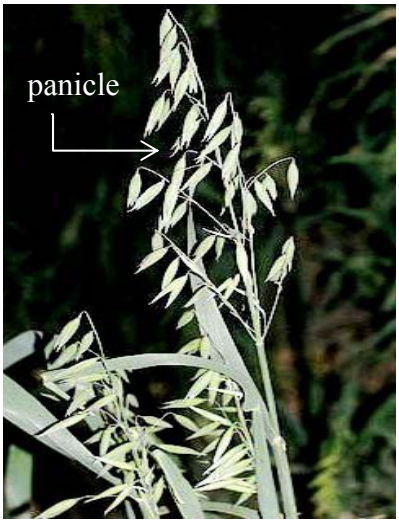

Figure 1.2 Shape of an oat plant (http://en.wikipedia.org/wiki/File:SK-OatAvena-sativa.JPG[Accessed 19th Jan 2013])

This problem is caused by certain features of an oat plant. For example, compared with wheat (Figure 1.1), the geometry of an oat plant (Figure 1.2) is more complicated. Also, the oat *panicle*, a branched cluster of flowers, may affect wind loading, because

there is a larger surface area than on a wheat spike (Berry *et al*., 2004). What is more, when oats mature, the grains become heavier, and the panicles of individual plants tend to become interlocked. This interlocking can affect the motion of an individual plant, i.e., sections of the plant canopy tend to move as a whole. These factors, including the structure of the oat plant, the interaction of the wind with the plants and the interaction of a single oat with its neighbours, may influence oat lodging (Doare *et al*., 2004; Gardiner *et al*., 2008). It is possible that the previous models, which do not consider these factors, cannot effectively represent an oat plant and its movement under the wind loading.

As a result, it is necessary to propose a model that can accurately evaluate oat lodging. To develop such a model, four problems have been identified:

1) How to capture and reproduce the effect of natural wind.

2) How to develop a typical model that represents the features of an oat plant.

3) How to model the interaction of oat crops with wind.

4) How to model the interaction of a single oat plant with its neighbours.

1.2 Aim and objectives

In order to find solutions to the above problems, the aim of the current project is to establish a model which accounts for the interaction of oat plants with wind. It is hoped

that this will provide an insight into the factors which affect lodging in oats. To that end, the following four objectives are outlined:

1) To generate an appropriately correlated wind field over a series of oats containing the appropriate energy-frequency relationship, in order to capture and reproduce the effect of natural wind.

2) To construct an idealised plant model, capable of modelling the dynamic movement of an oat plant subjected to a time varying loading, in order to develop a typical model that represents the features of an oat plant.

3) To use the outcomes from objectives (1) and (2) in order to examine the behaviour of an oat plant in wind and model the likelihood of lodging to solve the problem of the interaction of a single oat plant with wind.

4) To examine the interaction of the oat plant with its neighbours and how this affects lodging in oat plants.

To accomplish these objectives, several key knowledge gaps need to be filled.

1.3 Knowledge gaps in research

This section discusses the knowledge gaps in the existing research.

i. Previous assumptions adopted for wind have limitations because natural winds are neither constant nor sinusoidal as has previously been assumed.

In the last decade, using simplified assumptions applied to wind, analysis has been conducted to examine the lodging in crops. The wind loading is considered as a constant force at the maximum value, which impacts on the plant canopy as a sail does on a ship. Further implicit assumptions, often not stated, are made when the analysis uses mathematical equations of harmonic motion, which are the oscillatory motions of individual plants. As expected, the outcome is that a plant sways backwards and forwards in wind at its natural frequency. These assumptions have serious limitations for studying oat lodging, because, in reality, wind gusts are stochastic rather than sinusoidal (Deodatis, 1996). Moreover, for predicting oat lodging on a large scale, the temporal (instantaneous) and spatially distributed natural wind field needs to be considered. Experiments on modern boundary layers (Py et al., 2006) have shown that crop movement was correlated with the flow of wind, but this phenomenon has never been quantified in an oat canopy.

ii. Oat plants have a different morphology to other cereals that have been studied previously.

Previous studies attempted to model plant structure and movement by ignoring branches, or treating them as static masses on the single central trunk (Baker, 1995; Sterling *et al*., 2003; Berry *et al*., 2003). These models have a limitation in their application to oats, because, being a flexible structure, the motion of an oat plant is influenced by the swaying branches. Thus, a more complex method than a simple static model needs to be used. Great caution also should be exercised in considering the oat morphology and properties because they vary with the age of the plant (Niklas, 2002), which has been evidenced by the fact that plant properties vary according to at which growth

stage they are (Mencuccini et al., 1997). Therefore, a new model that can represent an oat plant and model the dynamic movements in wind becomes a prerequisite.

iii. Nonlinearities are likely to be significant during high winds, but the previous models are based on the linear theory.

Wind blows over oat crops resulting in oscillatory motions of individual plants and oat lodging (Baker, 1995; Finnigan, 2000). The interaction of the oat plant with wind involves a fluid-structure coupling effect. It is difficult to analyse this characteristic using the analytical solution that was used in the previous models. Moreover, the previous models based on the linear theory did not consider a large deflection of the plant under the action of high winds, i.e., the wind speed exceeds 6m/s. This is a serious limitation for the study of lodging. It is therefore desirable to obtain a better understanding of the fundamental mechanisms of the interaction of oat plants with wind taking into account the large deflections, and to model the likelihood of lodging.

iv. The interaction of the neighbouring plants may influence the oat lodging, but there is no research that considers this.

When oat plants mature, the panicles of individual plants become interlocked. However, current methods (Baker, 1995, Sterling et al., 2003, Berry et al., 2003) cannot account for this effect or for the damage to plants caused by this factor. Therefore, it is necessary to gain a deeper insight into this phenomenon.

Finally, there is very little experimental data available on this problem.

In summary, the knowledge gaps in the research have been presented in this section. These gaps link to the objectives as follows.

1) The first objective, the generation of an appropriately correlated wind field over a series of oats having the appropriate energy-frequency relationship, will overcome the limitations of the previous assumptions applied to wind.

2) The second objective, the construction of an idealised plant model, can study the complex structural form of an oat plant.

3) The third objective, the investigation into the behaviour of oat plants in wind and modelling the likelihood of lodging, examines the geometric non-linearity of an oat plant in high winds.

4) The forth objective, the study of the interaction of the oat plant with its neighbours, attempts to study how this effect influences lodging in oats.

1.4 Methodology to cover the knowledge gaps in the research

This section briefly introduces the methodology to cover the knowledge gaps in the research. Numerical simulations are performed in order to achieve the aim of this project in an efficient way. The reasons are listed as follows.

a) Experiments can only supply limited data and in some cases, they are not

feasible, in particular, on a large scale.

Currently, the approaches used by wind engineers to capture the effect of the natural wind are field test, wind tunnel measurement, and numerical simulation. The field test is most commonly used because of the realistic conditions. However, the wind in the field is uncontrollable, and it is hard for a field test to fully cover the studied problem. Wind tunnel measurement is feasible for an isolated oat plant or a group of plants; however, a wind tunnel is limited in size. For instance, there is a limitation on the length scales that can be generated. Thus a wind tunnel test fails to apply to oat plants on a large scale, for example, oats growing in the field.

b) No analytical solution under real wind conditions.

This problem is rather complicated, involving the fluid (the wind), the structure (the oat plant) and their interaction. In addition, geometric non-linearity in the lodging process has been observed. These lead to a lack of analytical solutions in natural wind.

For the above reasons, numerical simulations are preferred in order to achieve the aim of this project efficiently. The weighted amplitude wave superposition method (WAWS) and Finite Element (FE) technique are identified as appropriate tools for the study of this complicated problem. A statistical model is used to describe the fluctuant wind and a new oat plant model is proposed to represent a realistic oat plant. This new approach will be validated against the existing experimental findings.

1.5 Novelties

The primary contribution of this project is to present a new approach which forecasts lodging in oats. Several factors that may affect the lodging in oats are considered in detail as follows.

i. Instantaneous and spatially correlated wind field

In previous models, the wind load is represented by using empirical formulas. Simplified assumptions are applied to the wind that is considered as a constant force or sinusoidal load (Mattheck and Breloer, 1994). However, wind gusts are proved to be stochastic (Deodatis, 1996). Moreover, the temporal (instantaneous) and spatially distributed wind fields need to be considered to predict the oat lodging on a large scale. To take these issues into account, an artificial spatial and temporal wind field is generated using a numerical method which will be discussed in detail in Chapter 3.

ii. Complex structural form

Current models (Baker, 1995; Sterling *et al*., 2003; Berry *et al*., 2003) use the simplifying assumption, under which the plant can be considered as two masses connected by a light element. These models are limited in their applicability to the oat plants, whose branches influence the dynamic response to wind. To overcome this difficulty, a new model is proposed in this thesis.

iii. Nonlinearities

In the last decade, many attempts, based on the linear assumptions, have been exercised to model wind induced damage in crops or trees (Baker, 1995; Sterling et al., 2003; Berry et al., 2003). However, these models have a serious limitation as they ignore the nonlinearities in kinematic quantities such as the strain-displacement relationships in structures, i.e. large deflections, which are likely to be significant in the lodging process (Miller, 2005). The geometric nonlinearity behaviour of the oat plant will be studied in this thesis.

iv. Mechanical interactions between the plant and its neighbours

There have been very few attempts to study the effect of the interaction of individual plant with its neighbours in wind (Doare *et al.*, 2004). Furthermore, almost no work focuses on how this interaction affects the damage to plants. As stated in Section 1.1, it may affect lodging in oats. Thus a better understanding of the fundamental mechanisms of the interaction of oat plants is desired. Nonlinear springs are applied here to model the interaction of the oat crop with its neighbours.

1.6 Layout of the thesis

The layout of the thesis is listed as follows.

- Chapter 1 lists the research motivation, aim, knowledge gaps and innovations.
- Chapter 2 outlines fundamental information on wind and oat plants, especially the wind in and above the plant canopy and the parameters relating to oat

lodging. The approaches adopted in this project are reported. Previous attempts to model plant lodging are also documented.

- In Chapter 3, as the preliminary work to examine the interaction of oat plants with wind, a spatially correlated and temporal wind field is generated to achieve the first objective. The weighted amplitude wave superposition method (WAWS) is adopted here to model the natural wind. An agreement of the simulated wind fluctuations with the theoretical (Von Karman) power spectrum, theoretical correlations, and measured wind data above the oat canopy, verifies this approach.

- In order to achieve the second objective, in Chapter 4, the mechanical models of an isolated oat are proposed and validated by experimental data.

- The third objective, the dynamic behaviour of an isolated oat subjected to wind loading is examined in Chapter 5. The simulation is then compared with experimental data from the wind tunnel test. The failure wind speed is predicted using the envelope of maximum bending moments along the plant height and is compared with Baker's model (Baker, 1995).

- Chapter 6 outlines a new model that is capable of simulating the response of a group of oats in order to achieve the fourth objective. In this chapter, the interaction between the oat plants is examined, and the percentage of oat lodging on a large scale is predicted.

- Finally, in Chapter 7, the concluding remarks are summarised. Suggestions for further work are also provided.

2 LITERATURE REVIEW

2.1 Introduction

The purpose of this chapter is to provide background information on the research project, including the characteristics of wind and the plant properties. Firstly, fundamental meteorological characteristics are introduced in section 2.2. In section 2.3, the nature of wind above and within the plants canopy is provided. Section 2.4 focuses on the methods to describe atmospheric turbulence, and is followed by a section to discuss the techniques used to simulate the wind fluctuations. Secondly, an oat plant is introduced in Section 2.6. The structure of the oat plant and the parameters related to oat lodging are illustrated here. In section 2.7, the methods used by wind engineers to assess the plant lodging are discussed and followed by the summary at the end.

2.2 Basic meteorology

Wind is caused by the differential solar heating at different locations on the earth's surface and an effect of the rotation of the Earth (Holmes, 2001). Such differences lead to large-scale atmospheric circulation systems, with both horizontal and vertical orientations (Holmes, 2001). In 1735, Hadley (1735) proposed the first atmospheric circulation model (Figure 2.1). This model, a single large cell in each hemisphere (Hadley, 1735), well explained the observed wind trades at each side of the equator. However, this

model did not consider the prevailing winds at temperate latitudes. Accounting for this omission, as well as the influences of the rotation of Earth and *friction*, transmission through shear between layers of air in the atmospheric boundary layer (Holmes, 2001), a modern model (Figure 2.2) has been yielded (Cook, 1985). Between the equator and the poles, there are three cells next to the Earth's surface, whilst, near the equator two extra cells are elevated. The mean global winds of this model close to the Earth's surface are presented in Figure 2.3. This figure also shows the planet is divided into three bands on either side of the equator.

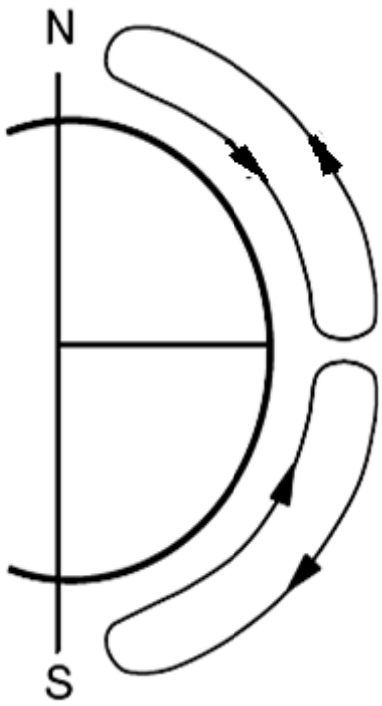

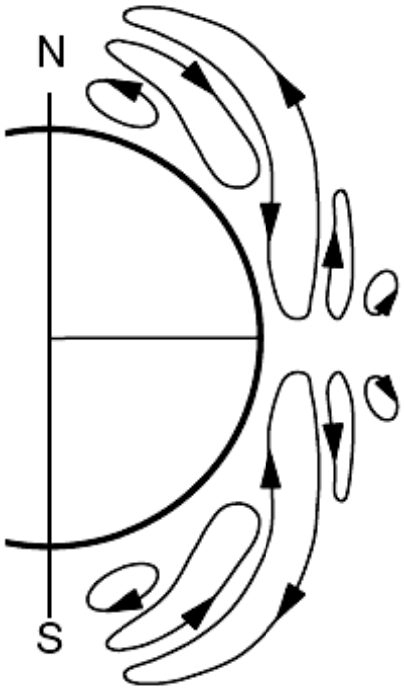

Figure 2.1 Hadley's model (Hadley, 1735) **Figure 2.2** Modern model (Cook, 1985)

The region of the Earth's atmosphere where the winds are largely influenced by the

effects of the Earth's surface, such as heating, cooling, and friction, on a time scale of less than a day, is called the atmospheric boundary layer (Garrat, 1991). This region ranges from a few hundred meters to several kilometres (Figure 2.4). Approximately 10% of the atmospheric boundary layer (ABL) close to the Earth's surface is referred to as the surface layer, where intense small-scale turbulence is generated by friction and thermal convection (Azad, 1993). Within the surface layer, the momentum between adjacent moving atmospheric boundary layers exchanges by way of the vertical movement of small-scale turbulence, which is of different sizes and strengths, are embedded in one another and are apparently a random function of both space and time (Tennekes and Lumley, 1972; Panofsky and Dutton, 1984).

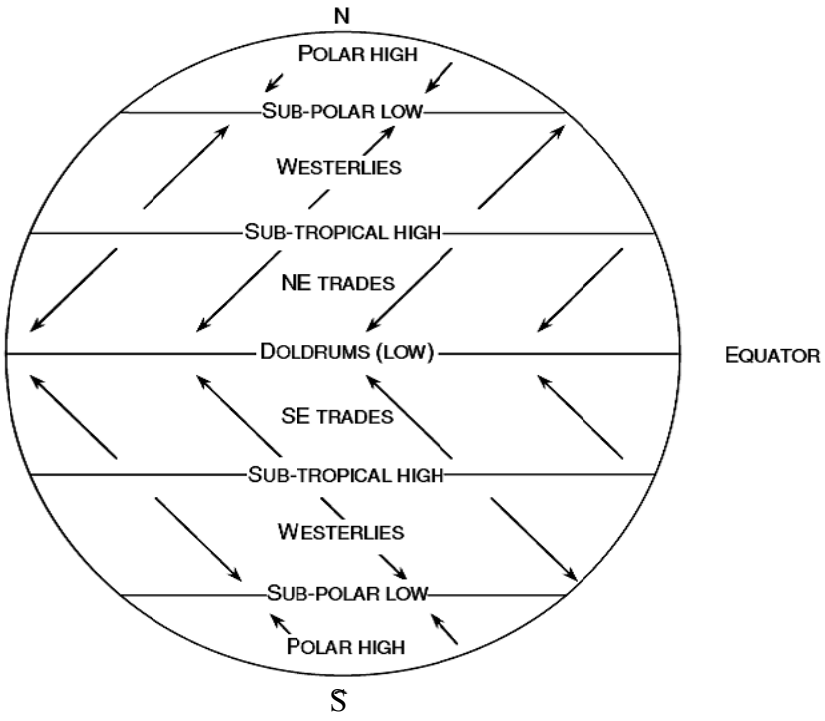

Figure 2.3 Mean global surface winds (Cook, 1985)

The characteristics of turbulent flow are listed as follows (Tritton, 1977; Panofsky and Dutton, 1984):

- Turbulent flow, interpreted as a population of eddies of different sizes and strengths, is nonlinear and chaotic.
- The flow is strongly diffusive and intermittent, rotational in three-dimensions, and apparently a spatial and temporal random function.
- Gradients in the turbulent flow, occurring in all directions, are created by stretching vortices.

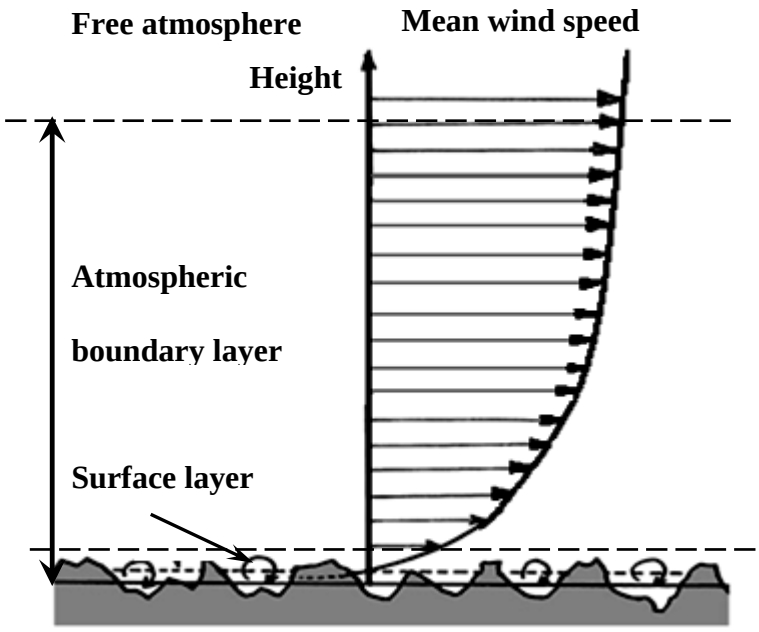

Figure 2.4 The variation of mean wind speed within the atmospheric boundary layer (Garratt, 1992)

Hence, the energy from the gradient wind is transmitted down to the lower layers, and the effects of surface friction are transmitted upwards by such eddies (Byers, 1959). In the atmospheric boundary layer, due to the frictional drag of the surfaces and all bodies (mountains, buildings and plants etc.), the wind speed increases from zero at the surface to a maximum value at the top of the atmospheric boundary layer. This is because the momentum is given up in the form of pressure forces on the roughness elements (Garratt, 1992).

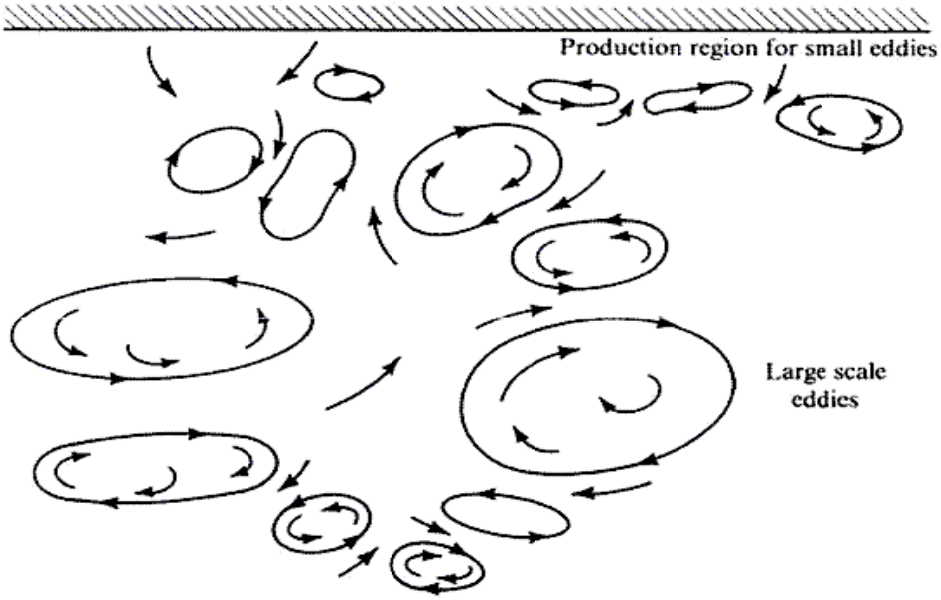

Figure 2.5 Turbulence involves a multitude of eddies on various scales (Tritton, 1977)

The mean velocity profile can generally be expressed by (Garratt, 1992):

$$U(\mathrm{z}) = \frac{u_*}{\kappa} \ln \frac{z - d_0}{z_0} \tag{2.1}$$

Where, U (z) is the mean horizontal wind speed at height z above the ground, u_* is the friction velocity ($u_* = \sqrt{\tau_b / \rho_a}$, where ρ_a is the density of air and τ_b is the surface shear stress), κ (= 0.4) is the von Karman constant (Kolmogorov, 1941), d_0 is the zero plane displacement, the height above ground where a mean wind speed is zero, and z_0 is the roughness length (presented in Table 2.1). Values of z_0 range from about 0.001m for very smooth coastal sites to around 0.7 m for very rough city centre sites.

Large expanses of water, mudflats, snow covered farmland	0.001 m
Flat grassland without hedges, very few isolated obstructions	0.01 m
Meteorological standard, typical UK undulating farmland	0.03 m
Farmland with regular boundary edges and sporadic structures	0.1 m
Plant canopies	0.2m
Dense woodland and domestic housing	0.4 m
City centres comprising four story buildings or higher	0.7 m

Table 2.1 Terrain roughness parameters (Cook, 1985)

2.3 Flow over a plant canopy

Wind, one of the important influences that plants experience, has the potential for plant damage (Jaffe, 1980; James et al., 2006; de Langre, 2008). Motivated by this reason, an important meteorology challenge is to improve understanding of the spatial variation of the wind flow over a forest or a cereal farm (see Belcher and Hunt, 1998).

In 1965, Wright **(**1965**)** was perhaps one of the first to examine the flow through a plant canopy. He established an exponential function to model the variation of the mean longitudinal wind velocity in terms of height above the ground (and within the canopy). Further investigations confirmed the existence of such a law (Baines, 1971; Cionco, 1972; Oliver and Mayhead, 1974; Finnigan and Mulheran, 1978), which can be represented via the equations below:

$$U(z) = u_h e^{-\alpha(1-z/h)} \tag{2.2}$$

Here, U (z) is the mean horizontal wind speed at height z ($z \le h$) above the ground; h is the height of the top of the plant canopy; u_h is the wind speed at height h; and α is the constant, which depends on the structural characteristics of vegetation.

The wind includes two components: mean and fluctuation. In order to describe the effect of the wind completely, the features of the turbulence within and above the plant canopy have been examined. Several turbulence models were devised to predict on this

turbulence (Wilson and Shaw, 1977; Mellor and Yamada, 1982). Further developing these turbulence models, Raupach et al. (1996) proposed a plane mixing layer model, which showed good agreement with the data from the experiments and measurements. Finnigan (2000) confirmed Raupach's work, that is, large coherent structures control the dynamics of the turbulence. Py et al. (2006) and Dupont et al. (2010) then examined these coherent structures, and found that an idealized plant canopy alters the frequencies of the wind fluctuations when these frequencies are near to the natural frequency of the swaying canopy. They called this phenomenon the canopy-atmosphere "lock-on". In addition, it was found that plant movement is correlated with coherent wind turbulences (Py et al., 2006; Dupont et al., 2010), which has not identified in an oat canopy yet. Therefore, it is necessary to have an understanding about the coupling of plant canopy with wind in order to determine the wind energy being transported to an oat plant canopy.

2.4 Methods used to describe turbulent flows

The behaviour of turbulent flows is governed by a group of coupled non-linear partial differential equations, beginning with 1) the law of conservation of mass and 2) Newton's second law of motion, which describes the conservation of momentum in the flow. These laws are valid at every point in a flow, thus the equations can describe every point in the flow field.

2.4.1 Navier-Stokes equation

According to the law of conservation of mass and Newton's second law of motion, the motion of viscous incompressible fluids can be described as follows. These equations are also referred to as the Navier-Stokes equations (Temam, 2001).

$$\frac{\partial u}{\partial t}+u\frac{\partial u}{\partial x}+v\frac{\partial u}{\partial y}w\frac{\partial u}{\partial z}=-\frac{1}{\rho}\frac{\partial p}{\partial x}+\frac{\mu}{\rho}\left(\frac{\partial^2 u}{\partial x^2}+\frac{\partial^2 u}{\partial y^2}+\frac{\partial^2 u}{\partial z^2}\right)+X$$

$$\frac{\partial v}{\partial t}+u\frac{\partial v}{\partial x}+v\frac{\partial v}{\partial y}w\frac{\partial v}{\partial z}=-\frac{1}{\rho}\frac{\partial p}{\partial y}+\frac{\mu}{\rho}\left(\frac{\partial^2 v}{\partial x^2}+\frac{\partial^2 v}{\partial y^2}+\frac{\partial^2 v}{\partial z^2}\right)+Y \qquad (2.3)$$

$$\frac{\partial w}{\partial t}+u\frac{\partial w}{\partial x}+v\frac{\partial w}{\partial y}w\frac{\partial w}{\partial z}=-\frac{1}{\rho}\frac{\partial p}{\partial z}+\frac{\mu}{\rho}\left(\frac{\partial^2 w}{\partial x^2}+\frac{\partial^2 w}{\partial y^2}+\frac{\partial^2 w}{\partial z^2}\right)+Z$$

Where, t is the time, x, y, and z are coordinate axes with the corresponding velocity components u, v, and w, respectively. Whilst, ρ, p and μ is the density, the pressure and the dynamic viscosity, respectively. X, Y and Z are body forces, which combine gravitational and Coriolis force (force acting on moving objects and caused by the Earth's rotation). $X = 2v\omega_e \sin\varphi_e$, $Y= 2v\omega_e \sin\varphi_e$ and $Z = -g$, where ω_e is the angular velocity of the Earth (7.27 rad/s), φ_e is the latitude, and g is the acceleration due to gravity.

At the same time, the continuity equation based on the law of conservation of mass is given by:

$$\frac{\partial u}{\partial x}+\frac{\partial v}{\partial y}+\frac{\partial w}{\partial z}=0 \tag{2.4}$$

Equations (2.3) and (2.4) cannot be solved, except in a few simple cases, i.e. laminar flows (Temam, 2001).

2.4.2 Reynolds averaged Navier-Stokes (RANS) equations

The Reynolds averaged Navier-Stokes equations, which overcome the challenges faced when dealing with turbulent flows, are used as alternative approaches. These equations separate flow variables (such as velocity) into a mean (time-averaged) component (such as $\bar{u}$) and a fluctuating component (such as u') via an equation below:

$$u=\bar{u}+u' \tag{2.5}$$

This method is called Reynolds decomposition. Using this approach, equations (2.3) and (2.4) can be rewritten as:

$$\begin{aligned}
&\frac{\partial \bar{u}}{\partial t}+\bar{u}\frac{\partial \bar{u}}{\partial x}+\bar{v}\frac{\partial \bar{u}}{\partial y}+\bar{w}\frac{\partial \bar{u}}{\partial z}=-\frac{1}{\rho}\frac{\partial \bar{p}}{\partial x}+\frac{\mu}{\rho}\left(\frac{\partial^2 \bar{u}}{\partial x^2}+\frac{\partial^2 \bar{u}}{\partial y^2}+\frac{\partial^2 \bar{u}}{\partial z^2}\right)-\left(\frac{\partial \overline{u'^2}}{\partial x}+\frac{\partial \overline{u'v'}}{\partial y}+\frac{\partial \overline{u'w'}}{\partial z}\right)+\bar{X}\\
&\frac{\partial \bar{v}}{\partial t}+\bar{u}\frac{\partial \bar{v}}{\partial x}+\bar{v}\frac{\partial \bar{v}}{\partial y}+\bar{w}\frac{\partial \bar{v}}{\partial z}=-\frac{1}{\rho}\frac{\partial \bar{p}}{\partial y}+\frac{\mu}{\rho}\left(\frac{\partial^2 \bar{v}}{\partial x^2}+\frac{\partial^2 \bar{v}}{\partial y^2}+\frac{\partial^2 \bar{v}}{\partial z^2}\right)-\left(\frac{\partial \overline{v'^2}}{\partial y}+\frac{\partial \overline{u'v'}}{\partial x}+\frac{\partial \overline{v'w'}}{\partial z}\right)+\bar{Y}\\
&\frac{\partial \bar{w}}{\partial t}+\bar{u}\frac{\partial \bar{w}}{\partial x}+\bar{v}\frac{\partial \bar{w}}{\partial y}+\bar{w}\frac{\partial \bar{w}}{\partial z}=-\frac{1}{\rho}\frac{\partial \bar{p}}{\partial z}+\frac{\mu}{\rho}\left(\frac{\partial^2 \bar{w}}{\partial x^2}+\frac{\partial^2 \bar{w}}{\partial y^2}+\frac{\partial^2 \bar{w}}{\partial z^2}\right)-\left(\frac{\partial \overline{w'^2}}{\partial z}+\frac{\partial \overline{u'w'}}{\partial x}+\frac{\partial \overline{v'w'}}{\partial y}\right)+\bar{Z}
\end{aligned} \tag{2.6}$$

$$\frac{\partial \bar{u}}{\partial x}+\frac{\partial \bar{v}}{\partial y}+\frac{\partial \bar{w}}{\partial z}=0$$

These new equations combine new terms involving velocity fluctuations and a similar form as the original equations (2.3) using the mean quantities to replace the total quantities. The new additional nonlinear terms, called Reynolds stresses, represent the effect of fluctuations on the mean flow. This approach partly solves the problem in terms of known quantities, such as the mean flow. However, additional unknowns such as fluctuating quantities are generated. This is the point of departure for approximations like the statistical models of turbulent flows to examine the wind fluctuations.

2.4.3 Statistical model

Statistical models that attempt to describe the physical process occurring in the turbulent flow hypothesise that the flow is a random function of both space and time. The basic characteristics of the statistical model are listed in the following sections.

2.4.3.1 Correlation and covariance functions

The covariance function, the mean product of fluctuating velocity components, details the relationship between turbulent characteristics measured at one or more points in space, either simultaneously or with a time lag between them. The function provides information on eddies and gusts in a time sense at a single point, or alternatively at two points in space (Carlson, 1998). The covariance functions are denoted as:

$$C_{ij}(\tau) = \overline{i(t)\,j(t+\tau)} \tag{2.7}$$

Where $i, j = u, v \text{ or } w$. Among these velocity correlation functions given by three velocity components, auto-covariance functions are the most important. This is because the auto-covariance coefficient (denoted as $c_{ii}(\tau)$, $i = u, v \text{ or } w$) is regarded as a measure of the extent to which the fluctuation of the wind at time t as a function of the fluctuation at time $t+\tau$ shows the velocity components are independent from or dependent on each other.

If equations (2.7) are normalized by the appropriate standard deviations (σ_i, $i = u, v \text{ or } w$) of the constituent velocity components, the auto-correlation functions are formed:

$$\rho_{ij}(\tau) = \frac{C_{ij}(\tau)}{\sigma_i \sigma_j} \tag{2.8}$$

Where $i, j = u, v \text{ or } w$. $\rho_{uu}(\tau)$, $\rho_{vv}(\tau)$ and $\rho_{ww}(\tau)$ are referred to as auto correlation functions, which are the cross-correlation of a signal with itself. The auto correlation function is a mathematical tool for finding repeating patterns. If the value of $\rho_{ii}(0)$ (i = u, v or w) is very small (such as 0.05), then the two quantities are almost independent. When $\rho_{ii}(0)$ closes to 1.0, the two quantities are completely dependent on each other.

2.4.3.2 Spectral density functions

A spectral density function is another important function that describes the feature of

natural wind. The spectral density function, commonly accepted as a measure of energy within the wind (Carlson, 1998), can be expressed as Fourier transforms of the auto-covariance function $C_u(\tau)$ as follows.

$$S_u(n) = 4\int_0^\infty C_u(\tau)\cos(2\pi n\tau)\,d\tau \tag{2.9}$$

$S_u(n)$ is the spectral density function, n is the frequency. When the time lag $\tau = 0$, then $C_u(\tau) = C_u(0) = \sigma^2(u)$.

In keeping with the previous work (Baker, 1995; Martinez-Vazquez and Sterling, 2011), the wind spectrum used in this study is the von Karman spectrum (von Karman, 1948; Cook, 1985), which is given by:.

$$\frac{nS_u(n)}{\sigma_u^2} = \frac{4\left(\frac{n^x L_u}{\overline{U}}\right)}{\left[1+70.8\left(\frac{n^x L_u}{\overline{U}}\right)^2\right]^{\frac{5}{6}}} \tag{2.10}$$

Here $S_u(n)$ is the spectral density, σ_u^2 is the RMS value of the fluctuating wind speed, ${}^xL_u$ is the *turbulence length scale,* a measure of the size of the gusts (Baker, 1995), and $\overline{U}$ is the mean velocity at a height above the ground, where the wind force acted. The plot of the normalized von Karman power spectrum is given in Figure 2.6.

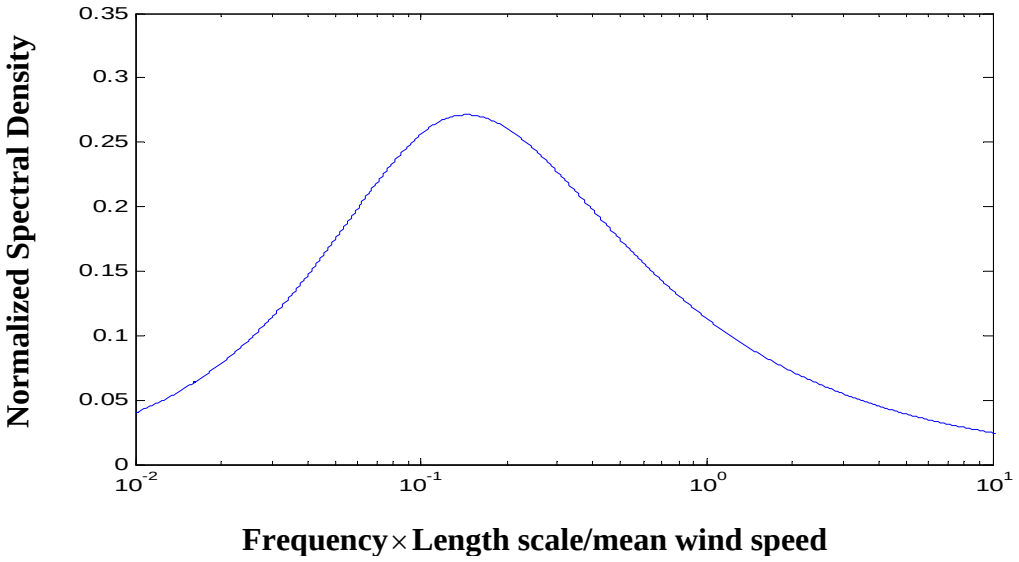

Figure 2.6 Normalized von Karman power spectrum (Baker, 1995)

2.4.3.3 Turbulence intensity

Turbulence intensity is a measure of the dispersion of the wind speed around its mean value, which is given by:

$$I_t(z) = \sigma_u(z) / \overline{U}(z) \tag{2.11}$$

Where, $\sigma_u(z)$ is the standard deviation at height z, and $\overline{U}(z)$ is the mean wind speed value at the same height.

2.5 Techniques used to simulate the turbulent wind field

Several numerical techniques are proposed to be commonly employed to model the external wind loads in order to analyze the response of slender structures, whose dynamic behavior is strongly nonlinear, in the time domain (Casciati and Ubertini, 2008; Faravelli and Ubertini, 2009). Due to the feature of the oat plant (this will be discussed in the following section), i.e. that the oat stem is slender and the geometric non-linearity occurs in the lodging process as observed, one of these techniques is used in this study. These approaches could be generally divided into two categories: the spectral representation approaches (such as the weighted amplitude wave superposition method and proper orthogonal decomposition based techniques) and auto-regressive filters methods (AR, MA, ARMA, etc.). Compared with the autoregressive filters algorithm, the spectral representation approach is proved to guarantee better simulated results, the unconditional stability of the simulation and an easier definition of the simulation parameters (Casciati and Ubertini, 2008). What's more, the AR method cannot be used for vortex excitation simulation purposes (Lipecki and Flaga, 2010), while streamwise vortices were detected by the experiments (Mellor and Yamada, 1982). Therefore, the spectral representation approaches are chosen for this study.

Among the spectral representation approaches, the weighted amplitude wave superposition method (WAWS method) has the best simulation results (Rossi, et al., 2004), although it requires high computational expenses (Faravelli and Ubertini, 2010). Therefore, the WAWS method is applied in this study. The details are briefly introduced as

follows.

The weighted amplitude wave superposition method (WAWS method) is a mathematical method based on the power spectral density function (PSD) of the analysed process. If we assume there are M stations (i.e. nodes, denoted as 1, 2, …, i, …, M) spaced at every length (L) × width (W) meter intervals within an area of $(M+1)LW-2\sqrt{M}LW \quad m^2$ at the height h in the wind field, wind fluctuation at station i can be generated according to the following equation:

$$u_i^{'}(t)=\sum_{k=1}^{N}\sum_{j=1}^{i}H_{ij}(f_k)\cos\left(2\pi f_k^{'}t+\phi_k\right) \tag{2.12}$$

where $u_i^{'}(t)$ is the velocity of a time series of point i ($i=1,2,\ldots,M$); t is the time; N is the number of spectrum internals; $H_{ij}\left(f_k\right)$ ($i=1,2,\ldots,M$ $j=1,2,...,i$ $k=1,2,\ldots,N$) is the set of N lower-triangle matrixes of dimension $M\times M$, which are determined on the basis of power spectral density (PSD) functions; $f_k(k=1,2,\ldots,N)$ is the central frequency of frequency interval Δf of the processes; $f_k^{'}$ is the set of N frequencies; the k-th element is a sum of central frequency in interval Δf and ϕ_k is the set of N random values of phase shift angles taken from the range 0, 2π.

$H_{ij}\left(f_k\right)$ can be obtained by the equation below.

$$\mathbf{H}(f_k)\mathbf{H}(f_k)^{\mathrm{T}} = 2\Delta f_k \mathbf{G}(f_k) \tag{2.13}$$

Where, $\mathbf{H}(f_k)$ is in lower triangular form, $\mathbf{G}(f_k)$ is the two-side PSD matrix; $\mathbf{H}(f_k)$ is calculated from $\mathbf{G}(f_k)$ using Cholesky decomposition.

The matrix element $\mathbf{G}(f_k)$ (its real part) can be written as:

$$G_{ab}(f_k) = \sqrt{G_a(f_k)G_b(f_k)}Coh_{ab}(f_k) \tag{2.14}$$

Where, $G_a(f_k)$ and $G_b(f_k)$ are one sided power spectral density functions for two points a and b. $Coh_{ab}(f_k)$ is the coherence function between these two points.

The procedure of the simulation is given below and outlined further in the bullet points.

- Step 1 Define the input parameters: the frequency interval (Δf) and number of frequency intervals (N_f) about the PSD function, the time step (Δt), number of time steps (N_t).
- Step 2 Give the known power spectrum of particular points
- Step 3 Determine the covariance function($Coh_{ab}(f_k)$)
- Step 4 Determine the cross PSD matrixes $\mathbf{G}(f_k)$ for particular frequencies
- Step 5 Apply Cholesky decomposition to get $\mathbf{H}(f_k)$

- Step 6 Generation of N random numbers: ϕ_k and construct the time history segments.

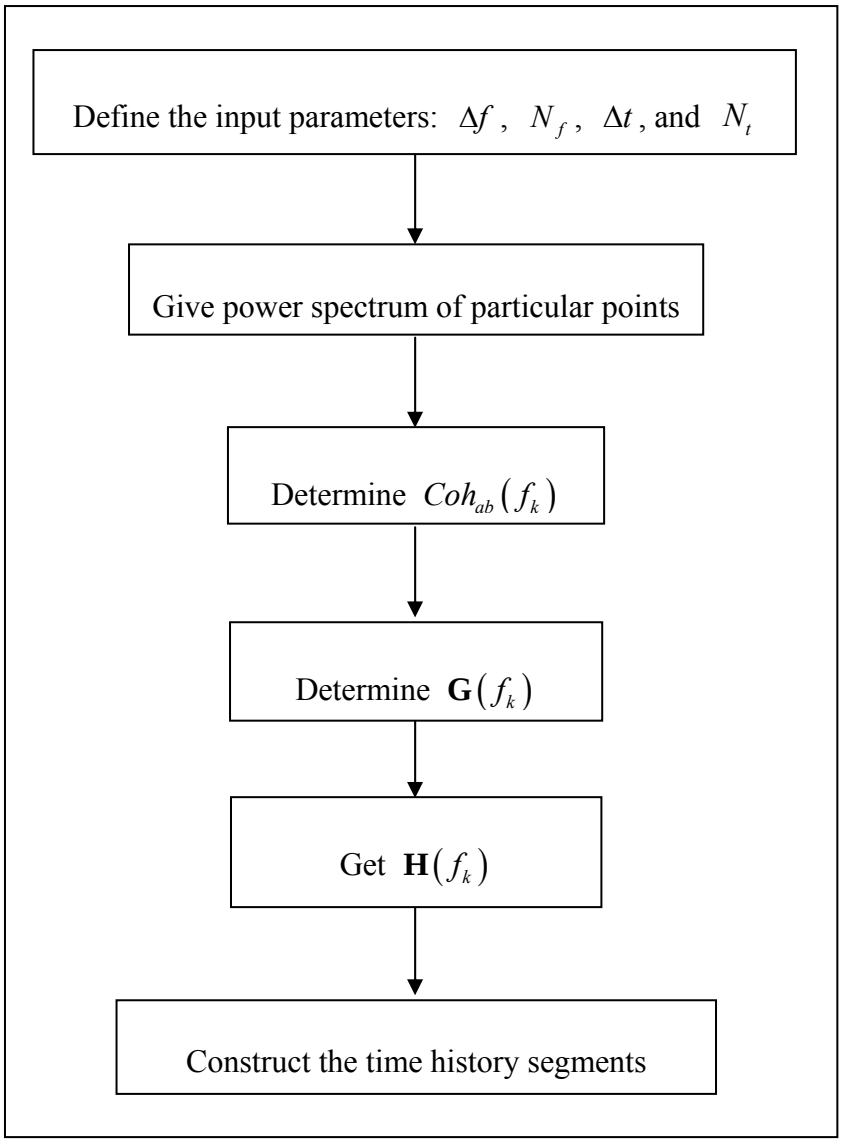

Figure 2.7 Flow Chart of WAWS Simulation

2.6 The features of an oat plant

This section provides background information on oat plants and the structural parameters relating to oat lodging.

2.6.1 A description of an oat plant

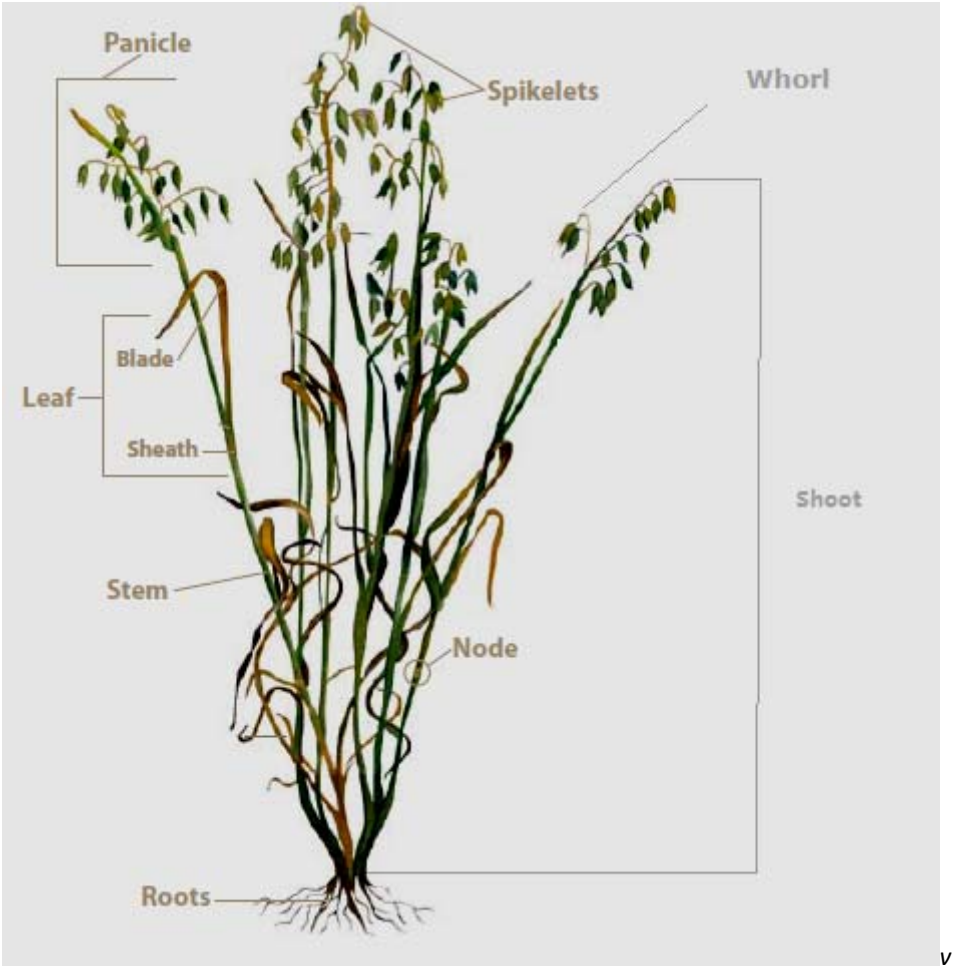

Figure 2.8 An oat plant

An oat plant is an annual grass belonging to the *Gramineae family,* a large and nearly ubiquitous family of monocotyledonous flowering plants, and combines two root systems, stems, leaves and *panicles*, the branched cluster of flowers in which the branches are racemes (Agriculture, Forestry & Fisheries, 2010, see Figure 2.8).

The two root systems are called the seminal and the adventitious roots. The seminal roots, originating during the development of an embryo, are two or three lateral roots, whilst the adventitious roots, constituting the major root system of an oat plant, extend beneath the soil surface at least 1 m deep (Agriculture, Forestry & Fisheries, 2010).

The shoot grows above the ground surface. There can be one to more than nine shoots per plant. Each shoot is composed of a stem, leaf blade and leaf sheath. A shoot may also be referred to as a tiller. Each stem is composed of a series of nodes and internodes (the nodes hold buds where the leaves emerge, and the internodes are the parts between two nodes). The nodes are solid, but the internodes change from solid during the early development stage to hollow at their maturity (Agriculture, Forestry & Fisheries, 2010). The leaf consists of a blade and sheath. The blade is elongated, flat, narrow, linear and acute in its tip, and the sheath is an open cylinder, enclosing all or a portion of the stem above it (Agriculture, Forestry & Fisheries, 2010).

At the head of each oat shoot, there is a cluster of branches called a panicle. Each branch is known as a whorl. Each whorl consists of several spikelets. Seeds are developed (called ripening) in these spikelets each of which contains at least one grain. (Agriculture, Forestry & Fisheries, 2010).

2.6.2 The growth stage of an oat plant

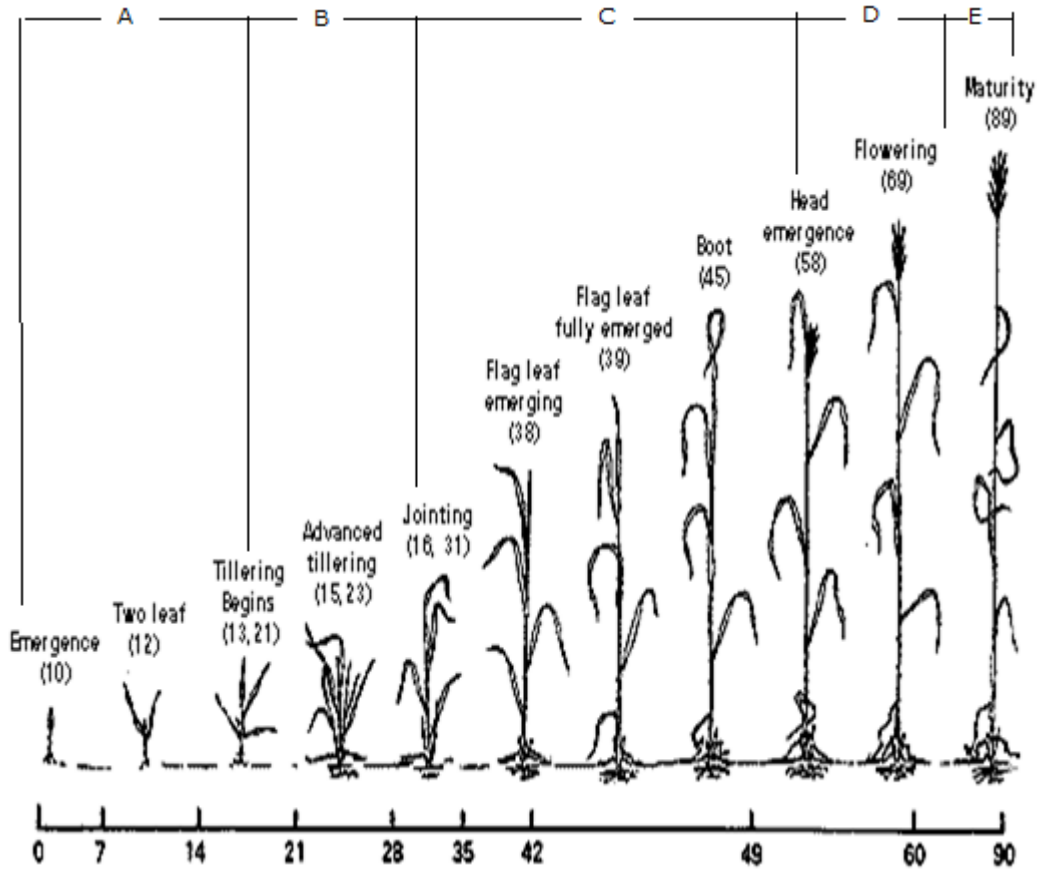

Figure 2.9 The growth and development of a cereal, A) germination and early seedling growth, B) tillering, C) stem elongation, D) heading, and E) ripening (Zadoks et al, 1974)

The cultivation of the oat can be divided into five main stages (Figure 2.9): 1) germination and early seedling growth, 2) tillering, 3) stem elongation, 4) heading, and 5) ripening (Zadoks et al, 1974).

The germination and early seedling growth stage starts after the kernel has seeded in

the soil, which is when the endosperm provides nutrients for growth until the first true leaves have emerged and the seminal root system is established. The seminal root system provides the developing seeding with water and nutrients, and supports plant growth until tillering, when the adventitious root system, which first appears at the tillering node at the two or three-leaf stage, becomes the main root system of the plant.

Synchronously with the development of the adventitious root system, the tillers emerge. The number of tillers is influenced by plant density (there are more with low plant density), nutrient supply (there are more with high supply), and cultivar, etc. At the end of the tillering, the spikes (panicles in the oat plant) develop.

After the spikelet primordia have formed inside the stem base, the main stem and tillers begin to elongate. During stem elongation the internodes increase in length to its final size. Then, the panicle begins developing at the tip of the panicle branches and proceeds towards the base. This is called heading, which is completed when the base of the spike is visible. After heading, there is a stage called grain ripening, and the grain is harvested at the end of this stage.

2.6.3 Parameters relating to oat lodging

Oat plants can fail in two ways: (a) by buckling at the stem (Figure 2.10a) or (b) by uprooting and overturning (Figure 2.10b) due to root failure (Baker 1995; Sterling *et al.*, 2003; Berry *et al.*, 2003).

Wind can produce dynamic forces that act on an oat canopy, which in turn results in the

overturning moment along the oat plant. Lodging occurs when the overturning moment applied to the crop exceeds either the resisting moment arising from the material properties of the strength or from the root/soil interaction (Baker, 1995, Sterling *et al.*, 2003). This assumption is well proven in wheat by previous tests (Sterling *et al.*, 2003).

a) Buckling at the stem (Berry *et al.*, 2004)

b) Root lodging (Berry *et al.*, 2004)

Figure 2.10 A close view of failure (Berry *et al.*, 2004)

Therefore, the two useful measures with respect to oat lodging are the anchorage failure moment and the stem failure moment, and the wind loading (Nm) applied to the oat plant under natural wind conditions. If there is accurate information on these parameters, a structural analysis can be undertaken to evaluate the risk of lodging. Thereby, the structural information on an oat is useful for assessing the likelihood of wind damage to oats.

As an oat plant matures, the panicle expands to larger surface areas, develops greater wind-loading and elongates the plant to reach higher wind speeds. All of these changes result in larger bending moments along the stem and at its base (Niklas and Spatz, 2000),

which may cause the stem break or root failure. At the same time, the development of the stem and root enhances the strength of the stem or the root-soil system. Therefore, the properties relating to oat lodging are the projected area of the panicle which the wind drags on; the height of the oat; Young's Modulus, a measure of the resistance to bending; the mass, which provides a quantitative measure of an object's resistance to movement, the stem failure moment and root-soil failure moment. As for the strength of an oat plant, it is assumed that the *anchorage failure moment*, the moment that the ground cannot hold the plant root, depends on two parameters, namely, the spread of the root plate and the shear strength of the surrounding soil (see Section 5.6.1, Equation 5.13), whilst the stem failure moment is related to one material parameter (failure yield stress) and two geometric factors (the stem radius and wall width). These assumptions are validated in wheat and barley by previous scholars (Crook and Ennos, 1993; Baker *et al*., 1998; Sterling *et al*., 2003; Martinez-Vazquez and Sterling, 2011). Thus, stem radius, wall width, failure yield stress, the spread of the root plate, and the shear strength of the surrounding soil also relate to oat lodging.

2.7 Methods used to study plant lodging

Many previous attempts have been made to model the interaction of plants with wind in order to predict wind induced failures (Oliver and Mayhead, 1974; Peltola *et al.*, 1999; Saunderson *et al.*, 2000; Peltola, 2006; Bergeron, 2009).

There are two main methods used to study this problem: static analysis and dynamic

analysis. Many models have been proposed using static analysis, for example, Forest-GALES and HWIND (Gardiner *et al.*, 2000). These models simplified the wind load based on empirically derived formula and only consider the wind mean speed component.

However, static analysis may not accurately examine the conditions plants experience because of the wind turbulence (Silins *et al.*, 2000). The static analysis hypothesizes that dynamic sway is not directly responsible for wind throw and assumes that plants deflect to a point of failure under constant wind speed. However, it was found that the plant failure at wind speeds that were less than those predicted by static pull tests (Oliver and Mayhead, 1974; Gardiner, 1995), because the dynamic forces during gusts are different to the static forces applied to the plant during the test.

Dynamic approaches, although they are more complex (Sellier et al., 2006, 2008; Webb and Rudnicki, 2009), are required to study the response of the plant to winds. Generally speaking, there are mainly three different tools applied to study this aspect (Clough and Penzien, 1993): a) the lumped-mass method, b) the generalised displacements for uniformly distributed beams method, and c) the finite element method. A further review of the approaches used to study this issue can be found in de Langre (2008).

2.7.1 The lumped mass method

The lumped mass method assumes the mass of a plant to be concentrated at discrete points (Figure 2.12, 2.13), whereby simplifications can make the analysis easy because inertial forces only develop at these mass points. The branch of this aerodynamic aspect has been heavily influenced by the work of Baker and his colleagues (Baker, 1995; Baker *et al.*, 1998; Sterling *et al.*, 2003; Martinez-Vazquez and Sterling, 2011).

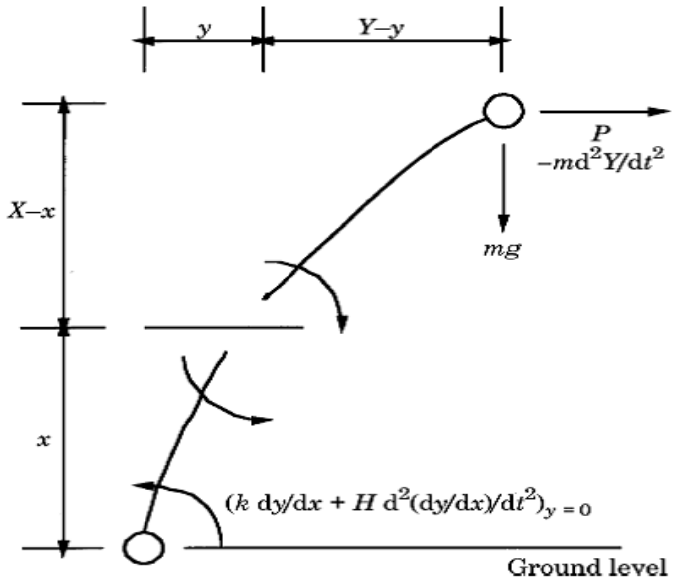

Figure 2.11 The mechanical model, origin of x and y axes at stem base (Baker, 1995)

Baker (1995) firstly proposed a model to study the damage of both trees and cereal crops in winds (Figure 2.10). The model assumed that cereal plants such as wheat or isolated trees, e.g., plane tree and sitka spruce, could be idealized as two masses connected by a light inextensible element, one mass represented the crown of the tree or the

ear of the cereal plant, and the other represented the root ball. The natural frequency of the model was calculated, and the gust wind force with the inertial forces of the moving masses was taken into account. The bending moment spectrum was derived by spectral analysis, and then the specified failure moments (uprooting or stem failure) were determined by extreme value analysis.

The failure wind speed (V_g) is calculated by the equation that follows Baker *et al.* (1998) and Sposaro *et al.* (2010):

$$V_g = \left[\frac{2B_m}{(\rho_a A_{pj} C_D X_{hcg})(1+\frac{g}{(2\pi n)^2 X_{hcg}})(1+\exp^{-\pi\delta}\frac{\sin(\pi/4)}{\pi/4})} \right]^{\frac{1}{2}} \tag{2.12}$$

in which the measured inputs are the failure base bending moment (B_m), the density of air (ρ_a), the ear area (A_{pj}), the drag coefficient (C_D), the main stem's height at the centre of gravity (X_{hcg}), the natural frequency (n), the acceleration due to gravity (g), and the plant damping ratio (δ).

The failure base bending moment is given by:

$$B_m = \frac{F_s l_n}{4} \tag{2.13}$$

in which F_S is the measured breaking force using the three-point-bending-test, and l_n

is the internode length.

A good prediction confirmed the application of such a model to assess the lodging in wheat (Baker et al., 1998; Berry et al., 2003; Sterling et al., 2003). However, this simplification is somewhat questionable when applied to a tree (Martinez-Vazquez and Sterling, 2011). For example, a case study which has been undertaken (Baker, 1995) showed the mean failure wind speeds were 12m/s and 27m/s for a plane tree with leaves and without leaves, respectively. These values were lower than the calculated wind speeds which would lead to the tree failing by stem lodging. It is possible that trees can minimize their projected surface areas which leads to a reduction in drag than the paper (Baker, 1995) assumed. Thus, the representation of the model has to be carefully considered before using it to study any plant.

In developing Baker's (1995) model, Martinez-Vazquez and Sterling (2011) generated complete time histories of response (Figure 2.13). This new approach provided more information on the correlation between the instantaneous load and the response of the plant, so that it could study some important effects, such as fatigue, which the previous model could not do. Another merit of this model might lie in the estimation of the percentage of lodging in wheat fields, which showed a great economic contribution.

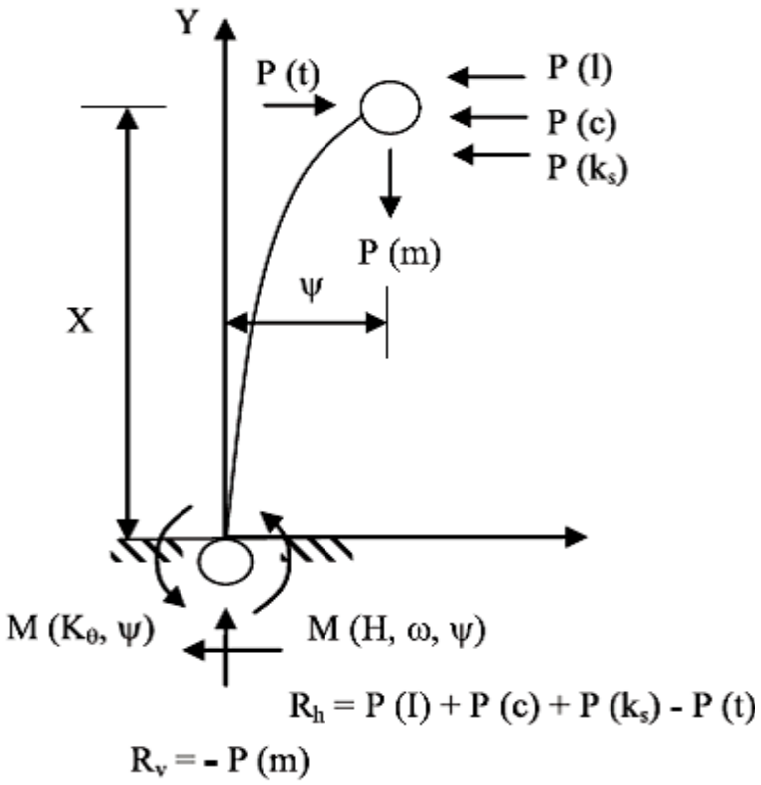

Figure 2.12 Idealisation of a wheat plant (Martinez-Vazquez and Sterling, 2011)

However, although these attempts have successfully applied to some crops, such as wheat (Baker, 1995; Sterling et al., 2003; Berry et al., 2003), using the existing models to assess oat lodging is not always proper. It is possible that the different structural form of an oat plant results in the inappropriate application of existent models. Thus, two simple masses with a light inextensible stem are not suitable to represent a realistic oat plant.

2.7.2 Generalised displacements for uniformly distributed beams

The second method is called the generalised displacements for uniformly distributed beams, which is a common analysis tool to study the dynamic behaviour of structures. This method is based on an assumption that the structural deflection can be expressed as the sum of a series of generalized expressions for displacement (Clough and Penzien 1993). Peltola (1995) adopted this method to model a tree as a single beam in the ground, and found that taller, more slender trees were more susceptible to failure. To further extend this model, Saunderson et al. (1999, 2000) used a tapered cantilever beam to model the dynamic behaviour of a sitka spruce. The dynamic behaviour of the plants was investigated using a transfer function. An agreement between the displacement spectrum calculated from the model and the measured spectrum for frequencies up to about 0.7 Hz showed that a beam set in the ground provides a good model for studying the behaviour of an isolated plant, for example the sitka spruce. However, this method may be valid for some limited types of slender plantation plants but is not representative of most plants that have different forms, because these trees, where the branches constitute a significant proportion of the total mass or where there is no central trunk, cannot be simplified as only a beam. Thus, it is not suitable to be used to study an oat plant due to the complicated shape of this crop. Another limitation is related to the assumption that the deflection of the plant is "small". This assumption may sometimes be inadequate, especially when modelling the bending of an oat plant's stem in a very strong wind when nonlinearities are likely to be significant.

2.7.3 Finite element method

The third method is the finite element method, which combines the features of both the lumped mass method and the generalised displacement for uniformly distributed beam method. This method could be applicable to all structures. Using this method, a structure is divided into an appropriate number of elements whose size and shape may be different. The deflection of the structure can then be expressed in terms of the sum of a series of generalised coordinates deriving from the ends of each element (nodes).

The advantages of this method lie in the ability to select the desired number of generalised coordinates by properly dividing the structure, and can obtain three-dimensional structures. For these reasons, Jin *et al.* (2009) produced a 3-D rice plant using this method to perform the numerical analysis of rice lodging. What's more, Rodriguez *et al.* (2012) obtained the vibration modes from a finite element computation using a detailed digitization of the tree's geometry. This was followed by a comparison between the computation and experiments, which confirmed the specific organization of the modes of such branched trees. These evidences illustrate that the FEM has promise for the study of the dynamic behaviour of an oat plant.

In addition, applying this method to plants could consider the interaction between adjacent plants which requires a complex mathematical solution, as well as the interaction of wind with a group of plants, whose canopy show the wavelike motion called ‘‘honami’’ (Inoue, 1955). These two aspects may be the important factors causing the lodging in oats. Therefore, the finite element method is used in this study to model an oat plant.

2.8 Summary

In this chapter the background information on the research project is introduced. From literature, the harmonic superposition method (WAWS method) and the Finite Element (FE) technique are identified as effective tools for the simulation of the complicated problem caused by the nature of wind and the features of oat plants, respectively.

3 CORRELATED TURBULENT WIND FIELD SIMULATION

3.1 Introduction

In order to achieve the first objective of this study, namely, to capture and reproduce the effect of the natural wind, this chapter evaluates the artificial spatially correlated and temporal wind fluctuations generated by the weighted amplitude wave superposition (WAWS) method. The layout of this chapter is as follows: the production of correlated turbulent wind field is outlined in Section 3.2. In Section 3.3, the simulated wind spectrum is compared to the theoretical (Von Karman) power spectrum and measured wind data outlined in section 3.3.3. The correlation between wind speeds located at the different spatial distances are also compared to the theoretical values. Finally, concluding remarks are made in Section 3.4, which shows this method is promising to produce artificial wind field above an oat canopy.

3.2 Production of correlated turbulent wind field

In this section, the features of the methodology (weighted amplitude wave superposition, WAWS) to capture and reproduce the effect of the nature wind are explored. The

detail of this method has been introduced in section 2.5. The Decimation-in-time Fast Fourier Transform Method (DIT-FFT method) has been adopted in order to ensure an efficient calculation (Skinner, 1976; Hu, 2011). A MATLAB Computer Program was written to perform the fluctuant wind. Simple examples are undertaken in section 3.2.2 to show the capabilities of the methodology.

3.2.1 The values of the controlling parameters in the simulation

In this section, the values of the controlling parameters in the wind simulation are discussed. The simulation procedure discretizes the frequency domain as well as the time domain. These two discretisations are not independent from each other and are determined by two parameters: 1) the time step, Δt and 2) the number of time steps during the whole the simulated time, N_t. Other parameters can be calculated through these two parameters, i.e., the *cut-off frequency* (a boundary at which the energy transference from the excitation to the system starts to decrease). $n_{in} = 1/2\Delta t$; the time history $T_t = \Delta t N$, where N=2^x (x is an integer); and the frequency step $\Delta n = 2n_{in}/N = 1/T_t$.

Figure 3.1 shows a normalized von Karman power spectrum at which the turbulence length scale L_u refers to 10m (ESDU, 2000), and the mean velocity $\overline{U}$ is 10m/s. It is also shown that different choices of the parameters time step Δt and the time history T_t, which equals to $\Delta t N_t$, lead to different cut-off values of the spectrum. In terms of

the problem at hand, the choice of the parameters Δt and T_t depends on the properties of the wind turbulence as well as the dynamic behaviour of oat plants.

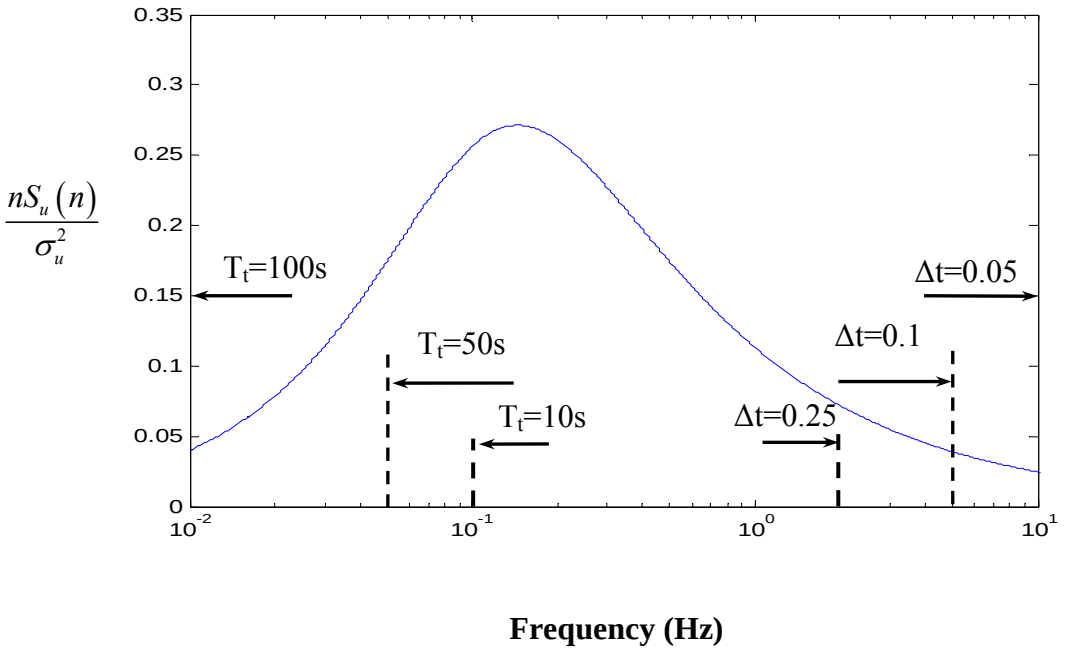

Figure 3.1 Normalized von Karman power spectrum. Cut-off values due to the simulated time step and the simulated time history (Carassale *et al.*, 2006)

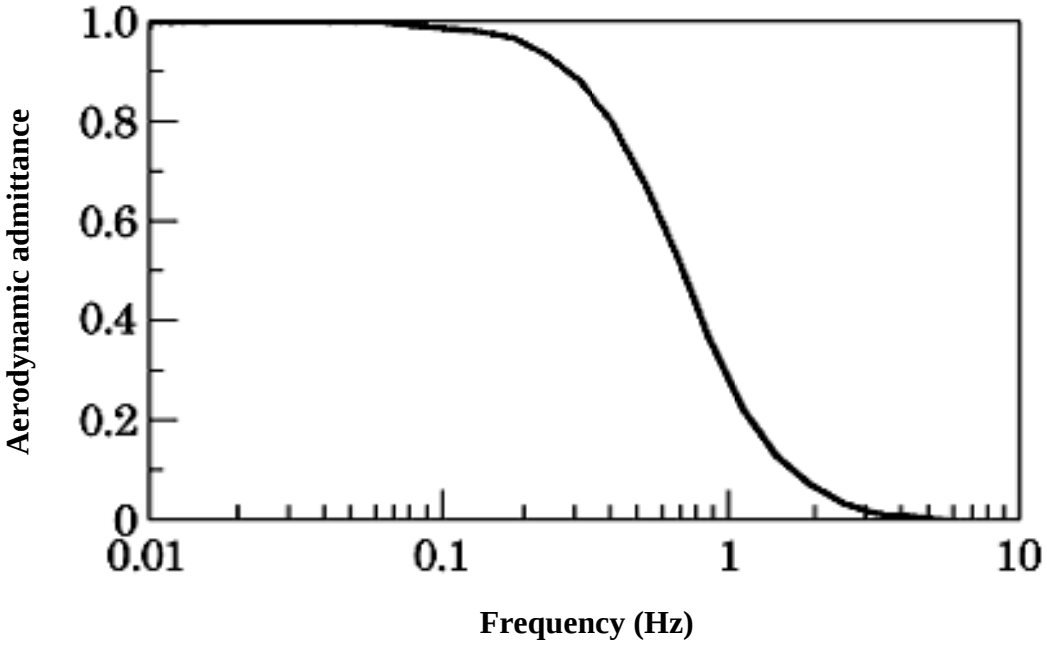

Figure 3.2 Aerodynamic admittance function (Baker,1995)

Due to the attenuating effect of the aerodynamic admittance function (Davenport, 1964), there is very little (less than 5%) energy transference to plants above 5Hz (**Figure 3.2**). Therefore, the cut-off frequency (n_{in}) of the simulation should be no less than 5Hz. In order to match this requirement, the time step Δt is assumed to be 0.1s in keeping with the work of the wind data measurement in July 2011(see section 4.3.1 for further reference). For the field data, the sampling frequency was 10Hz. In addition, considering the frequency of the plant motion (ranging from 0.70Hz to 1.12Hz, see table 4.11 in section 4.3.1), the frequency step should be less than 0.02Hz. Therefore, the time history for examination must be more than $50s$. The simulation parameters are therefore chosen and shown in **Table 3.1**

Controlling parameters	**value**
Number of time steps during the whole the simulated time N_t	512
Time step Δt (s)	0.1
Simulation time history (sampling period) T_t (s)	51.2
Interceptive frequency n_{in} (Hz)	5
Frequency step Δn (Hz)	0.02

Table 3.1 Controlling parameters of the simulation

3.2.2 Numerical examples

This section shows numerical examples in order to explore the features of the WAWS method.

In the wind field simulation with the aid of MATLAB software, a horizontal grid of 25 stations (i.e. nodes, denoted as $P-n, n=1,\ 2,\ldots,\ 25$) is spaced at intervals of 1m within an area of 16 m^2(see Figure 3.3a, $d=1m$) at the height h (Figure 3.3b). The grid is located in a global Cartesian reference system with an origin O, where the wind direction is parallel to the x axis (Figure 3.3b), and the z axis is the vertical direction. The wind velocity field $\mathbf{U}(x,y,t)$ is considered to be a sum of two components: the

mean value, $U(z)$, which is a function of the elevation from the top of the oat canopy obeying a classic logarithmic law given in Equation 2.1, and a fluctuating component $\mathbf{u}(x, y, t)$, which depends on the location and the time. This stationary zero-mean turbulence in the horizontal plane can be modelled as a longitudinal fluctuation and a lateral fluctuation, respectively. These fluctuations are correlated through equation (3.1) (Dyrbye and Hansen, 1997).

$$\phi(x_i, y_i, x_j, y_j, n) = [1 - \frac{n_x}{2\overline{U}}\sqrt{(C_x(x_i - x_j))^2 + (C_y(y_i - y_j))^2}\,]e^{-\frac{n_x}{\overline{U}}\sqrt{(C_x(x_i - x_j))^2 + (C_y(y_i - y_j))^2}} \qquad (3.1)$$

where, $n_x = \sqrt{n^2 + (\frac{\overline{U}}{2\pi L_u})^2}$, n is the frequency, $\overline{U}$ is the mean wind speed, L_u is the integral length scale, C_i , $i = x, y$ is the longitudinal and lateral delay constant, respectively (Table 3.2).

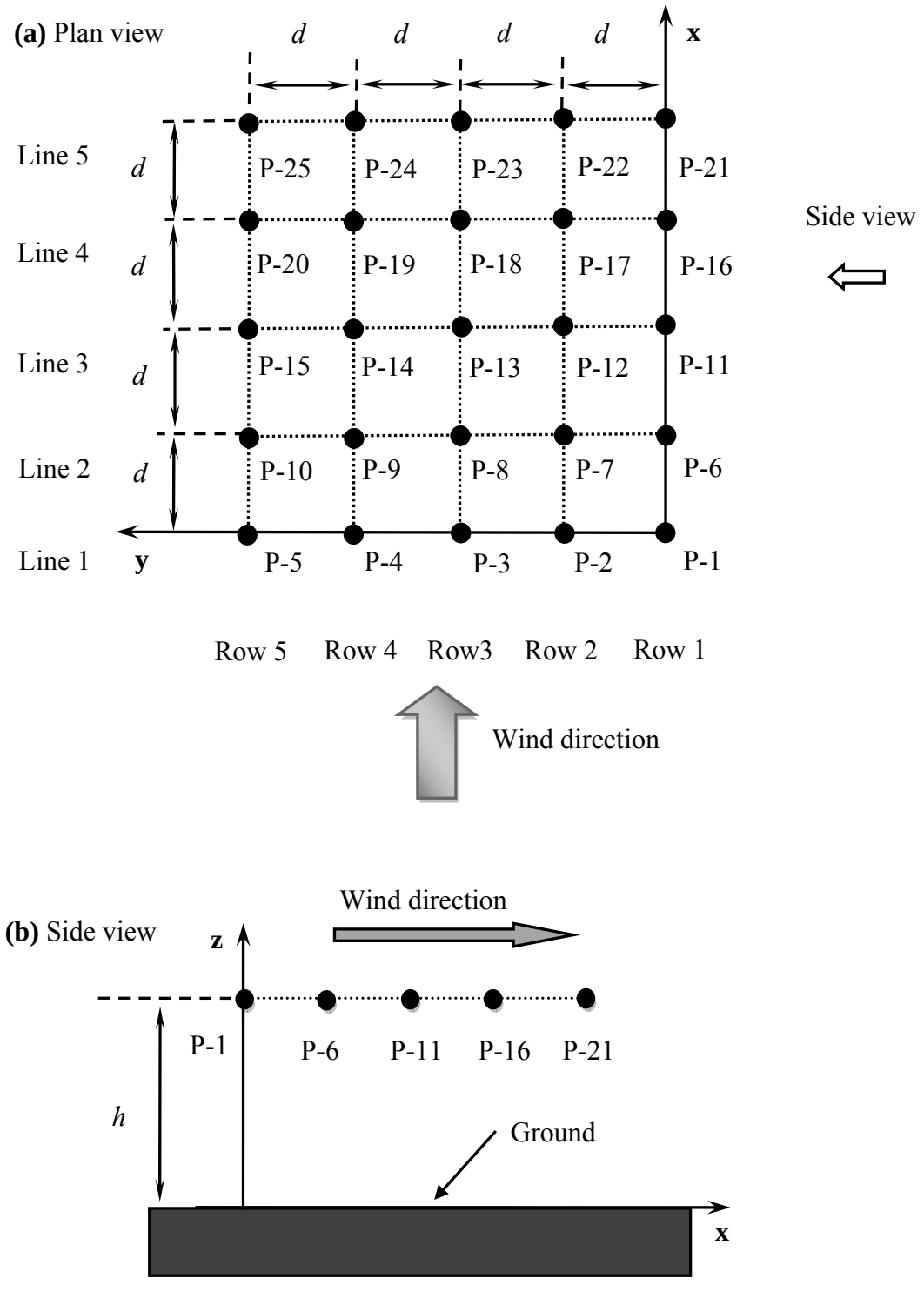

Figure 3.3 Grids for wind simulation: (a) plan view; (b) side view

Parameters	Value	Source
Friction velocity u_* (m/s)	0.16	MS2011
Von Karman constant κ	0.41	OM74
Height of the zero displacement plane d_0 (m)	0.52	MS2011
Roughness length z_0 (m)	0.20	MS2011
Longitude delay constant C_x	10	DH97
Lateral delay constant C_y	10	DH97
Longitude Turbulence length scale ${}^{x}L_u$ (m)	10	ESDU
Lateral Turbulence length scale ${}^{x}L_v$ (m)	10	ESDU
Turbulence intensity I_t	0.40	M2011

Table 3.2 Wind characters parameters (M2011: measured wind data, 2011; ESDU: ESDU (2000); MS2011: Martinez-Vazquez and Sterling (2011); OM74: Oliver and Mayhead (1974); DH97: Dyrbye and Hansen (1997)).

To evaluate the performances of the WAWS method, the simulated wind velocities of 25 stations with mean wind speeds of 5.0m/s, 7.0m/s and 9.0m/s were calculated. The wind parameters used in these simulations are shown in Table 3.2. In keeping with the work of Baker (1995), the von Karman power spectrum (see Equation 2.10) is applied here as the target wind power spectrum. The turbulence intensity is assumed to be 0.40 in accordance with the work of wind data measurement (see Figure 3.4). The turbulence length scale L_u is taken as 10m (ESDU, 2000), and the mean velocity $\overline{U}$ is considered at a height of 1.4m, where the anemometer is located.

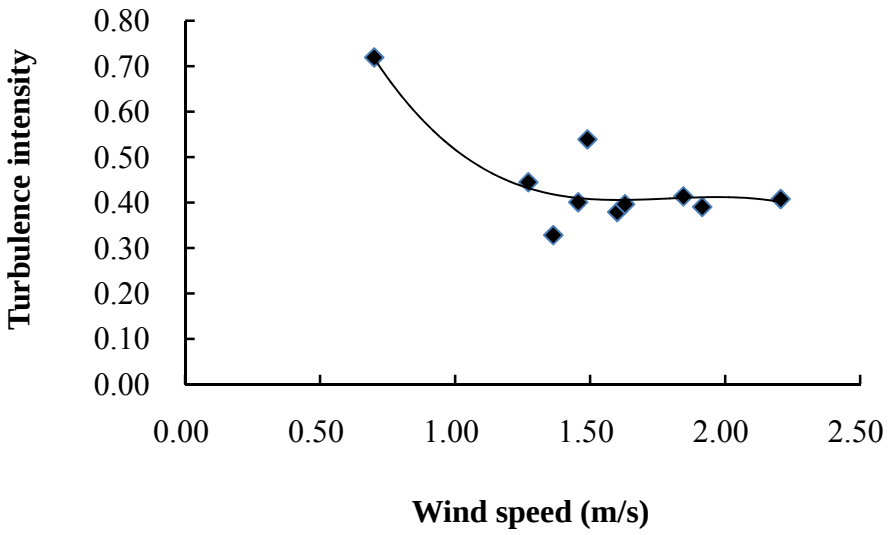

Figure 3.4 The turbulence intensity against the wind speed

The velocities simulated at three points, i.e., P-1, P-4, and P-16, are shown in Figure 3.5, Figure 3.6, and Figure 3.7, respectively. These figures show a raise of mean wind speed increases the maximum value of the wind fluctuations. All the wind fluctuations

have zero mean and are located in a horizontal grid of 5×5 stations spaced at every 1m intervals within an area of 16 m^2. A further discussion of the turbulent wind is given in the following section.

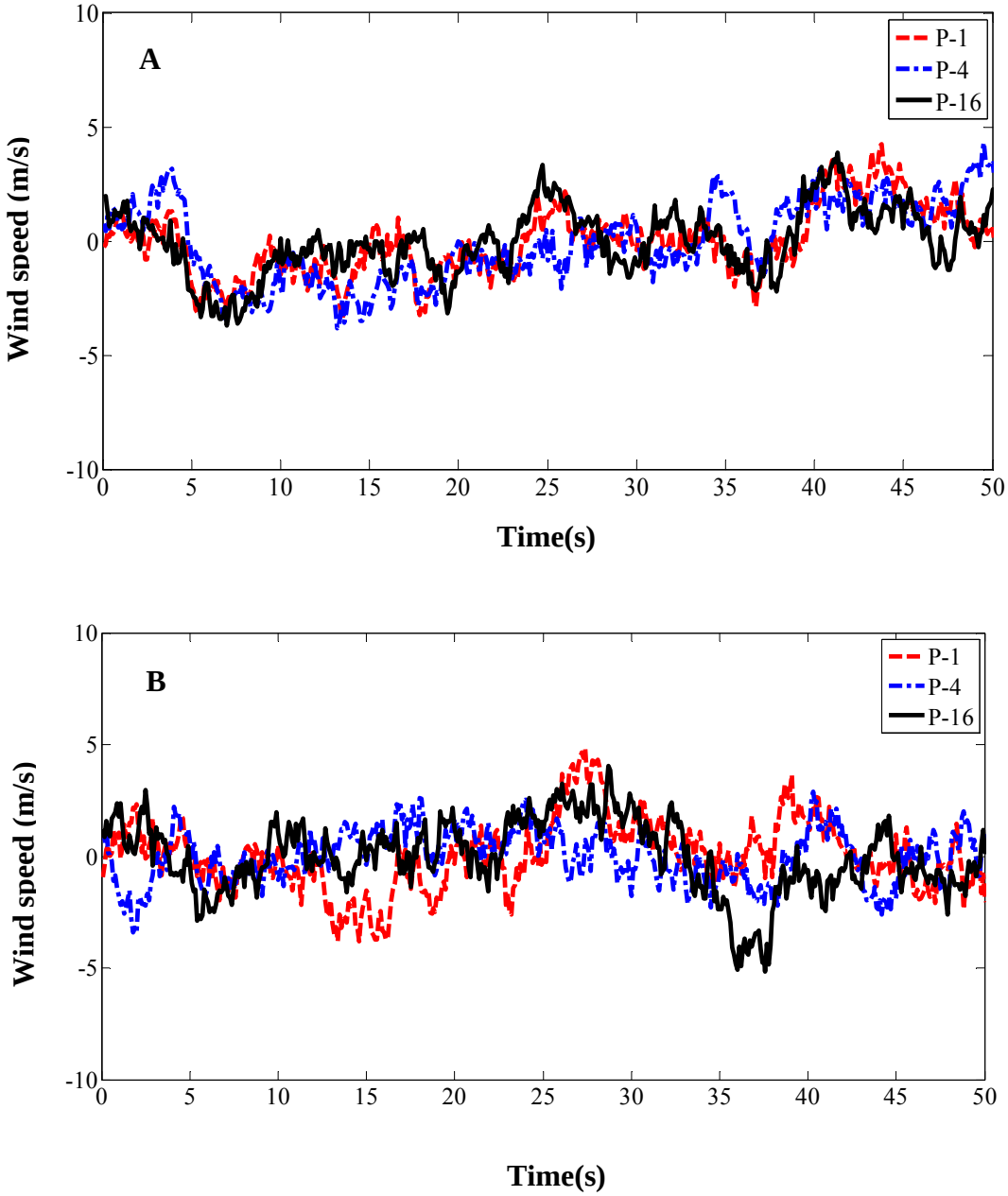

Figure 3.5 Simulated fluctuant wind at $\overline{U}$ =5m/s; A) along-wind; B) cross-wind

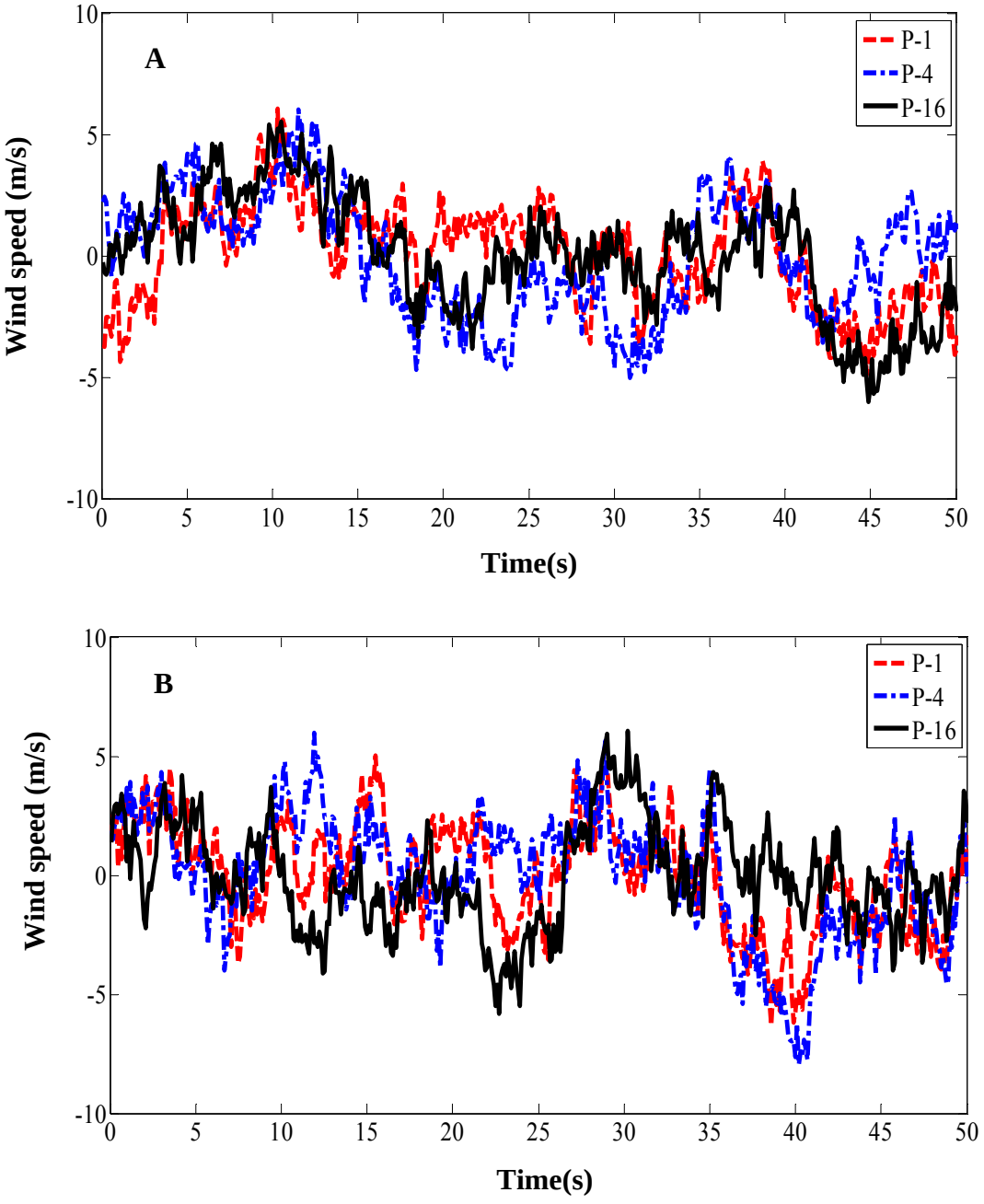

Figure 3.6 Simulated fluctuant wind at $\overline{U}$ =7m/s; A) along-wind; B) cross-wind

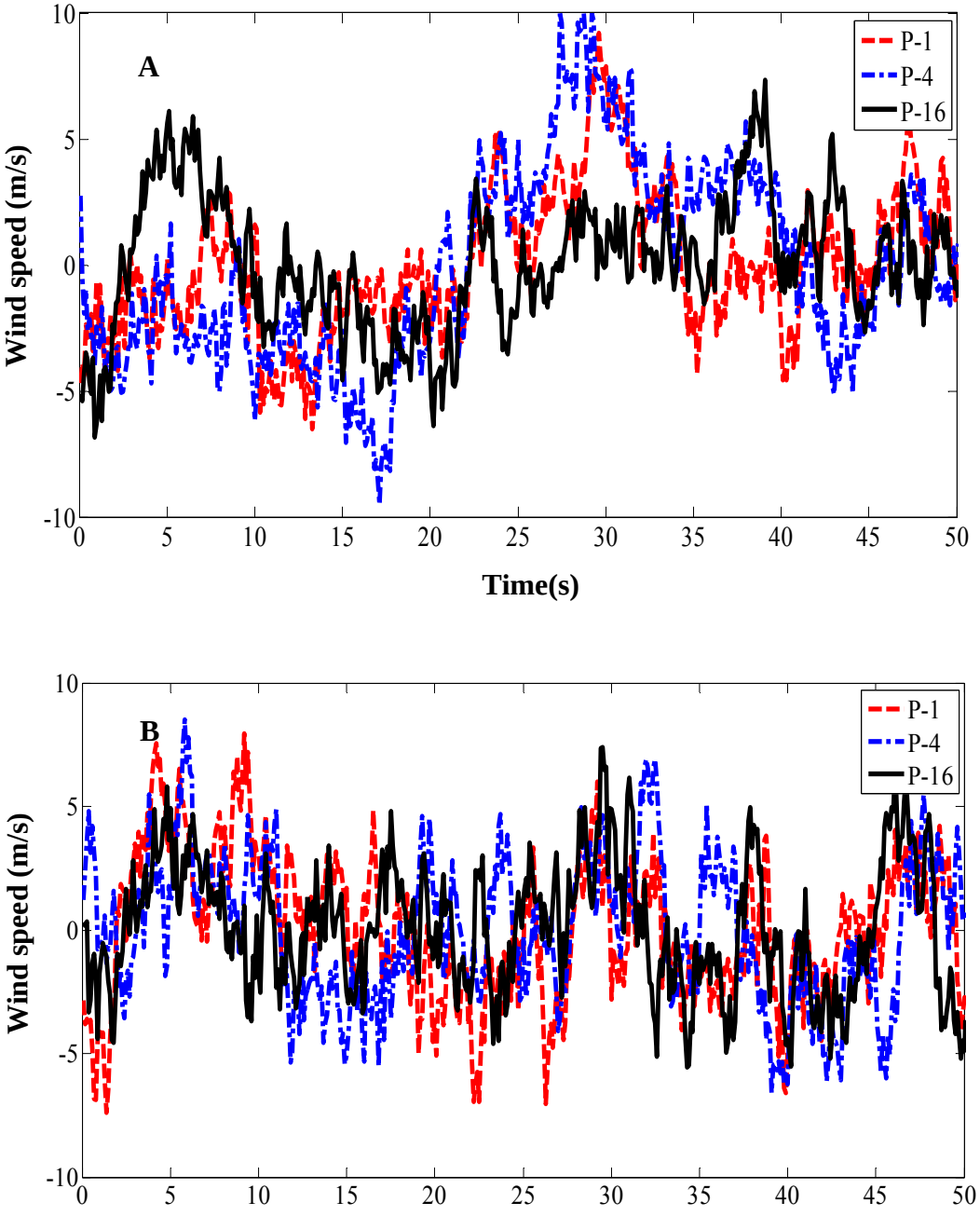

Figure 3.7 Simulated fluctuant wind at $\overline{U}$ =9m/s; A) along- wind; B) cross-wind

A 'quiver' plot of the vector field of simulated turbulent wind is shown in Figure 3.8, which is indicated by a weighted arrow pointing in a direction. The wind vortices are

presented in this figure, which is what we have observed in the field, i.e., the plants often rotate in a circular/elliptical direction. This indicates the simulated turbulent wind field is suitable to achieve the aim of the research.

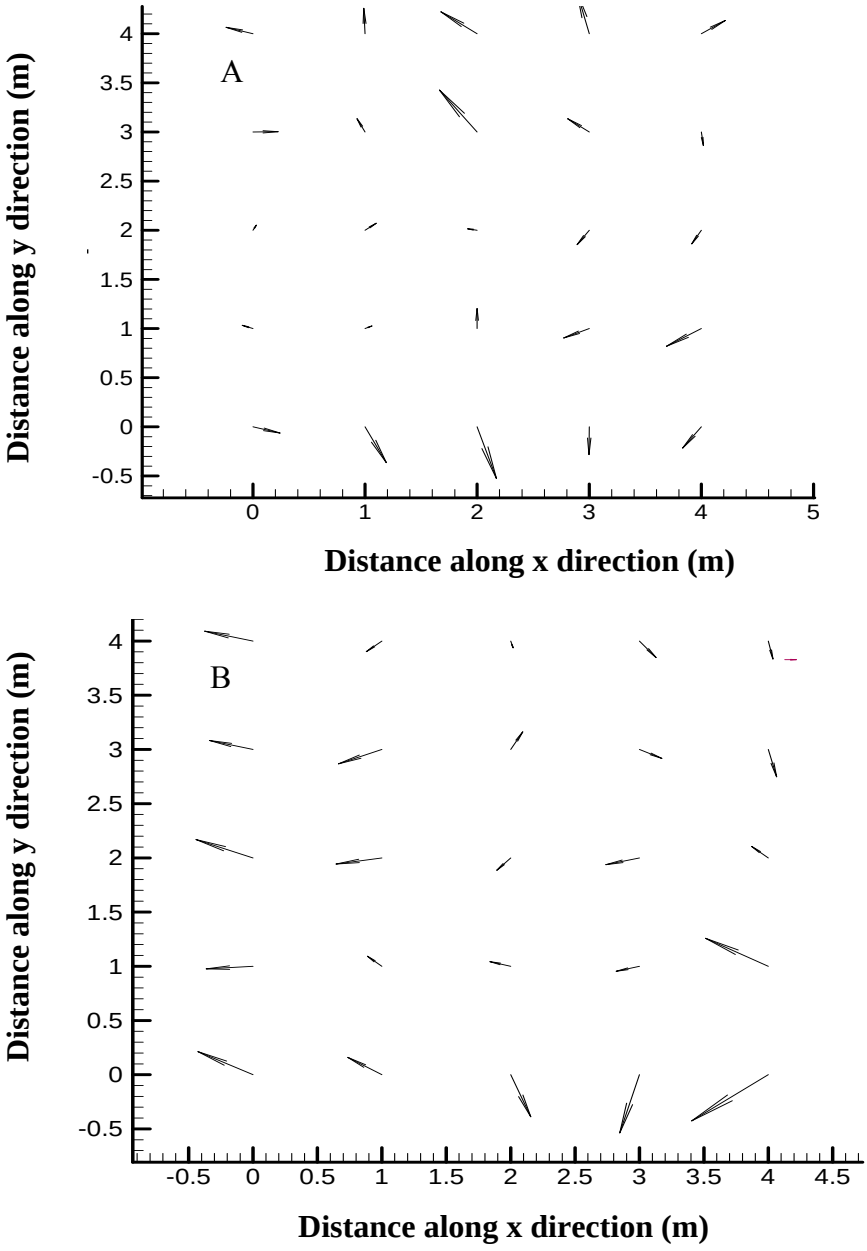

Figure 3.8 Quiver plot of the wind field; A) Simulated fluctuant wind field at $\overline{U}$ = 7m/s, t = 25s; B) Simulated fluctuant wind field at $\overline{U}$ = 9m/s, t = 10s

These wind simulations will apply on an oat plant through a drag force shown in equation (5.9) to examine the dynamic behaviour of oat plants in wind.

3.3 Validation of simulated turbulent wind

In this section, the simulated wind fluctuations are compared with the theoretical (Von Karman) power spectrum, theoretical correlations, and measured wind data above the oat canopy in order to check whether the method could accurately simulate the wind fluctuations or not. A comparison between the simulated wind spectra and theoretical wind spectrum is introduced in section 3.3.1; Section 3.3.2 compares the correlation of simulated wind fluctuations with the theoretical values, and Section 3.3.3 evaluates the simulated wind with a comparison of the measured wind data above an oat canopy.

3.3.1 Comparison between simulated wind spectrum and Von Karman power spectrum

In this section, the simulated wind is investigated by comparing with the theoretical target power spectrum. The simulated and theoretical power spectrums of three points, i.e., P-1, P-4, and P-16, corresponding to mean wind speeds of 5m/s, 7m/s and 9m/s, are shown Figure 3.9, Figure 3.10 and Figure 3.11, respectively. It is found that the curves of the simulated spectrums tend to the theoretical spectrum. This agreement (see Figure 3.9-Figure 3.11) indicates that the current approach to generate the artificial wind field is

suitable for the problem at hand.

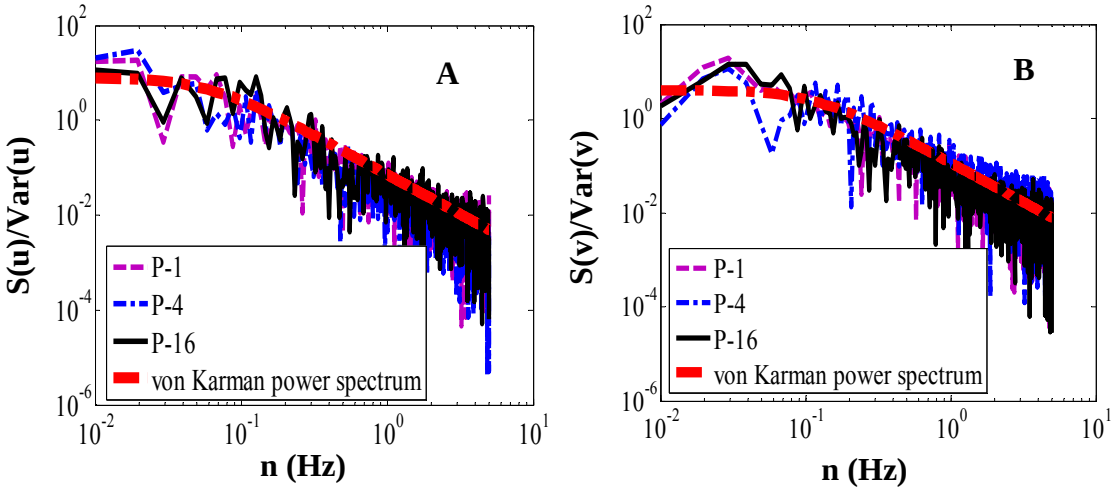

Figure 3.9 Simulated wind spectrums and theoretical power spectrum at $\overline{U}$ = 5m/s; A) along-wind; B) cross-wind

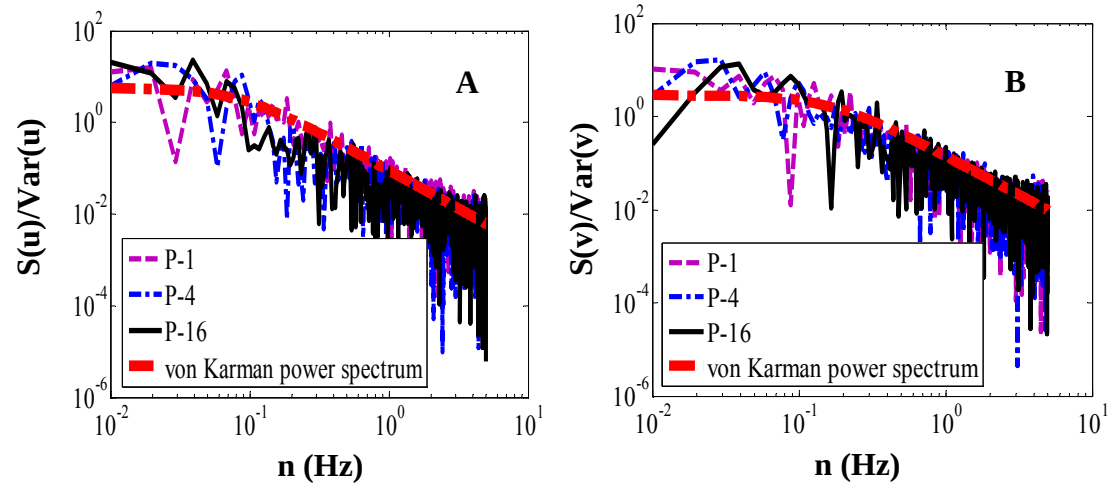

Figure 3.10 Simulated wind spectrums and theoretical power spectrum at $\overline{U}$ = 7m/s; A) along-wind; B) cross-wind

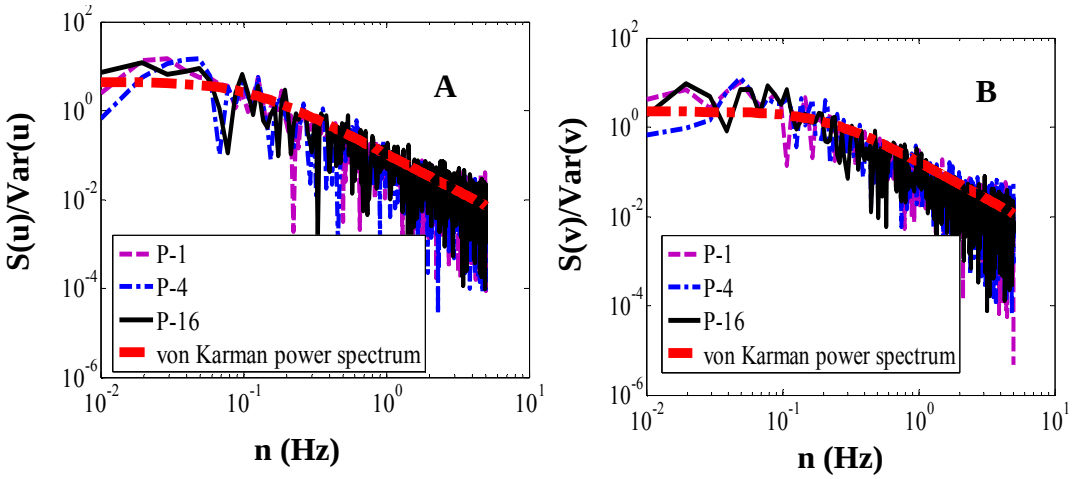

Figure 3.11 Simulated wind spectrums and theoretical power spectrum at $\overline{U}$ = 9m/s; A) along-wind; B) cross-wind

3.3.2 Comparison between simulated correlations and theoretical values

Before proceeding further, the correlations between the simulated wind fluctuations need to be investigated in order to determine if the turbulence-induced velocity fluctuations field is correctly simulated by the WAWS model. The theoretical correlation is given by (Martinez-Vazquez &Sterling, 2011):

$$\phi(r) = e^{-r_i/L_i} \tag{3.2}$$

Where, r_i, L_i is the distance and the integral length scale in the direction i $(i = x, y)$,

respectively.

The theoretical and simulated correlations of a selection of four points (P-*j*): P-1, P-5, P-9 and P-16 are shown in Figure 3.12. The abscissa represents the group of the points, i.e., P-*n* (*n*=1, 2, 3, …, *n*), with which the target point (P-*j*) correlates, and the y-axis presents the normalized correlation factor. This normalized correlation factor includes the cross correlation factor (when $n \neq j$) and the auto correlation factor (when $n=j$).

From Figure 3.14, an oscillation in data is found, because the points do not lie in a line but space in 5 lines within an area. For example, in Figure 3.12A, the correlation factor decreases followed by a decrease in distance between the target point-1 and points in the first line, i.e., point-1 to point-5, and increases suddenly at point-6 in the second line, which is near to point-1 (see Figure 3.3a). For this reason, five peaks in the vibrant curve are observed, i.e., the points space in 5 lines that causes an oscillation in data.

It is also found that simulated correlation tends to follow the theoretical curves. A mean square error defined to evaluate the accuracy of the simulated data compared to the theoretical value is given by:

$$\sigma = \sqrt{\sum_{i=1}^{N} (Simulations_{(i)} - \text{Theoretics}_{(i)})^2 / N} \qquad (3.3)$$

The mean square errors of simulated correlations compared to the theoretical ones shown in the figure 3.12 are provided in table 3.3. The average of the RMS errors is

0.07, which indicates the simulated correlations are acceptable because the error is less than 10%.

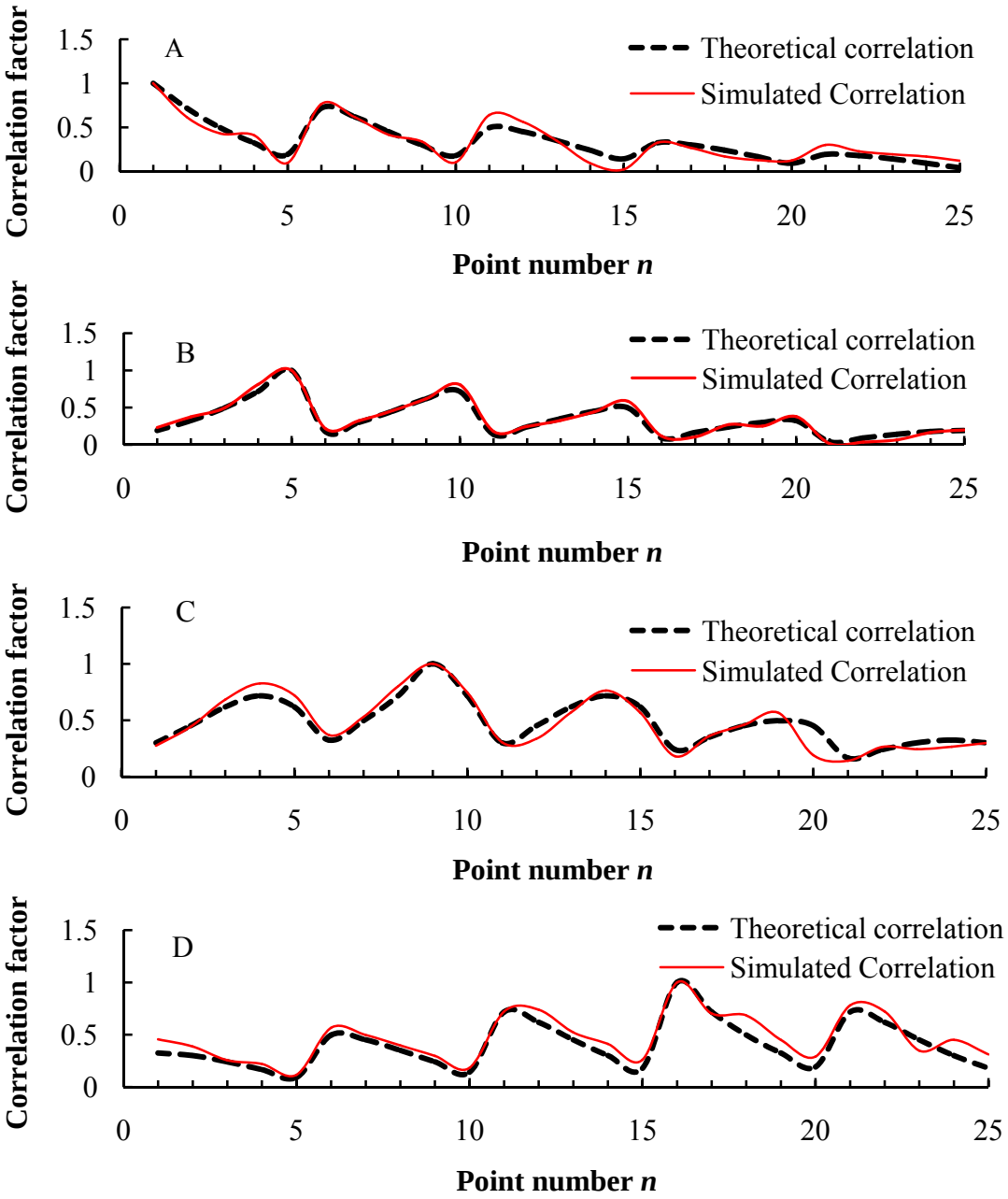

Figure 3.12 The theoretical and simulated correlations of the selected points

The theoretical and simulated correlations between the group of the points and point-1 (A), point-5 (B), point-9 (C), and point-16 (D), respectively.

Point ID	Mean square error
P-1	0.08
P-5	0.05
P-9	0.08
P-16	0.09
Mean	0.07

Table 3.3 The mean square errors of simulated correlations compared to the theoretical values

3.3.3 Comparison between simulated turbulent wind and experimental data

To further evaluate the method, the simulated wind is compared to measured field data obtained over an oat canopy. The wind speed data was recorded by an anemometer installed 1.4m above the oat field ground at Colwall Malvern (County of Herefordshire, UK,

52.08N,-2.38 E, 96m above the mean sea level) in July 2011. A typical result of this test is shown in **Figure 3.13**. A further description of this test can be found in Section 4.3.1.

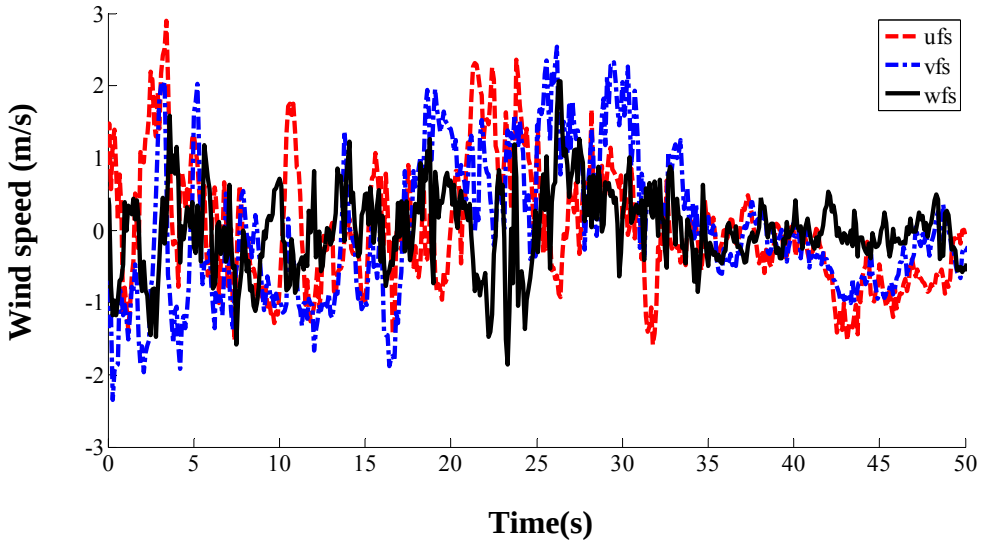

Figure 3.13 Fluctuant wind speed data corresponding measurement made on 6th July (The record began at 17:40:00pm); red (ufs), the longitudinal wind fluctuation; blue (vfs), the lateral wind fluctuation; black (wfs), the vertical wind fluctuation. The mean wind speed is 1.48m/s.

Comparing the simulated power spectrum with measured natural wind fluctuation spectra, it is found that the trend of the spectra of simulated wind fluctuation and recording natural wind is the same, and these two curves follow the theoretical curve. This agreement (**Figure 3.14**) indicates that this method is promising to produce an artificial wind field above the oat plants.

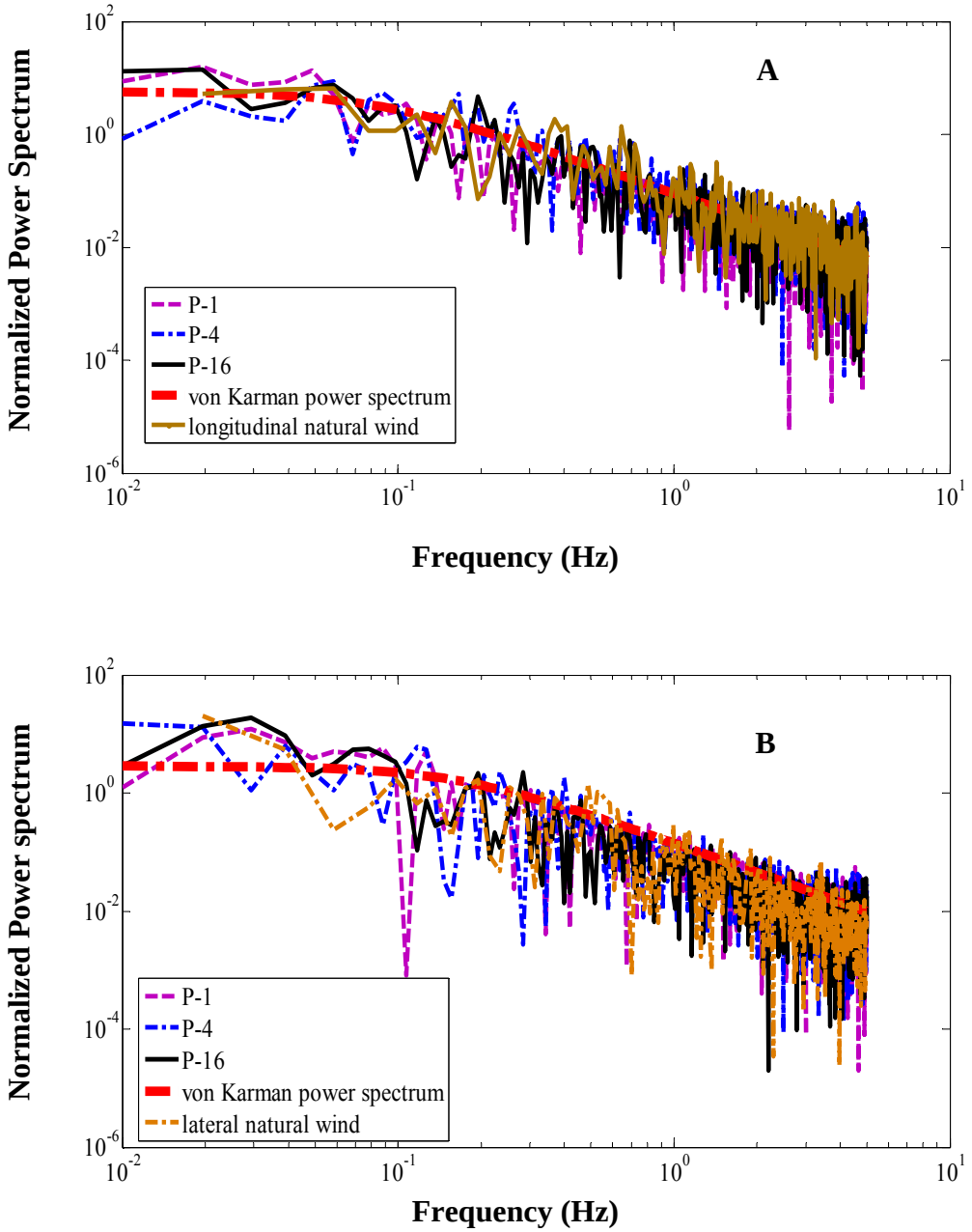

Figure 3.14 Comparison of the simulated wind spectrum with the theoretical power spectrum and measured wind spectrum when the mean wind speed is 1.48m/s; A) along wind; B) cross wind

3.4 Summary

In the present Chapter, the first objective of this study, capturing and reproducing the effect of the natural wind, was achieved. The WAWS method was applied in order to produce an appropriately correlated wind in time and space which possessed the relevant spectral characteristics. Case studies have been undertaken to show the capabilities and features of the simulation methodologies. The simulated correlations of a selected four points were agreed with their theoretical values. Nine pairs of simulated wind fluctuations, i.e. along-wind and crosswind, were compared with their theoretical (Von Karman) power spectrum, whilst three pairs of wind turbulences with the mean wind speed of 1.48m/s were further evaluated with the corresponding measured wind data over an oat canopy. An agreement of these comparisons validated the methodology and indicated that the generated wind field could produce the correlated transient natural wind field over an oat canopy.

4 THE NUMERICAL MODELLING OF AN OAT PLANT

4.1 Introduction

The aim of this chapter is to achieve the second objective of the research, i.e., the construction of an idealised plant model that is capable of modelling the dynamic movements of oats subjected to a time varying loading. However, because the plant's morphology varies with age, i.e., it has been shown that two main distinct morphologies (stem elongation and panicle development and grain ripening , please refer to Section 2.6) appear on the same plant at different growth stages, two models are required to represent these two distinct growth stages. During the stem elongation, the panicles are inside the stem and the size of them is relatively small (Figure 4.1a), whilst in the panicle development and grain ripening stage, the panicle expands to larger surface areas and becomes visible (Figure 4.1b).

Section 4.2 introduces the mechanical models of an isolated oat plant that are equivalent to each of the two growth stages. The behaviours of these models subjected to dynamic loading are studied in this section. A comparison of this proposed model with the experimental data is provided in Section 4.3. Finally, the summarising remarks are made in Section 4.4.

a

b

Figure 4.1 Shape of an oat plant at two different growth stages, a) stem elongation b) the panicle development and grain ripening

4.2 The mechanical model of an isolated oat plant

This section discusses features of two mechanical models of an isolated oat plant with and without the visible oat panicle, a branched cluster of flowers (Figure 4.1b). The two mechanical models are proposed in Section 4.2.1. The analytical equations of these models subjected to dynamic load are introduced in Section 4.2.2. This is followed by a study of the behaviour of an isolated oat plant subjected to a time varying loading in Section 4.2.3, and a parametric analysis in Section 4.2.4. Finally, the morphology of the isolated oat plant is examined in Section 4.2.5, and a modified analytical formula with regard to predication of the natural frequency is produced in Section 4.2.6.

4.2.1 An isolated oat plant model

This section proposes the mechanical model of an isolated oat plant. An oat plant, which grows vertically, bends as a result of the leverage exerted by wind (Figure 4.2). If the bending along the plant exceeds the strength of the stem, then stem lodging is expected, whilst if the ground cannot hold the oat root when the stem bends then root failure occurs (Baker, 1995; Sterling et al., 2003). In addition, different to the previous studies in wheat or barley which failures at the bottom, from the observation it is find that the oat plant can lodge at any point along the stem.

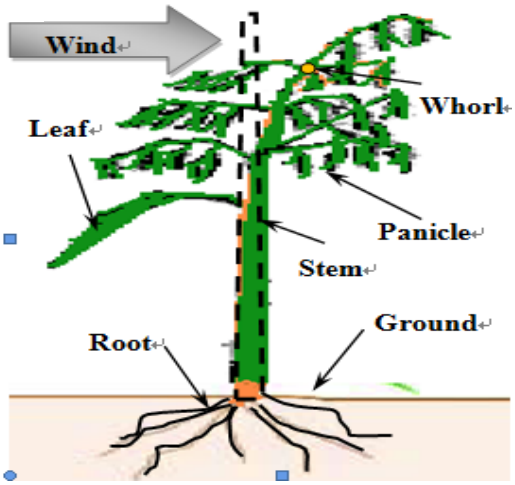

Figure 4.2 The leverage of the oat exerted by the wind

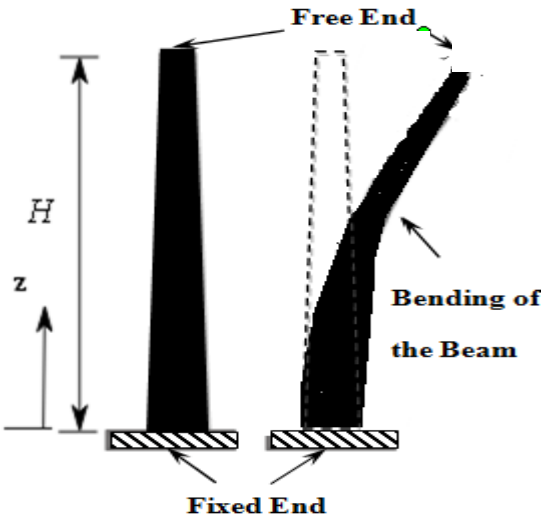

Figure 4.3 A cantilever beam

The slender stem, can as a first approximation, be represented as a vertical tapered cantilever (Figure 4.3).The anchorage of the plant ensures that the top of the plant can

move freely in the lateral direction and also undergo rotational displacement. Similarly, the branches of the panicle also bend under the wind forces and can be considered as sub-beams attached to the cantilever.

A beam is characterized by its material, its profile (the shape of its cross-section) and its length. Young's Modulus is an important parameter because it gives a measure of the resistance to bending. The mass density, mass per unit volume, is also an important parameter since it provides a quantitative measure of an object's resistance (per unit volume) to movement. In what follows it is assumed that the material of the oat is isotropic (the properties are not dependent on the direction) and homogeneous (the material properties are the same at each point). Thus, the density and Young's Modulus are considered to be a constant along the stem. In reality, plant tissues should be considered to be a composite material (Jin, et al., 2009) because the material of the oat plant is neither homogeneous nor isotropic. However, our aim is to build up a realistic but simple model that is easy to use in industry. The assumption proposed here simplifies the model, and some scholars (Saunderson *et al.*, 1999, Jin, *et al.*, 2009) have also adopted this assumption. In addition, previous attempts showed material properties only play a limited role in plant dynamics (Sellier *et al.*, 2009).

As for the root system, studies have shown that the root is near to a hinge on which the root plate turns (Coutts, 1986; Ennos and Crook, 1993). Thus, a plastic hinge at the bottom of the cantilever beam is used to model the root. The plastic hinge is formed at a certain value of moment, known as the plastic moment (M_p), which allows large rotations to occur.

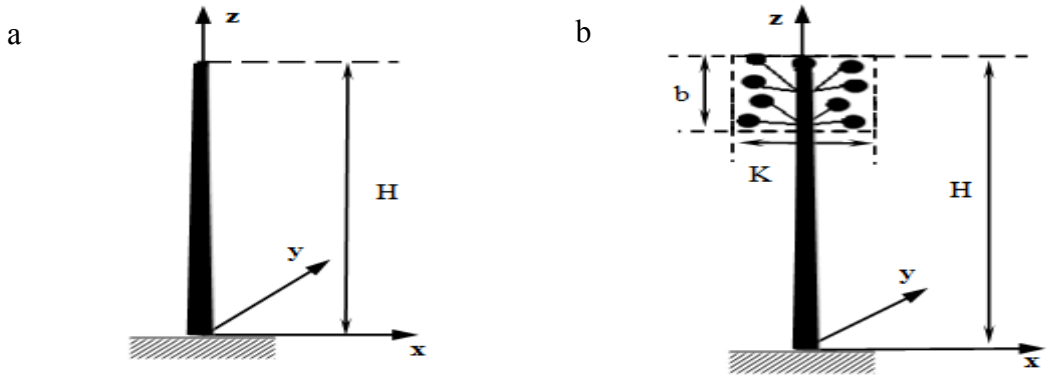

Figure 4.4 The idealized oat plant model used for two different growth stages, a) An idealized model corresponding to an isolated oat plant at an early stage before the panicle has emerged, b) An idealized model corresponding to an isolated oat plant at maturity

According to the characteristics of the oat plant at different growth stages shown in Section 2.6, it is hypothesized that due to the size of the panicle it provides little in the way of aerodynamic resistance to the motion of the plant during the early stage of growth, namely the stem elongation, but does provide additional mass to the stem. Therefore, the whole plant can be ideally modelled as a tapered cantilever beam (see Figure4.4a). However, when oats mature, the panicle is fully integrated and distributed around the height of the plant and plays an important role in governing the motion of the plant (Figure4.4b). Each branch of the panicle carries a concentrated load attached to the stem via a sub beam. As the ratio of the weight of the total grain and the weight of the whole panicle with grains is more than 90% (Table 4.1), the weight of other parts in the panicle are relatively small, for example the branches. Therefore, a branch is considered as a weightless-elastic beam. Thus, each branch of the panicle could be regarded as the top

half of Baker's model (Baker, 1995) and carries a concentrated load, which locates at the centre of gravity of the branch. The whole plant can be ideally modelled as a tapered cantilever with several sub-beams (Figure 4.4). It is necessary to note that the panicle is ideally assumed to be symmetrically distributed in this model. The strength of this assumption is to easily study each factor separately and clearly. In fact, an oat panicle is normally asymmetrically distributed. This effect will be examined in Section 4.2.5.

Parameter	**Average value (± S.D.)**	**Source**
Total grains weight per panicle m_G (g)	7.25 ± 1.30	ADAS
Total weight of whole panicle m_P (g)	8.03 ± 1.48	ADAS
m_G / m_P	0.90	CA

Table 4.1 Ratio of measured grain weight per panicle and the weight of the whole panicle

Key to sources: ADAS: test data from ADAS; CA: value calculated by the author using the data given in this table.

a b

Figure 4.5 Profile of the cross section of a) stem; b) branch

It is assumed that the profile of the stem is a hollow circle (Figure 4.5a). With respect to the branch (the sub-beam), the profile is a solid circle because of the cross section of a natural branch from field observation (Figure 4.5b).

The cross-sectional area of the stem at height z above the base of an oat plant is given by:

$$A(z) = \pi[R(z)^2 - (R(z) - t_w(z))^2] \quad (4.1)$$

Where, $R(z)$ is the radius of the stem at height z above the base of an oat plant, $t_w(z)$ is the thickness of the stem wall at a height z. $R(z)$ and $t_w(z)$ are related to the radius at

the plant base R_0 and the thickness of the stem wall at the plant base t_{w0} by the equations as follows:

$$R(z) = R_0(1-\frac{z}{H})^{\beta}$$
$$t_w(z) = t_{w0}(1-\frac{z}{H})^{\beta} \quad (4.2)$$

Where, H is the plant height, and β is a tapered parameter (Saunderson *et al.*, 1999). Finally, the cross-sectional area of the branch is given by:

$$A_b = \pi r^2 \quad (4.3)$$

Where r is the radius of the branch.

In summary, in this section, a new model of an oat plant has been proposed to be equivalent to each of the two growth stages. To further examine these models, the following section will explore the dynamic response of the idealised models.

4.2.2 Analytical equation of an isolated oat plant subjected to dynamic loading

This section introduces the analytical equation of an isolated oat plant subjected to dynamic loading. Plant motion induced by the wind is proposed using a vibration equa-

tion with a forcing function. The dynamic responses of the isolated oat at the early growth stage and at maturity are provided in Section 4.2.2.1 and Section 4.2.2.2, respectively, with the solutions given in Section 4.2.2.3.

4.2.2.1 Analytical equation of an isolated oat at the early growth stage subjected to dynamic loading

This section discusses the analytical equation of an isolated oat plant at the early growth stage subjected to dynamic loading. According to Clough and Penzien (1995), the dynamic response of this model acted on a laterally distributed force (x direction) can be expressed as:

$$m(z)\frac{\partial^2 x(z,t)}{\partial t^2}+c\frac{\partial\, x(z,t)}{\partial t}+E\frac{\partial^2}{\partial z^2}(I(z)\frac{\partial^2 x(z,t)}{\partial z^2})=F(z,t) \tag{4.4}$$

In which the **z** axis is the direction along the stem, the **x** axis is the direction of deflection; $m(z)=\rho A(z)$, where ρ is the material density, $A(z)$ is the area of the stem cross section at height z; t is the time; c is the viscous damping, E is Young's Modulus of the stem; $I(z)$ is the stem second moment of area at height z, where $I(z)=\frac{\pi[16R^4(z)-(2R(z)-2t_w)^4]}{64}$. $F(z,t)=f(z,t)$, where $f(z,t)$ is the wind force per unit length along plant height z.

If $f(z,t)=0$ Equation (4.5) can be rewritten as

$$\rho A(z)\frac{\partial^2 x(z,t)}{\partial t^2}+c\frac{\partial\ x(z,t)}{\partial t}+E\frac{\partial^2}{\partial z^2}(I(z)\frac{\partial^2 x(z,t)}{\partial z^2})=0 \tag{4.5}$$

Equation (4.6) is referred to as a free vibration response equation.

4.2.2.2 Analytical equation of an isolated oat at maturity subjected to dynamic loading

Now the analytical equation of an isolated oat plant at maturity acted on the dynamic loading is given in this section. The differences between the early growth stage model and maturity model are listed as follows:

- The maturity model has a mass at the top of the main stem.
- The maturity model contains Baker's (1995) models (the sub-beam systems).

It is hypothesized that 1) the mass at the top of the main stem offers the inertia force in the motion, and 2) the branches sway by themselves in winds and transfer their base bending moment to the stem.

Thus, the dynamic response of the stem at maturity can still be expressed as the Equation (4.5), where $m(z)=\rho A(z)+m_g(z)$, ρ is the material density of the plant, $A(z)$ is the area of the stem cross section at height z, and $m_g(z)$ is the grains weight at height z; $F(z,t)=f(z,t)+\frac{\partial}{\partial z}\sum_i^{N_b} M_{Bi}(z,t)$, $M_{Bi}(z,t)$ is the effect of the base bending moment of the branch i, $i=1,2,\ldots,N_b$, N_b is the number of the branches,

and $m(z)$ is the mass distribution at height z.

$m_g(z)$ can be denoted as:

$$m_g(z) = \begin{cases} 0 & z \neq H_{wj} \\ m_{gj} & z = H_{wj} \end{cases} \qquad j = 1, 2, ..., N_{whorl} \tag{4.6}$$

Where H_{wj} is the height of whorl j; N_{whorl} is the number of the whorls.

The wind-induced base bending moment of the branch $M_{Bi}(z,t)$ can be modified according to Baker (1995), and is expressed as:

$$M_{Bi}(z,t) = (f(z,t) L_{Bi} \cos\theta_{Bi} \cos\varphi_{Bi})(1 + \frac{g}{(2\pi n_{Bi})^2 L_{Bi} \cos\theta_{Bi} \cos\varphi_{Bi}})(1 - \exp^{-2\pi n_{Bi}\delta_{Bi}t} \cos(2\pi n_{Bi} t)) \tag{4.7}$$

in which $f(z,t)$ is the wind force per unit length along plant height z, L_{Bi} is the length of the branch i, $L_{Bi}\cos\theta_{Bi}$ is the height at centre of gravity between the branch top and its base, where θ_{Bi} is the acute angle between the branch i and the stem, φ_{Bi} is the acute angle between the branch i and the wind direction; n_{Bi} is the natural frequency of the branch i, g is the acceleration due to gravity, and δ_{Bi} is the damping ratio of branch *i*.

The wind force per unit length along the plant height can be denoted as

$$f(z,t) = \frac{1}{2} \rho_a A_{pj} C_D [\overline{U}(z) + u'(z,t) - \frac{dx(z,t)}{dt}]^2 \tag{4.8}$$

in which the inputs are the density of air (ρ_a), the projected area of the panicle (A_{pj}), the drag coefficient (C_D), the mean wind velocity ($\overline{U}(z)$), the fluctuation velocity ($u'(z,t)$) at height z; and the velocity of plant ($\frac{dx(z,t)}{dt}$) at height z.

If $f(z,t) = 0$, the free vibration response of the maturity model is given by:

$$m(z)\frac{\partial^2 x(z,t)}{\partial t^2} + c\frac{\partial x(z,t)}{\partial t} + E\frac{\partial^2}{\partial z^2}(I(z)\frac{\partial^2 x(z,t)}{\partial z^2}) = 0 \tag{4.9}$$

Where, $m(z) = \rho A(z) + m_g(z)$

From equation (4.10), it is found that, in the free vibration response case, the effect of the branches and grains is adding additional mass to the stem. This finding will be examined further in Section 4.2.6.

4.2.2.3 The solution of analytical equations

This section provides the solutions of the dynamic response equations. The bending moment function will be provided because of the assumption that if the bending moment along the plant exceeds the strength of the material or the bending moment at the plant base preponderates over the ground's capacity of holding the oat root, lodging will be expected (Baker, 1995; Sterling, 2003).

According to Clough and Penzien (1995), the solution of the dynamic response equation can be written as:

$$w(z,t)=\sum_{r=1}^{+\infty}W_r(z)q_r(t) \tag{4.10}$$

Where $w(z,t)$ is the lateral deflection, $W_r(z)$ and $q_r(t)$ are the spatial function and the temporal function of the *r*-th mode, respectively. Followed by the work of Clough and Penzien (1995) and Saunderson et al., (1997), they can be further rewritten as:

$$\begin{aligned} &W_r(z)=a_{1r}\cos\lambda_r z+a_{2r}\sin\lambda_r z+a_{3r}\cosh\lambda_r z+a_{4r}\sinh\lambda_r z-\frac{\overline{F_r}}{M_r\omega_{dr}^2}\\ &q_r(t)=e^{-\zeta_r\omega_{nr}t}(b_{1r}\cos\omega_{dr}t+b_{2r}\sin\omega_{dr}t)+\frac{1}{M_r\omega_{dr}}\int_0^t e^{-\zeta_r\omega_{nr}(t-\tau)}\sin\omega_{dr}(t-\tau)F_r(\tau)\mathrm{d}\tau\\ &r=1,2,\cdots \end{aligned} \tag{4.11}$$

Where a_{ir} and b_{jr} ($i=1,2,3,4$ and $j=1,2$) is the arbitrary constants to be determined from the boundary and initial conditions, respectively. ω_{dr} is the damped circular frequency, $\omega_{dr}=\omega_{nr}\sqrt{1-\zeta_r^2}$, ζ_r is the damping ratio, $\zeta_r=\frac{C_r}{2M_r\omega_r}$, where C_r is the viscous damping; M_r is the modal mass, $F_r(t)$ is the modal force. They can be calculated using the equations below:

$$\begin{aligned} &M_r=\int_0^H m(z)W_r{}^2(z)\mathrm{d}z\\ &F_r(t)=\int_0^H F(z,t)W_r(z)\mathrm{d}z\\ &r=1,2,\cdots \end{aligned} \tag{4.12}$$

In which, $m(z)$ and $F(z,t)$ are the mass distribution and force distribution, respectively. H is the plant height.

The time varying bending moment along the stem is the second partial differentiation of the response, which is given by:

$$M\left(z,t\right)=\frac{\partial^2 w(z,t)}{\partial z^2}=\frac{\partial^2 \sum_{r=1}^{+\infty} W_r\left(z\right)q_r\left(t\right)}{\partial z^2} \tag{4.13}$$

$q_r\left(t\right)$ is not affected by the partial differentiation, then Equation (4.14) can be divided as:

$$M\left(z,t\right)=\sum_{r=1}^{+\infty}(M_{1r}(z,t)+M_{2r}(z,t)) \tag{4.14}$$

Where, $M_{1r}(z,t)=\frac{\partial^2 W_r\left(z\right)}{\partial z^2}e^{-\zeta_r\omega_{nr}t}(b_{1r}\cos\omega_{dr}t+b_{2r}\sin\omega_{dr}t)$

$$M_{2r}(z,t)=\frac{\partial^2 \frac{W_r\left(z\right)}{M_r\omega_{dr}}\int_0^t e^{-\zeta_r\omega_{nr}(t-\tau)}\sin\omega_{dr}(t-\tau)F_r(\tau)\mathrm{d}\tau}{\partial z^2}$$

Equation (4.15) shows that the bending moment is a sum of the free vibration response ($M_{1r}(z,t)$), which is also called transient response, and the response to dynamic loading ($M_{2r}(z,t)$), namely steady state response. The frequency domain analysis considers only the steady state response, but ignores the transient response. This is a main limitation of the frequency domain analysis because it may underestimate the maximum

bending moment of an oat plant subjected to dynamic loading. Thus, in this thesis, the time history of a system's response is examined in order to obtain a deeper insight into the dynamic behaviour of an oat plant in natural wind.

Equation (4.15) also shows that the bending moment of the plant is a function of time, damping ratio, frequencies, position along the plant and the external force. In addition, boundary and initial conditions also affect the bending moment.

Considering the simplest situation, the boundary condition of a cantilever beam is listed in equation (4.16).

$$W(0) = 0 \qquad W'(0) = 0$$
$$W''(H) = 0 \qquad W'''(H) = 0 \tag{4.15}$$

Where H is the plant height.

Substituting equation (4.16) into (4.12), and letting $F(z,t) = 0$, the solution of spatial information equation of a uniform cantilever beam is obtained, which is given by:

$$\cosh \lambda H \cos \lambda H = -1 \tag{4.16a}$$

$$W(z) = \frac{1}{2}(\cosh \lambda z - \cos \lambda z) - \frac{1}{2}(\cosh \lambda H + \cos \lambda H)(\sinh \lambda z - \sin \lambda z)/(\sinh \lambda H + \sin \lambda H) \tag{4.17b}$$

$$\omega_{nr} = \lambda_r^2 \sqrt{\frac{EI}{\rho A}} = (\lambda_r H)^2 \sqrt{\frac{EI}{\rho A H^4}} \qquad r = 1, 2, \ldots \tag{4.17}$$

Giving $\lambda_r H = 1.87,\ 4.69,\ 7.85,\ \ldots,$

Where λ_r is *r*-th the non-dimensional coefficient; ω_{nr} is the *r*-th angular frequency; ρ is the material density of the plant; A is the area of the stem cross section; E is the Young's Modulus of the stem; I is the stem second moment of area; H is plant height.

Hence, in the free vibration case, the time varying bending moment along the stem is:

$$M(z,t) = \sum_{r=1}^{+\infty} \frac{\lambda_r^2}{2} [\cosh \lambda_r z + \cos \lambda_r z - C_r \sin \lambda_r z - C_r \sinh \lambda_r z](b_{1r} \cos \omega_{dr} t + b_{2r} \sin \omega_{dr} t) e^{-\zeta_r \omega_r t}$$

$$\lambda_r^2 = \omega_{nr} \sqrt{\frac{\rho A}{EI}} \quad \lambda_r H = 1.87,\ 4.69,\ 7.85,\ \ldots,\ \ r = 1, 2, \ldots \tag{4.18}$$

$$C_r = (\cosh \lambda_r H + \cos \lambda_r H)(\sinh \lambda_r H + \sin \lambda_r H)$$

Equation (4.19) suggests that each frequency contributes to the bending moment. Thus, the natural frequencies play a key role in the plant's damage. The phase angle, a result of the initial conditions and the natural frequency, also influences the lodging in oat.

In summary, in this section, the equations of the dynamic responses of the isolated oat are provided. It is found that the stem bending moment, caused by the free vibration re-

sponse and response to dynamic loading, is a function of time, damping ratio, natural frequency, position at the plant and the external force. Each frequency influences the bending moment, which is an important parameter related to the plant's damage (Baker, 1995; Sterling, 2003).

4.2.3 The dynamic characteristics of an isolated oat plant

In Section 4.2.2, the natural frequencies appear to be important in plant damage. However, how natural frequency plays a role in oat damage needs to be investigated. In this section, a transfer function, which reflects the inherent characteristics of the structure, is examined in order to determine the influence of different natural frequencies on oat lodging.

The case studies of the early growth stage and maturity model are undertaken. In keeping with the work of Martinez-Vazquez and Sterling (2011), the models are loaded by a linearly distributed force in the $\mathbf{x}$ direction (denoted as q), having a constant $\frac{1}{2}\rho_a K C_D$ for a distance αH from the top (Figure 4.5), where ρ_a is the density of the air, K is the diameter of the canopy, C_D is the drag coefficient, α is the ratio of the panicle length b and the plant height H. The standard values of these parameters are shown in Table 4.2 below.

Parameter	Standard value	Source of the data
panicle area K (m^2)	0.045	ADAS
panicle length b (m)	0.20	ADAS
air density ρ_a (kg/m^3)	1.2	EA
drag coefficient C_D	0.51	WTTEST

Table 4.2 Parameters of drag force

Key to sources of the data: ADAS, test data from ADAS Company; EA, data estimated by author from the existing air density data, WTTEST, wind tunnel test (Baker *et al*, 2012).

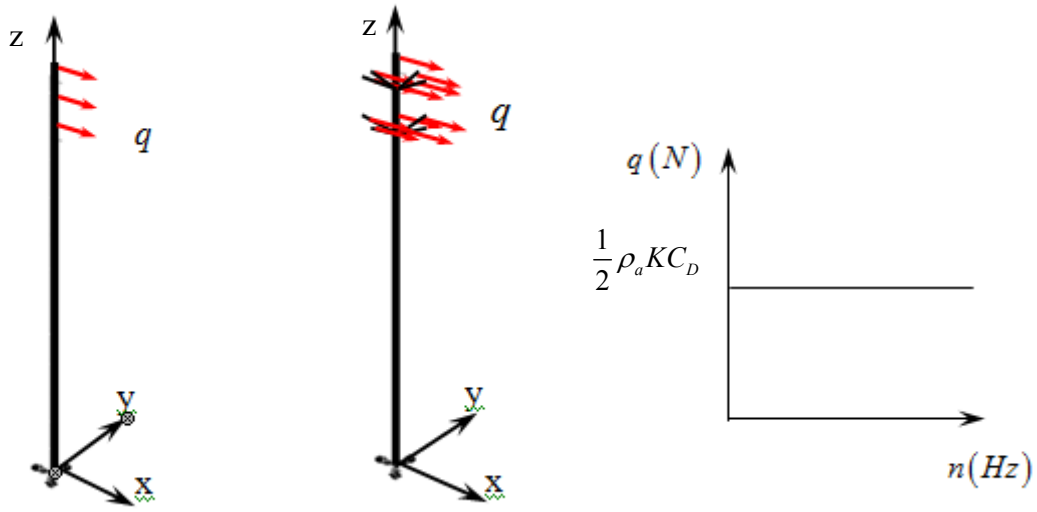

a) An isolated model at an early growth age

b) An isolated model at maturity

c) The force acting on an isolated oat plant

Figure 4.6 An isolated model acted on a constant and linearly distributed force

4.2.3.1 Construction of a numerical isolated plant

This section introduces how to generate a synthetic oat plant (Figure 4.5) using the ABAQUS software (Version 6.10, Hibbitt, Karlsson & Sorensen, Inc. USA) in order to calculate the transfer function. The beam element with hollow circular (Figure 4.4b), beam element with solid circular (Figure 4.4c) and inertia mass are adopted to describe the stem, branches and grains, respectively. The geometry of the model is shown in Figure 4.6 in accordance with the mechanical model. The main beam (stem), which is fixed at its base, has been divided into 10 elements, whilst each branch is divided into 4 elements. In addition, inertia masses (green points shown in Figure 4.6B) are attached

on the top of each branch and main beam.

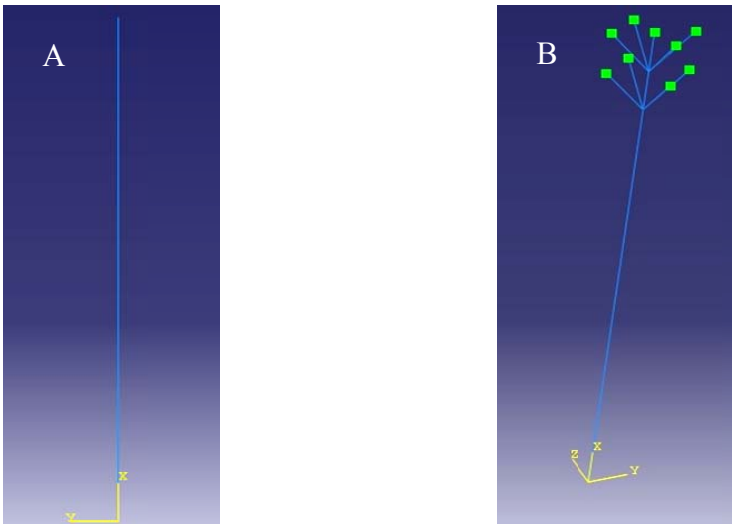

Figure 4.7 An idealized model corresponding to an isolated oat plant; A) at an early stage; B) at maturity

The parameters which may largely influence the motion of an oat plant are measured from the natural oat samples and are shown in Table 4.3 and Table 4.4, respectively, in order to explore the features of an oat plant as realisticly as possible. Note that, although the properties of an oat plant change at different growth stages, for example, in its early growth stage, the plant is shorter than it is at maturity, they are assumed to be un-changeable in these case studies in order to identify the effect of the panicle. Besides, in this section, we assume all the branches have the same parameters and are distributed symmetrically (the asymmetrical factor will be studied in Section 4.2.5).

Parameter	Standard value	Source of the data
Geometry parameter		
Plant height H (m)	1.1	ADAS
Radius of section at base R_0 (m)	3.5×10^{-3}	ADAS
Wall width t_w (m)	1×10^{-3}	ADAS
Tapered parameter β	0.3	EA
Material parameter		
Density ρ (kg/m^3)	600	EA
Young's Modulus E (MPa)	800	EA
Poisson's Ratio μ	0.3	EA

Table 4.3 Parameters of an isolated oat plant stem. Key to sources of data: ADAS, test data from ADAS; EA, data estimated by author using the test data from ADAS.

Parameter	Standard value	Source of the data
Branch parameter		
Branch number N_b	8	EA1
Branch length L_b (m)	4×10^{-2}	EA1
Branch angle θ (deg)	45	EA2
Branch Young's Modulus E_b (MPa)	500	EA2
Radius of branch section R_b (m)	0.005	EA2
Grain parameter		
Grain weight per node m_g (g)	1	EA1

Table 4.4 Parameters of an isolated oat plant panicle. Key to sources of data: EA1, data estimated by author using the test data from ADAS; EA2, data arbitrarily estimated by author

The steps "frequency" and "Steady-state dynamics, Modal" have been used to calcu-

late the transfer function. The result is shown in the following sections.

4.2.3.2 Results and discussions

This section shows the simulation result.

i. Natural frequencies

The first two natural frequencies of the models corresponding to the early growth stage are 1.1Hz and 7.1Hz, which are the natural frequencies of the main stem. The first two natural frequencies of the models at a maturity are 0.8Hz, 6.3Hz (corresponding to the main stem) and 3.4Hz and 3.8Hz (corresponding to the branches), respectively. Comparing these two models, it is found that the first two natural frequencies corresponding to the stem reduce when an oat plant grows up. At the same time, two more frequencies corresponding to the branches appear to be between the two stem frequencies when a plant matures.

ii. Transfer function of bending moment

The transfer function of the bending moment corresponding to an oat plant at an early growth stage is shown in Figure 4.8. In this figure, we can find that the bending moments shift due to the frequency of the loading changes. The bending moments increase suddenly when the frequency of the wind load approaches 1 Hz and 7 Hz, which are the first and second mode, respectively. Using the same analysis method and applying the same magnitude of the loading, the transfer function of the bending moment corresponding to the oat plant at maturity is shown in Figure 4.9.

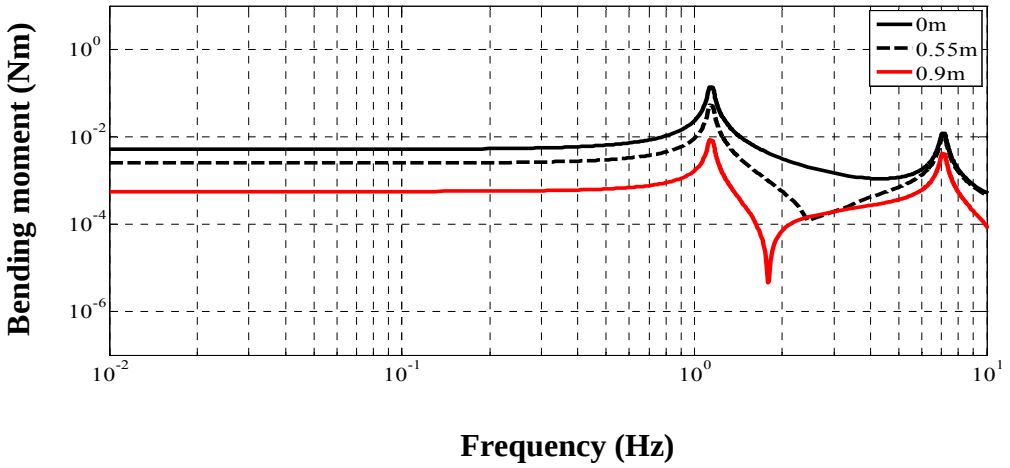

Figure 4.8 Transfer function of bending moment at an early growth stage model loaded by a linearly distributed force for a distance of 0.2m.

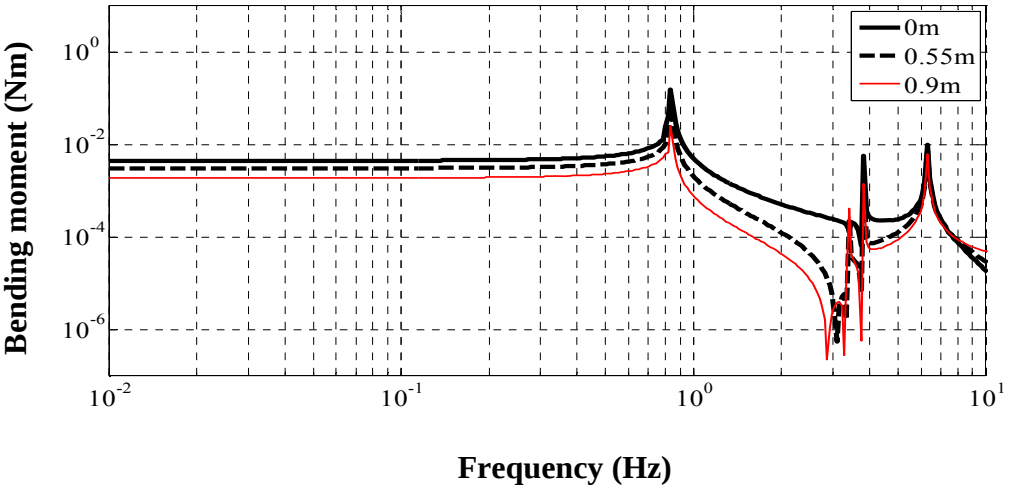

Figure 4.9 Transfer function of bending moment at maturity loaded by a linearly distributed force for a distance of 0.2m.

It is found that more modes of the bending moment occur in the frequency range from 3Hz to 10Hz, which is termed the high frequency range. Figure 4.8 illustrates that the branches do not affect the first mode significantly, in other words, the effect of the branches mainly lies in the high frequency range (3Hz-10Hz). Next, the transfer function of the bending moment corresponding to the oat plant at maturity also illustrates that the maximum bending moment occurs at the bottom when the frequency is at its first mode. While, at second mode (7.1 Hz in Figure 4.7 and round 3.4Hz in Figure 4.8), the bending moments in the middle point and the bottom are very close in accordance with the curves. In this case, rather than the bottom, the stem may fail in the middle point. However, if both the first and second modes occur, the maximum bending moment still occurs at the bottom. In reality, the high frequency energy of the wind load is filtered (Davenport, 1964). Above 3Hz, there is very little energy (Baker, 1995, see Figure 3.2). It seems the wind induces the plant motion at its first mode, which is also called fundamental resonant frequency. Therefore, this chapter focuses on how the structural parameters of the oat plant influence the fundamental natural frequency, and in the following chapter, Chapter 5, the relationship between the oat lodging and the fundamental natural frequency will be discussed.

Comparing the early growth stage model with the maturity model shown in Figure 4.7 and Figure 4.8, respectively, it is found that the oat plant is more likely to lodge when it matures because the maximum bending moment of the maturity model (0.16Nm) is larger than the value of the early growth stage model (0.064Nm) when the loading on the two models is the same. These maximum bending moments occur at the

fundamental natural frequency. This finding well matches the field observations (Berry et al., 2004). The following sections will therefore only examine the idealized model that corresponds to an oat plant at maturity.

In addition, these maximum bending moments occur at the fundamental natural frequency, which shows this natural frequency mainly influences the lodging in oat.

In summary, Section 4.2.3 has been found that the fundamental natural frequency played a leading role in oat damage. In addition, it was also found that the oat plant was more likely to lodging when it matures. The following sections therefore only examine the model that corresponds to the maturity stage and focus on how the structural parameters of the oat plant influence the fundamental resonant frequency.

4.2.4 Parametric investigation

In Section 4.2.2, equation (4.16), the time varying bending moment along the stem showed that the resonant frequencies of the plant may be the key factor to oat damage. In addition, Section 4.2.3 showed that compared with other natural frequencies, the fundamental natural frequency plays the leading role in oat damage. However, how the oat parameters of the oat plant influence the basic resonant frequency still needs to be investigated. In this section, a parametric analysis is undertaken in order to explore the sensitivity of fundamental natural frequency to oat parameters. The key parameters in-

volved in the calculation are illustrated in Table 4.3 and Table 4.4. Each key parameter has been varied by 10% and the results are shown in Table 4.5-Table 4.7.

Parameter	**% change in n_1 for 10% decrease in parameter**	**% change in n_1 for 10% increase in parameter**
Plant height H (m)	+22	-18
Radius of section at base R_0 (m)	-13	+13
Wall width t_w (m)	+0.4	-0.7
Tapered parameter β	-0.09	+0.09

Table 4.5 Sensitivity of fundamental natural frequency (n_1) to changes in geometry parameters of an isolated oat plant stem

First consider the geometry parameters shown in table 4.5: the effect of varying height, radius of cross section, wall width, and tapered parameter, respectively. A decrease in plant height increases natural frequency, and an increase in the radius of the cross section, wall width or tapered parameter increases natural frequency. Variation in plant height is

most significant, i.e., there is 30% change in frequency compared with other parameters that only change the frequency less than 15% by varying 10%, whilst variations in radius of section also produces a large (15% compared to less than 5% when varying other parameters) change in natural frequency due to an increase in stiffness.

Second, consider the material parameters. Table 4.6 shows the effect of varying density, Young's Modulus and Poisson's ratio, respectively. A decrease in density increases natural frequency and an increase in Young's Modulus increases natural frequency. However, the effect of Poisson's ratio is found to have no significant effect on oat frequency.

Parameter	**% change in n_1 for 10% decrease in parameter**	**% change in n_1 for 10% increase in parameter**
Density ρ (Kg/m^3)	+4	-4
Young's Modulus E (MPa)	-5	+5
Poisson's Ratio μ	$+2\times10^{-3}$	-3×10^{-3}

Table 4.6 Sensitivity of fundamental natural frequency (n_1) to changes in material parameters of an isolated oat plant stem

Parameter	% change in n_1 for 10% decrease in parameter	% change in n_1 for 10% increase in parameter
Branch parameters		
Branch number $N_b^{\,b}$	+0.001	-0.002
Branch length L_b (m)	+0.8	-0.6
Branch angle θ (deg)	-0.05	+0.1
Branch Young's Modulus E_b (MPa)	-0.2	+0.2
Radius of branch section R_b (m)	+0.6	-0.9
Grain parameter		
Total Grain weight m_g (g)	+2	-2

Table 4.7 Sensitivity of fundamental natural frequency (n_1) to changes in parameters of an isolated oat plant panicle. Notes: $N_b^{\,b}$, in this case, grain weight does not change. In addition, the variation in fundamental natural frequency could up to 10% resulting from a 50% change in the grain weight which exists in reality.

Finally, consider the branch and grain parameters. The effect of varying branch number, branch length, the angle of branch and stem, Young's Modulus of branch, radius of branch section and grain weight is shown in Table 4.8. All the branch parameters have insignificant effects on the fundamental natural frequency but an increase in grain weight will produce a change in natural frequency, where the natural frequency will be decreased.

In summary, a parametric investigation of fundamental natural frequency has been undertaken in this section. It has been found that the frequency was most sensitive to variations in plant height, and the radius of the stem cross section played the second role in the frequency. Material density, Young's Modulus and grain weight also produced a change in natural frequency, whilst the effects of section wall width, tapered parameter, Poisson's ratio and branch parameters, i.e. branch numbers, branch length, Young's Modulus of branch and radius of branch section, have been considered but have no significant effect on the oat plant's frequency. These findings also suggested that although these parameters, i.e., tapered parameter, Poisson's ratio, branch numbers, branch length, Young's Modulus of branch and radius of branch section, were estimated by the author, they do not influence the numerical result significantly.

4.2.5 Sensitivity of natural frequency to asymmetrical distribution of oat panicle

In Section 4.2.4, how the physical parameters of an oat plant with a symmetrically distributing panicle influence the fundamental natural frequency has been examined. However, whether the asymmetrically distributed oat panicles would affect the natural frequency or not is still unclear. In order to study this effect, several cases (Figure 4.9) are investigated. The case studies are listed as follows:

- Case 1: An idealized model corresponding to an oat plant at maturity.
- Case 2: A model with one superposed branch corresponding to an oat plant at maturity.
- Case 3: A model with two superposed branches corresponding to an oat plant at maturity.
- Case 4: A model with three superposed branches corresponding to an oat plant at maturity.
- Case 5: A model with four superposed branches corresponding to an oat plant at maturity.
- Case 6: A model with branch superposed four branches corresponding to an oat plant at maturity.

- Case 7: A model with randomly distributed branches corresponding to an oat plant at maturity.

- Case 8: A simplified model at maturity in which grains are attached to the main stem.

- Case 9: An idealized model corresponding to an isolated oat plant at an early stage.

The results of these case studies are shown in Table 4.8. It is found that if the weight of the grains and branches of each node are the same, the asymmetrical distribution of the panicles of a natural oat does not affect the fundamental natural frequency significantly.

Thus, if we only consider the fundamental natural frequency, the simplified model (case 8) could represent other cases (cases 1-7) with error less than 2%. It was also found that the effect of the branches and grains adds additional masses to the stem.

In summary, the asymmetrical distribution of the oat panicle has been examined in this section. It has been found that the effect of the asymmetrically distributed oat panicles is not significant if we only consider the fundamental natural frequency. The idealized model corresponding to an oat plant at maturity (Figure 4.9a) could be simplified to the model, where the masses of the grains are attached to the main stem (Figure 4.9h). In the next section, a further comparison of this simplified model with the early growth stage is provided.

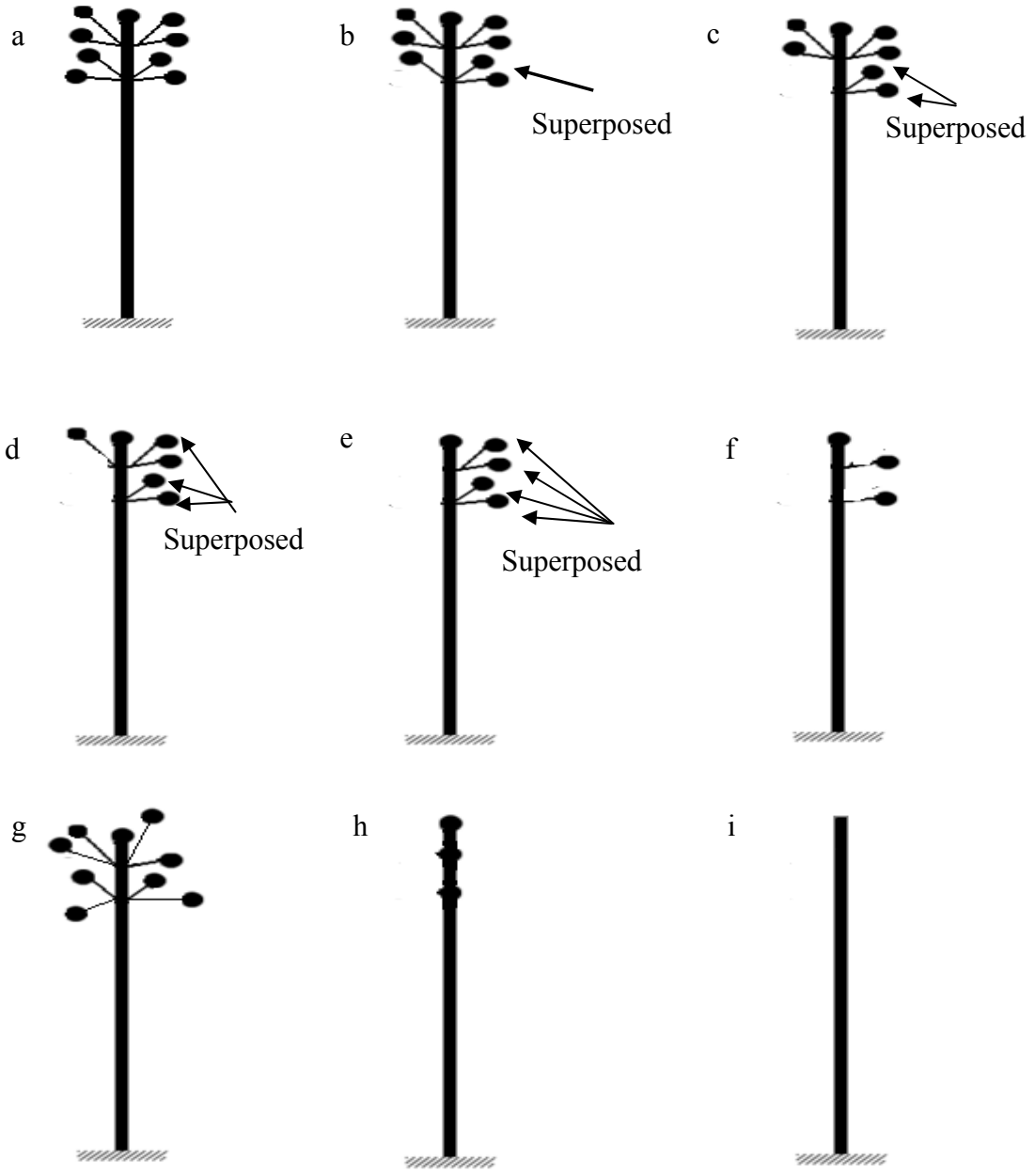

Figure 4.10 An oat model at maturity considering asymmetrical distribution of oat panicle; a) case 1, b) case 2, c) case 3, d) case 4, e) case 5, f) case 6, g) case 7, h) case 8, i) case 9

Cases	Frequency (Hz)	Discrepancy between the result of symmetrical case (case 1) and other cases (%)
1	0.84	0
2	0.84	0
3	0.84	0
4	0.83	-1
5	0.83	-1
6	0.82	-2
7	0.84	0
8	0.85	+1
9	1.13	+35

Table 4.8 Sensitivity of natural frequency to panicle distribution

4.2.6 The modified analytical formula considering the effect of oat panicle

Section 4.2.5 shows that the idealized model of an oat plant at maturity could be simplified. In this section, a further comparison of this simplified model with the early growth stage is undertaken. Compared with these two models (cases 8 and case 9 shown in Figure 4.10), it is also found that the effect of the branches and grains is adding additional mass to the stem. Taking this finding into account, Equation (4.18) of natural frequency could be modified as:

$$\omega_r = \lambda_r^2 \sqrt{\frac{EI}{\rho A}} = (\lambda_r H)^2 \sqrt{\frac{EI}{\rho A H^4}} = (\lambda_r H)^2 \sqrt{\frac{EI}{H^3(\rho A H + m_G)}}$$

$$n_1 = \frac{(\lambda_1 H)^2}{2\pi H} \sqrt{\frac{EI}{H(\rho A H + m_G)}} = \frac{(\lambda_1 H)^2}{2\pi H} \sqrt{\frac{EI}{H(m_s + m_G)}} = \frac{(1.87)^2}{2\pi H} \sqrt{\frac{EI}{H(m_s + m_G)}} \tag{4.19}$$

Where ω_1 is the fundamental angular frequency; n_1 is the fundamental natural frequency; λ_1 is the non-dimensional coefficient; ρ is the material density of the plant; A is the cross sectional area of the stem; E is Young's Modulus ; I is the second moment of area; H is plant height and m_G is the total grains mass, m_s is the masses of the stem.

To verify this modified formula, a comparison of the modified formula and numerical result is carried out. Table 4.12 illustrates the comparison of the modified analytical formula (MA) and Finite Element (FE) method. The discrepancy between the FE model

and the analytical formula (Equation 4.20) is less than 6% which indicates that this formula is reasonable (when one considers the variability that exists in the plant parameters).

Cases	Frequency(Hz)		Discrepancy (%)
	F E	MA	
1	0.84	0.87	3
2	0.84	0.87	3
3	0.84	0.87	3
4	0.84	0.87	3
5	0.84	0.87	3
6	0.82	0.87	6
7	0.84	0.87	3
8	0.85	0.87	2

Table 4.9 Comparison between the Finite Element analyses (FE) and the modified analytical formula (MA). Discrepancy is between FE model and the Equation (4.20).

4.3 Comparison between numerical simulations and experimental data

This section compares the numerical simulations with the experimental data in order to further validate the model. The model adopted above is considered to be reasonably realistic because this model could consider the realistic physical parameters, which may affect lodging, as much as possible in order to gain a better understanding of the lodging mechanism. The layout of this section is listed as follows: Section 4.3.1 briefly introduces the measurements; Section 4.3.2 compares the parametrical analysis result with the measurements; Section 4.3.3 evaluates the modified formula (Equation (4.20)) with a comparison of the experimental data, and Section 4.3.4 compares the numerical result with analytical predictions and data from the free vibration response test.

4.3.1 Introduction of the field measurement

This section briefly introduces the physical experiments to measure natural wind above the oat canopy and the fundamental natural frequency of oat samples. The experiments were conducted in an oat field at Colwall (County of Herefordshire, UK, 52.08N,-2.38 E, 96m above the mean sea level), 2011. The topography of the site is very flat exposed significantly in all directions. An oats field was grown under standard agro-technical procedures with different nitrogen treatment. One is no nitrogen, the other is 140kg/ha nitrogen.

The wind speed data was recorded by an anemometer installed 1.4m above the oat field ground. This height was chosen due to the highest oat plant was round 1.3m in that field, which ensured that the anemometer could record the wind speed that was very close to the oat canopy but did not influence the motion of the oat. Three components of wind speed were measured at a sampling frequency of 10 Hz and the longitudinal, lateral and vertical wind was obtained after coordinate rotation. One 50-second record of the wind data is used to validate the simulated wind. This data selected should be well representative of the wind flow and it had to display large wind gusts, exerting similar turbulence intensity value with the simulated data. The data starting at 17:40:00pm 16:40pm 6th July 2013 was chosen, and its streamwise and transverse horizontal wind velocities was compared with the simulated turbulent wind (See Section 3.3.3).

The fundamental natural frequency of oat was measured through free vibration test. The oat stem was pulled from its static equilibrium position and released gently. Each sample was tested 3 times, and then the average was calculated. The time of 3 oscillations was measured by a stopwatch. The natural frequency of the oat stem can be calculated from the equation below.

$$n = \frac{3}{t} \tag{4.20}$$

Where, n is the frequency of oscillation, and t is the recording time of 3 oscillations.

Afterwards, the corresponding plant height, the diameter of the stem cross section and

the wall width were measured.

1) The height (m) was measured using a tape measure. Each sample was measured three times from the ground to the plant top.

2) The diameter (mm) of each base internode was measured at its mid-point using digital callipers. Each sample was measured 3 times to calculate the average.

3) These internodes were then cut at their middle point. Afterwards, the wall width (mm) was measured using digital callipers. Again, each sample was measured 3 times and the average was calculated.

The data from measurement is shown in Table 4.10.

Plant	Height (m)	Radius of the section (mm)	Wall width (mm)	Natural frequency (Hz)
1	0.90	3.7	1.0	1.02
2	0.92	3.4	1.0	1.12
3	0.92	3.3	1.0	1.07
4	0.94	3.5	1.1	1.09
5	0.95	3.6	1.1	1.05
6	0.97	3.8	1.2	1.08
7	0.98	3.5	1.0	0.99
8	1.01	3.3	1.1	0.90
9	1.05	3.4	1.1	0.85
10	1.07	3.3	1.0	0.85
11	1.07	3.6	1.1	0.90
12	1.09	3.6	1.2	0.80
13	1.22	3.5	0.8	0.97
14	1.23	3.6	0.9	0.80
15	1.24	3.5	1.0	0.77

16	1.24	3.2	0.8	0.82
17	1.25	3.3	1.0	0.79
18	1.26	3.0	0.8	0.70
19	1.27	3.5	0.7	0.84
20	1.28	3.3	0.9	0.77
21	1.29	3.9	0.8	0.71
22	1.30	3.1	0.8	0.71
23	1.31	3.3	0.8	0.71
24	1.32	3.7	0.7	0.87
Mean	1.13	3.45	0.95	0.88
S.D.	0.15	0.22	0.1	0.13

Table 4.10 The measured proprieties of oat plants

4.3.2 Comparison of the parametric analyses with the field measurements

The parametric analyses result is compared with the measurement data in this section.

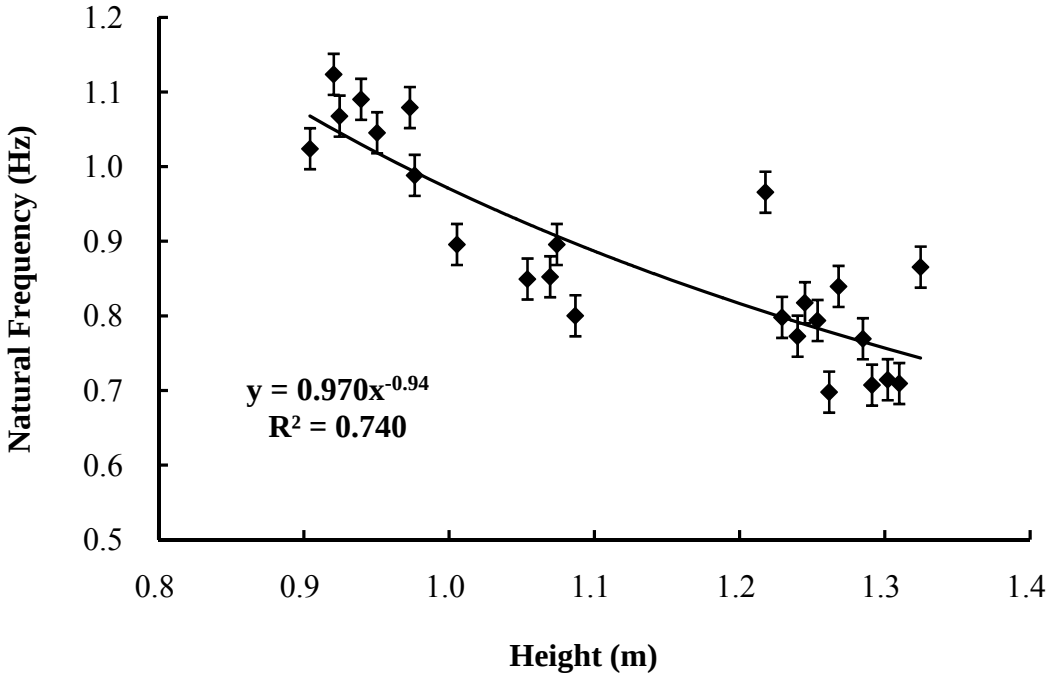

Figure 4.11 Relationship between measured heights of the oat shoots and measured natural frequencies of corresponding oat plants and variations in other physical parameters. The error bar refers to the standard deviation of the dataset.

The correlation between the measured natural frequency and the measured height is shown in Figure 4.10. Although there are variations in other physical parameters (e.g., the density, Young's Modulus, tapered parameter), the measured heights and the natural frequencies are reasonably correlated (R^2=0.74). Then, the relationship between the measured radius and the measured natural frequency corresponding to the height ranging from 0.9m to 1.3m is shown in Figure 4.11, which indicates no obvious relationship between the radius and the natural frequency (R^2=0.027).. This, together with the findings of Figure 4.10, provides evidence that plant height plays a leading role in funda-

mental natural frequency, which supports the findings in section 4.2.4.

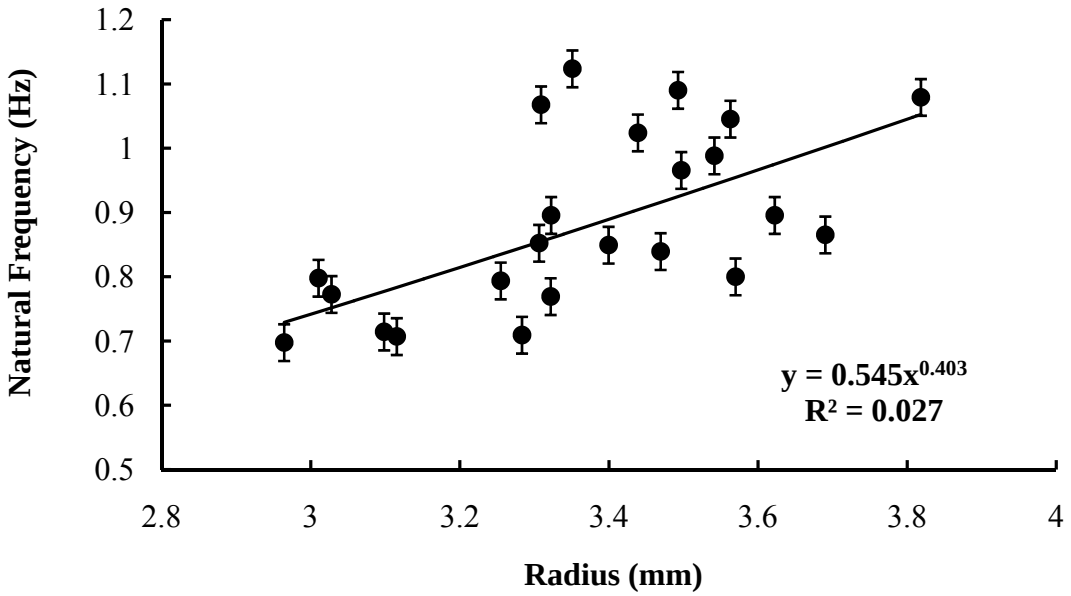

Figure 4.12 Relationship between measured radiuses and measured natural frequencies of corresponding oat plants and variations in other physical parameters. The error bar refers to the standard deviation of the dataset. This data corresponds to the height ranging from 0.9m to 1.3m.

Figure 4.13 examines the correlation between the radius and the natural frequency corresponding to the height ranging from 1.2m to 1.3m. With a similar height, the radius and the frequency are reasonably correlated (R^2=0.648). This matches the finding in Section 4.2.4, that is, the radius of the stem cross section plays the second role in fundamental natural frequency. All the findings above show that the model proposed in Section 4.2 seems reasonable. These, together with the outcomes in Section 4.2.4, show

that by using the parameters measured from real oat samples, the model can predict the trend and value of the natural frequency. In light of Equation (4.15), which tells us the time history of bending moment along the stem, a further conclusion that the model is sufficient to describe the dynamic behaviour of an isolated plant can be drawn.

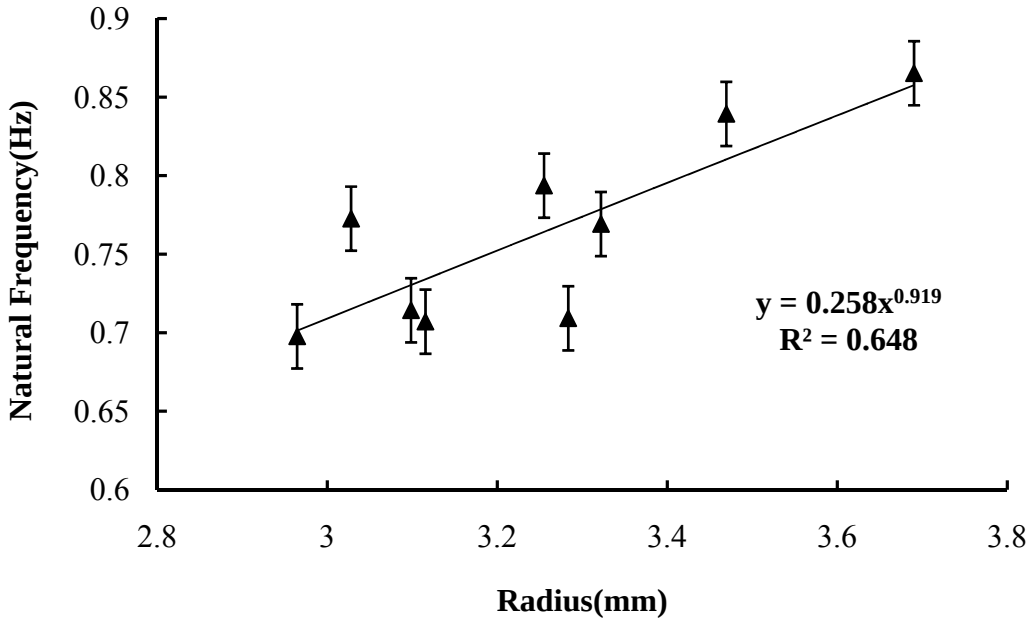

Figure 4.13 Relationship between radius of the oat shoot and natural frequencies of corresponding oat plants with a similar height and variations in other physical parameters. The error bar refers to the standard deviation of the dataset. This data corresponds to the height ranging from 1.2m to 1.3m.

4.3.3 Comparison of the modified formula with field measurements

The comparison of the modified formula (Equation 4.20) and field measurement at the

similar height, ranging from 1.2m to 1.35m, is shown in Figure 4.14. The value of the average of the squares of the difference is：

$$\sqrt{\sum_{i=1}^{12}(Calculation_{(i)} - Experiment_{(i)})^2}\ /12 = 0.38/12 = 3.2\% \tag{4.21}$$

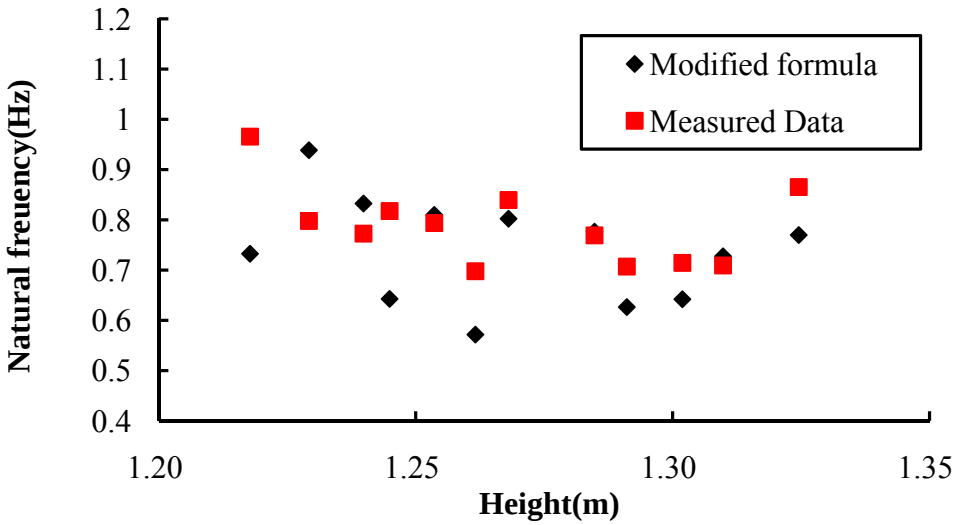

Figure 4.14 Comparison of the modified formula (4.20) and measurement

An agreement of these two with difference less than 5% indicates that this formula is reasonable. Furthermore, the finding that the effect of the branches and grains is adding additional mass to the stem is satisfactorily grounded.

4.3.4 Comparison of the numerical and analytical predictions with the data from free vibration test

To further evaluate the model, a free vibration response test for an isolated oat plant was undertaken in the School of Civil Engineering, University of Birmingham. In the test the oat plant was placed in front of a digital camera in order to ensure the plane of motion was perpendicular to the camera axis. The plant was pulled from its static equilibrium position and released gently. The movement was recorded by a digital video. A typical result for the test is shown in **Figure 4.15**.

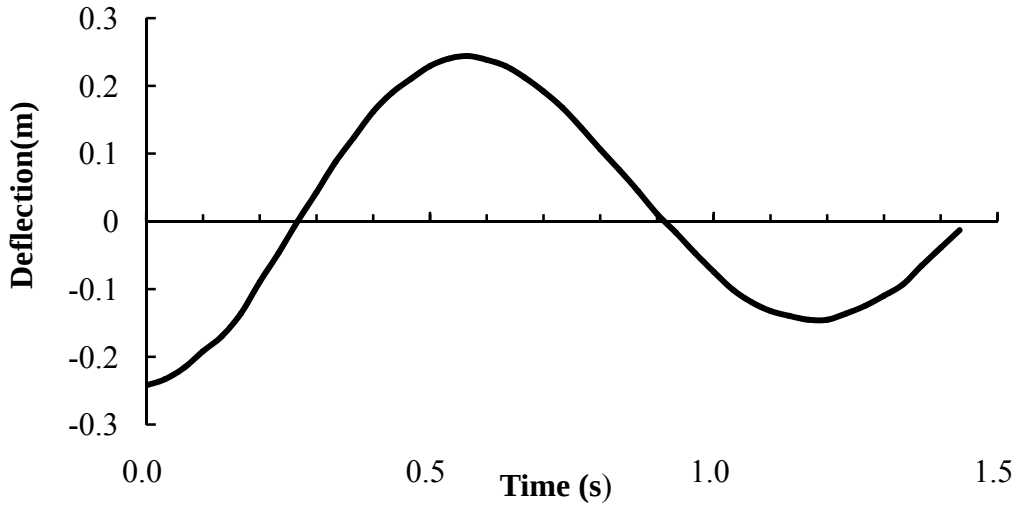

Figure 4.15 Free vibration response of an isolated shoot

From this figure, the values of damping ratio ζ and fundamental natural frequency n_1 can be calculated. The damping ratio is:

$$\zeta_1 = \sqrt{\frac{1}{1+(\frac{2\pi}{\ln(x_0/x_1)})^2}} = \sqrt{\frac{1}{1+(\frac{2\pi}{\ln(0.24218/0.14531)})^2}} = 0.081 \tag{4.22}$$

in which x_0 and x_1 are the heights of successive peaks. The recorded period of the vibration is 1.2s, thus the natural frequency is:

$$n_1 = \frac{1}{T\sqrt{1-\zeta_1^2}} = \frac{1}{1.2\sqrt{1-0.081^2}} = 0.8360Hz \tag{4.23}$$

T is the period between peaks (and troughs).

The lateral deflection of the beam at free vibration response can be denoted as (assuming constant cross-section)

$$w(z,t) = \sum_{r=1}^{+\infty} W_r(z) e^{-\zeta_r \omega_{nr} t} (b_{1r} \cos \omega_{dr} t + b_{2r} \sin \omega_{dr} t) \tag{4.24}$$

or

$$\begin{cases} W(z) = a_1 \cos \lambda z + a_2 \sin \lambda z + a_3 \cosh \lambda z + a_4 \sinh \lambda z \\ q(t) = e^{-\zeta \omega_n t} (b_1 \cos \omega_d t + b_2 \sin \omega_d t) \end{cases} \tag{4.25}$$

If we only consider the fundamental natural frequency, and take the height of the plant into account, the deflection of the plant can be written as:

$$w(z,t) = W_1(z)\, e^{-\zeta_1 \omega_{n1} t} (b_1 \cos \omega_{d1} t + b_2 \sin \omega_{d1} t)$$

$$\begin{aligned} W_1(z) &= \frac{1}{2}(\cosh \lambda_1 z - \cos \lambda_1 z) - \frac{1}{2}(\cosh \lambda_1 H + \cos \lambda_1 H)(\sinh \lambda_1 z - \sin \lambda_1 z)/(\sinh \lambda_1 H + \sin \lambda_1 H) \\ &= \frac{1}{2}[(\cosh 1.7z - \cos 1.7z) - 0.3(\sinh 1.7z - \sin 1.7z)] \end{aligned} \tag{4.26}$$

Where, $\lambda_1 H = 1.87$, with $H = 1.1, \lambda_1 = 1.7$

Considering the initial conditions, the shoot was gently pulled from its static equilibrium position. The initial position is $W_1(z)$ and the initial velocity is zero, which is shown as follows.

$$w(z,0) = W_1(z) b_1 = W_1(z) \tag{4.27a}$$

$$\begin{aligned} &\frac{\partial w(z,t)}{\partial t}\Big|_{t=0} \\ &= W_1(z)(\zeta_1 \omega_1 e^{-\zeta_1 \omega_1 t} b_1 + e^{-\zeta_1 \omega_1 t} b_2 \omega_{d1}) \\ &= 0 \end{aligned} \tag{4.28b}$$

Substituting Equation (4.23) and (4.28) into (4.27), we obtain

$$\begin{aligned} &w_1(z,t) = W_1(z)(\cos 5.24t + 0.081 \sin 5.24t) e^{-0.081 \times 5.25t} \\ &\omega_1 = 2 \times \pi \times n_1 = 5.25\ rad/s \quad b_1 = 1, b_2 = -\zeta_1 \omega_1 / \omega_{d1} = \frac{-\zeta_1}{\sqrt{1-\zeta_1^2}} \end{aligned} \tag{4.28}$$

The position of the measured point was 0.665m.

To calculate the free vibration of the numerical model, the steps in ABAQUS, namely

"frequency" and "Modal dynamics", have been used. The model is the same as in Section 4.2.3 which is shown in Figure 4.6B.

Figure 4.16 shows the numerical and analytical predictions compared to the test data, from which it can be concluded that both approaches predict the motion reasonably. This agreement indicates the model of an isolated oat plant can represent the dynamic behaviour of a natural isolated oat plant.

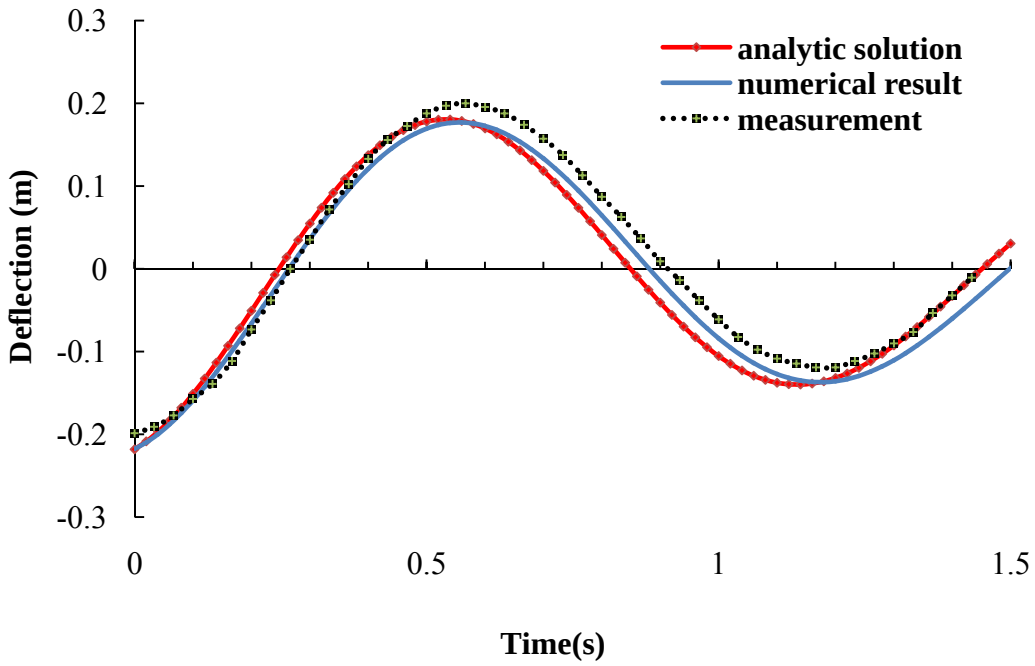

Figure 4.16 Comparison of predicted oscillation of oat plant (the analytical predictions and numerical result) against actual oscillation (measurement)

4.4 Summary

In this chapter the second objective of the research, the construction of an idealised

plant model that is capable of modelling the dynamic movements of oats, has been achieved. The main contributions of this chapter are identified:

- A new mechanical model with respect to an isolated oat plant has been originally constructed and validated against the experimental data.
- Analytical equations of an oat plant subjected to dynamic load have been given.
- The dynamic characteristics of an isolated oat plant have been explored.
- A good agreement of the numerical result, analytical formula and test data provides a satisfactory check that the generated isolated model is realistic and reasonable to examine the dynamic behaviour of a natural oat plant.

Besides, some findings regarding this oat model can be summarised as:

1) The bending moment of the plant was a function of time, natural frequency, damping, the external wind loading and position along the plant. The natural frequencies, especially the fundamental natural frequency, played a key role in the plant's damage.

2) The transfer functions of the bending moment illustrated that the branches did not significantly affect the first mode of the natural frequency.

3) Compared with the early growth stage, oat plants were more likely to lodge when they matured because the maximum bending moment of the maturity model was larger than the one at the early growth stage.

4) A parametric investigation of fundamental natural frequency showed that the frequency was most sensitive to variations in plant height, and the cross sectional radius of the stem, material density, Young's modulus, and grain weight also produced a change in the frequency. However, the effects of wall width, tapered parameter, Poisson's ratio and branch parameter, i.e. branch numbers, branch length, branch Young's Modulus and radius of branch section were found to have no significant effect.

5) The asymmetrical distribution of the panicle did not significantly affect the frequency. The branches and grains decreased the frequency by adding the additional masses.

6) Analytical formulas (4.20) and (4.27) have been produced to predict the fundamental natural frequency and the free vibration response of the oat plant, respectively.

5 THE DYNAMIC BEHAVIOUR OF AN ISOLATED OAT PLANT SUBJECTED TO REALISTIC WIND LOADING

5.1 Introduction

In order to achieve the third objective of this study, this chapter examines the dynamic behaviour of an isolated oat plant subjected to realistic wind loading. Section 5.1 gives the layout of this chapter. The numerical methods used in this chapter, i.e., random response and dynamic analysis methods, are briefly outlined in Section 5.2. Applying the random response method, in Section 5.3, the wind energy transference to the oat plant containing the appropriate energy-frequency relationship is examined. The bending moment spectrum along the plant as a result of the wind spectrum is calculated. Then, adopting the dynamic analysis method, the envelope of maximum bending moments corresponding to plant height in the time domain is explored. In section 5.5, a comparison between the numerical result and the wind tunnel test data is provided. The failure wind speeds are estimated using simple failure criterions and compared to Baker's (1995) model in section 5.6. The parametric study into the sensitivity of plant response is undertaken in section 5.7. Finally, the conclusions are drawn at the end.

5.2 The Methodology

This section briefly introduces two Finite Element (FE) methods used in this Chapter, i.e., the random response and dynamic analysis.

Using random response analysis, the wind energy transference to the oat plant containing the appropriate energy-frequency relationship will be examined. This is because if an object is forced to vibrate at a frequency near to this particular resonant frequency, lodging is mostly like to appear, i.e., large deflections of the object will occur (Den Hartog, 1985).

However, random response analysis has limitations as it can only analyse linear systems. Therefore the responses spectrum method is not appropriate for high winds because the geometric non-linearity of oat plants is significant as observed. In such a case, the time history of the wind flow must be found in order to obtain the system's response in the time domain, and a time domain dynamic analysis is a necessity.

In summary, because of the turbulent characteristics and dynamic properties of oat plants, the random response method and dynamic analysis method are used to study the behaviour of the oat plant subjected to wind. These methods are briefly introduced in sections 5.2.1 and 5.2.2, respectively.

5.2.1 Method 1-The random response method

In this section, the Random response analysis method is introduced. Random response analysis predicts the steady-state response of a system that is subjected to a series of non-deterministic vibrations of variant frequency. The responses, i.e., displacement, velocity or acceleration, are excited by an input spectrum. This analysis approach is widely used in Engineering, for example, to determine the response of an airplane to turbulence, the response of a structure to jet noise, or the response of a building to an earthquake (ABAQUS, 2010). However, there is a key limitation of this method, that is, it is only applicable for linear systems. If the non-linear factors in the system are important, this method is not appropriate and the time history of the excitation must be known.

5.2.2 Method 2-The dynamic method

In this section, the dynamic analysis in the time domain is discussed. Dynamic analysis broadly includes explicit and implicit analysis. Compared to the explicit dynamic method, which is only conditionally stable (ABAQUS, 2010), the implicit method has merits due to its unconditional stability. In addition, the *dashpots,* dampers which resist motion via viscous friction, can be applied to the model in order to represent the aerodynamic damping. Unfortunately, the explicit dynamic time stepping method in ABAQUS cannot simulate models with dashpots, whereas the implicit dynamic time stepping method can.

For these reasons, the implicit dynamic method is used to obtain the response of the oat plant in wind.

5.3 The wind energy transference to an isolated oat plant in the frequency domain

This section examines the wind energy transference to an oat plant. The wind spectrum (i.e., the input spectrum) is introduced firstly. Although there are several forms of wind spectrum, the von Karman formula (Equation 2.10) is frequently used (Baker, 1995; Baker et al., 1998; Berry et al., 2003; Sterling et al., 2003; Martinez-Vazquez and Sterling, 2011). The von Karman power spectrum which corresponds to different mean wind speeds ranging from 1m/s to 15m/s with an interval of 2m/s is shown in Figure 5.1.

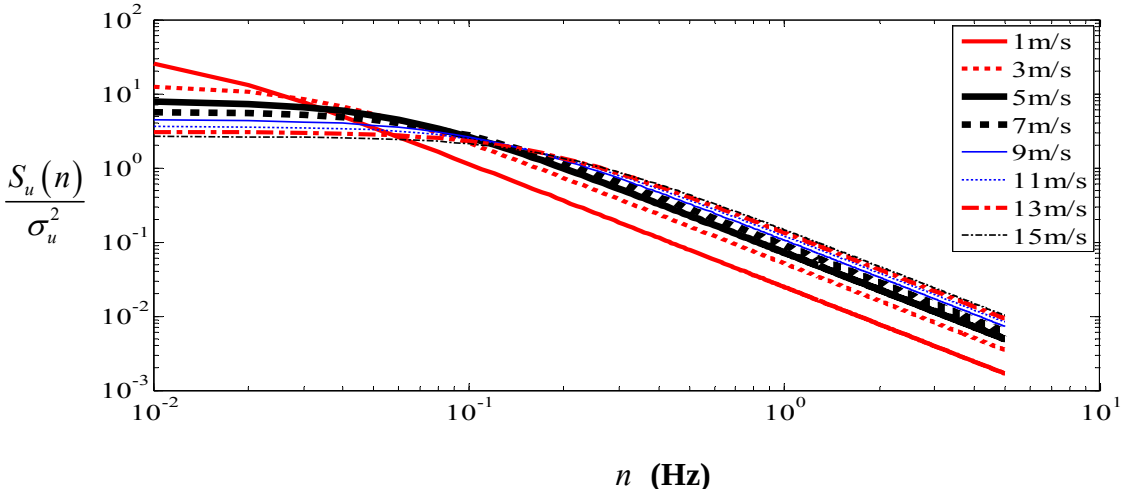

Figure 5.1 Von Karman power spectrum corresponding to different mean wind speed ranging from 1m/s to 15m/s with an interval of 2m/s

The corresponding force spectrum acting on the plant can be written as (Baker, 1995):

$$S_F(n) = (4\frac{\overline{F}^2}{\overline{U}^2})\chi^2(n)S_u(n) \tag{5.1}$$

In which n is the natural frequency, $\overline{U}$ is the mean wind speed, $\overline{F}$ is the mean force on the oat, where $\overline{F} = 0.5\rho_a A_{pj} C_D \overline{U}^2$ (ρ_a is the density of air, A_{pj} is the canopy area, $A_{pj} = bK$, C_D is the drag coefficient, see Table 4.2 and Figure 4.3b), and $\chi^2(n)$ is the aerodynamic admittance function. The form of $\chi^2(n)$ is given by:

$$\chi^2(\mathrm{n}) = \frac{1}{1 + 2.5(\frac{nK}{\overline{U}})} \tag{5.2}$$

Where K is the oat canopy diameter, the definition of this parameter is shown in section 4.2.1, Figure 4.3b. The key parameters involved in the simulations are listed in Table 4.2.

Secondly, the oat plant model is described. Chapter 4 showed that the oat plant was more likely to lodge when it matured. Thus two numerical models, 1) the isolated model at maturity (Figure 4.3b) and its simplified version (Figure 4.10h), are studied here with the aid of the ABAQUS software. The details of these models are provided in Chapter 4. The random response step in ABAQUS software was used to calculate the response

spectrum of the oat plant in winds. The results are shown in the following sections.

Now, the results of the wind energy transference to an oat plant are discussed. The base bending moment spectrum against the wind speed is examined firstly, because the previous study suggested that the maximum bending moment occurred at the base of the plant (Baker, 1995). The base bending moment spectrums of the oat at maturity that corresponds to different mean wind speed are shown in Figure 5.2. The abscissa represents the frequency, and the y-axis presents the bending moment spectrum.

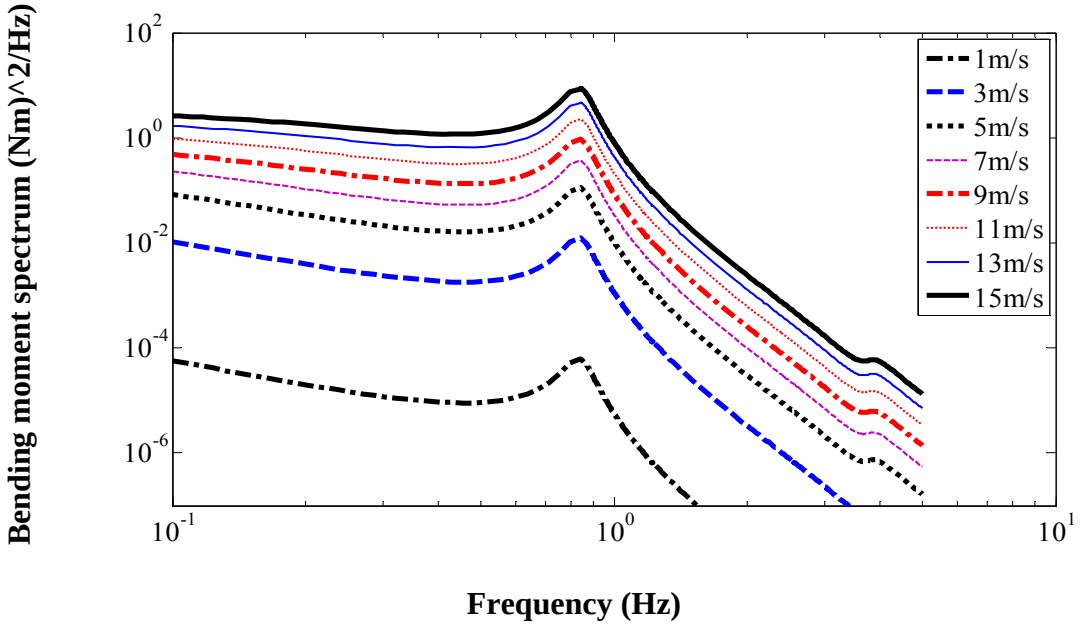

Figure 5.2 Base bending moment spectrum of the oat at maturity corresponding to different mean wind speeds from 1m/s to 15m/s with an interval of 2m/s.

From Figure 5.2, an increase in mean wind speed leads to an increase in the magnitude of the bending moment spectrum is found. In each bending moment spectrum

curve, the highest value appears at the plant's fundamental natural frequency, after which the wind energy transference to the oat plant decreases.

Next, the bending moment spectrum along the stem is explored. According to the failure wind speed predicted by Baker's (1995) model (i.e., 7.5m/s), two case studies are undertaken, that is, 1) the mean wind speed is less than the failure wind speed and, 2) the mean wind speed is higher than the failure wind speed. The mean wind speeds of 5m/s and 11m/s are chosen. The results related to this choice are shown in Figure 5.3 and Figure 5.4, respectively. The abscissa represents the frequency, and the y-axis presents the bending moment spectrum.

From Figure 5.3 and Figure 5.4, it can be determined that, whether the plant has branches or not, and what the wind speed is, the highest value of the bending moment spectrum appeared when the frequency is near 0.8 Hz, which is the oat plant's fundamental natural frequency identified in section 4.2.3. Also, above 0.8 Hz, the wind energy transference to the oat plant decreases. It is also found that the magnitude of the bending moment is largest at the plant's base, and an increase in the distance along plant height decreases the bending moment.

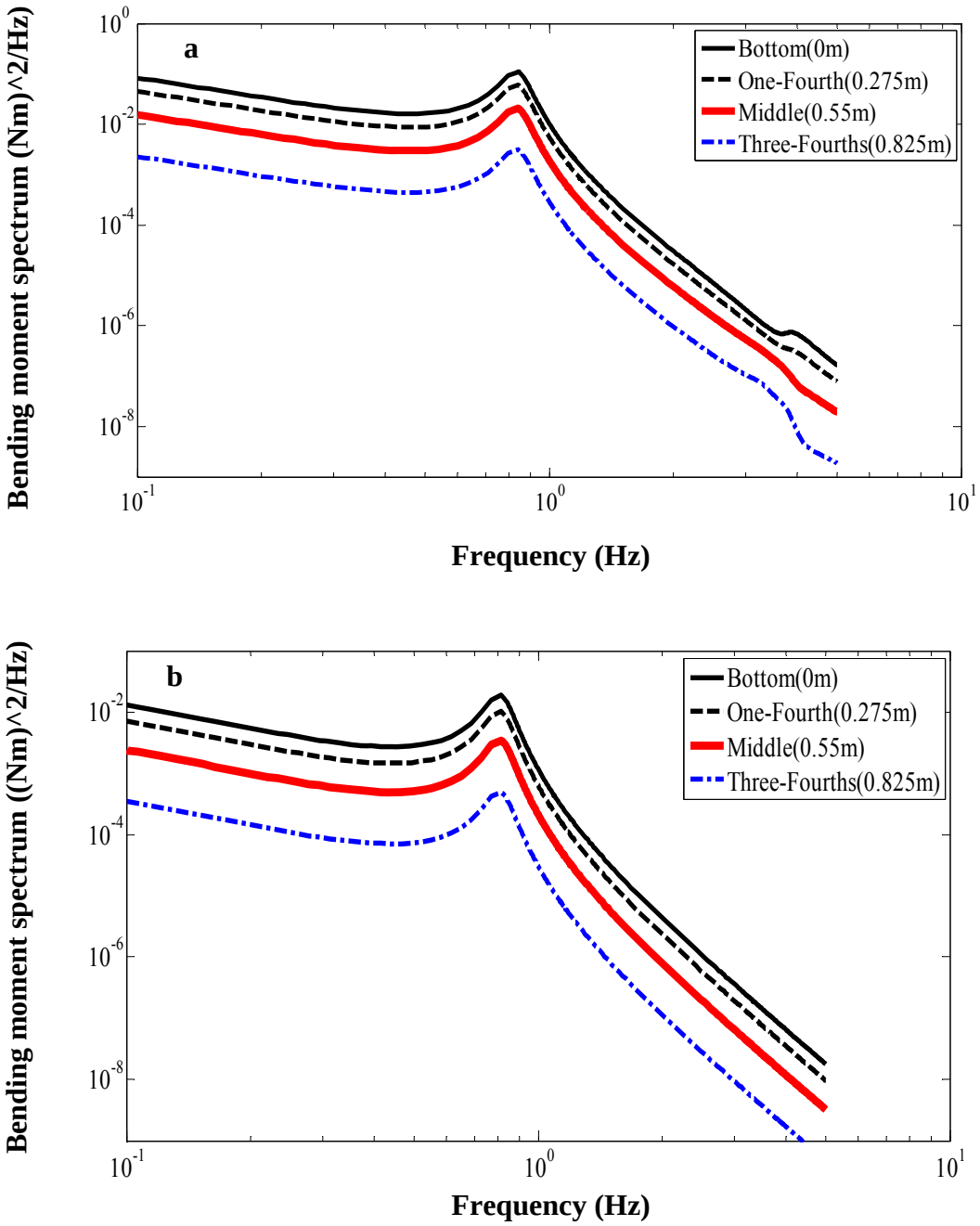

Figure 5.3 Bending moment spectrum along the oat plant height at the mean wind speed of 5m/s. a) the oat model at maturity; b) the simple version.

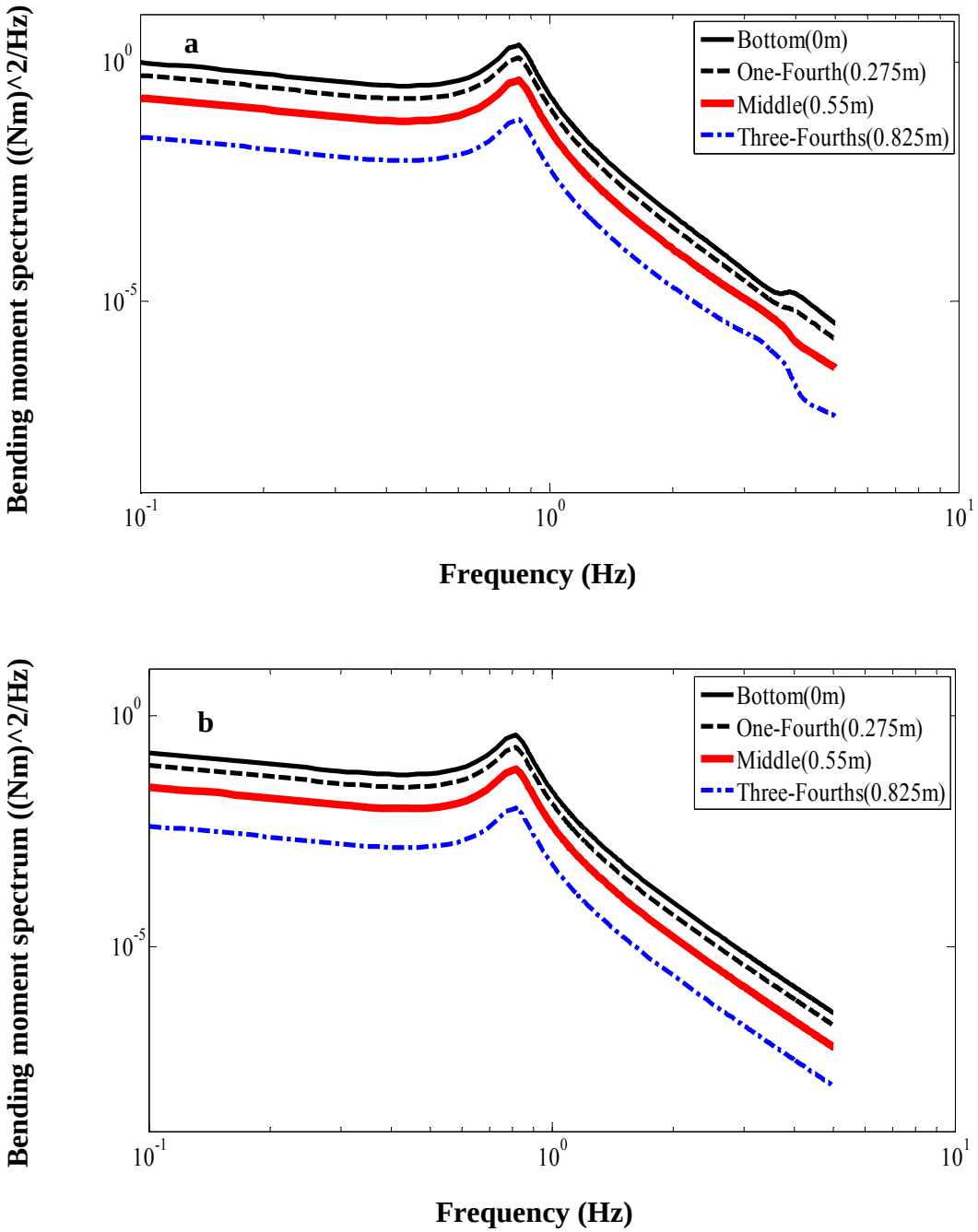

Figure 5.4 Bending moment spectrum along the oat plant height at the mean wind speed of 11m/s. a) the oat model at maturity; b) the simple version.

It is also found the bending moment spectrum of the maturity model (Figure 5.3a and Figure 5.4a) is larger than its simple version (Figure 5.3b and Figure 5.4b) when applying the same wind load. Comparing these two models, the only difference between them lies in that the maturity model has branches while the simple version does not. For the current work, we only identified the effect of the branches for one particular example shown in Chapter 4 (Figure 4.3b), where the branches are symmetrically distributed. It is found that the wind load acting on this model is 2.5 times that of the simple version. Therefore, a modification to the simple version model is produced by increasing the wind loading by 2.5 times.

The bending moment spectrum of the modified simple model that is related to the mean wind speeds of 5m/s and 11m/s are shown in Figure 5.5 and Figure 5.6, respectively. These figures are plotted to compare with the oat model at maturity.

From these figures, it is found that there is an agreement (error less than 5%) between the curves before 1.5 Hz. This, together with the finding that the plant is most likely to lodge when forced to oscillate at its natural frequency (around 0.8 Hz), suggests that the modified simple version can represent the model at maturity to examine the oat lodging with satisfactory accuracy. It also shows that the branches attract more wind loading.

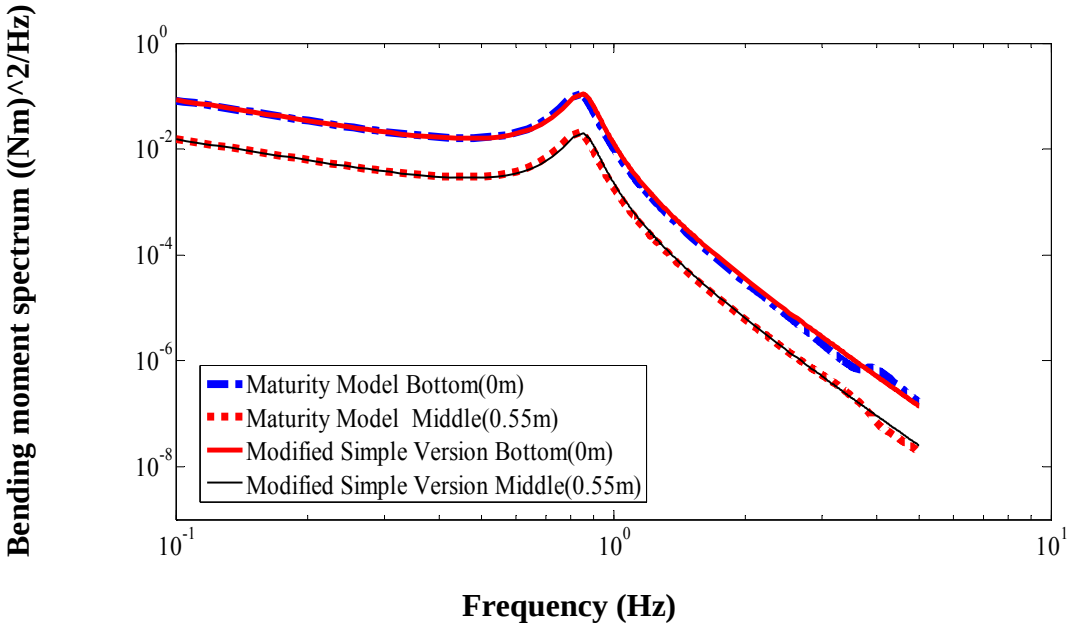

Figure 5.5 Bending moment spectrum of the oat stem at the mean wind speed of 5m/s by comparing the modified simple version with the oat model at maturity

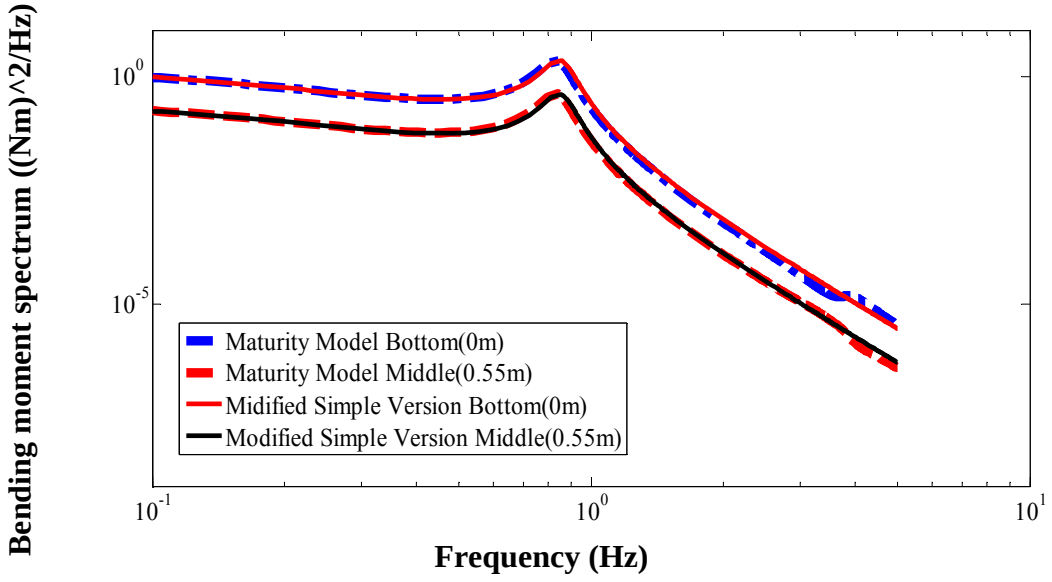

Figure 5.6 Bending moment spectrum of the oat stem at the mean wind speed of 11m/s by comparing the modified simple version with the oat model at maturity

In summary, in this section, it has been identified that the oat plant was most likely to lodge when forced to oscillate at its natural frequency and the plant's base was most susceptible to failure, and. In addition, the wind energy transference to the oat plant was very little above 3Hz due to the cut-off effect of the wind spectrum. Moreover, it was found that the bending moment spectrum of an oat plant at maturity was larger than its simple version, which indicated that the branches increase wind loading on an oat plant.

5.4 The behaviour of an isolated plant in the time domain

Because of the limitation of random response, i.e., steady-state response, the time history of a system's response must be known in order to obtain a deeper insight into the interaction of an isolated oat plant with real wind. Therefore, in this section, the time history responses of an isolated oat plant subjected to natural wind loading are examined.

Using the WAWS method introduced in Chapter 3, the wind fluctuations were simulated. Thirty series of the time history of wind speeds were generated using a Matlab program by the author. The mean speed of these wind fluctuations ranged from 3m/s to 11m/s with an interval of 2m/s, and six load cases for each mean speed were calculated in order to take the random characteristics of wind fluctuations into account. The typical results of the six wind load cases at the mean speed of 5m/s are shown in Figure 5.7 and Figure 5.8. The abscissa represents the time and the y-axis presents the wind speed. The

spectrums of these simulated fluctuant wind are similar with the figure 3.9A.

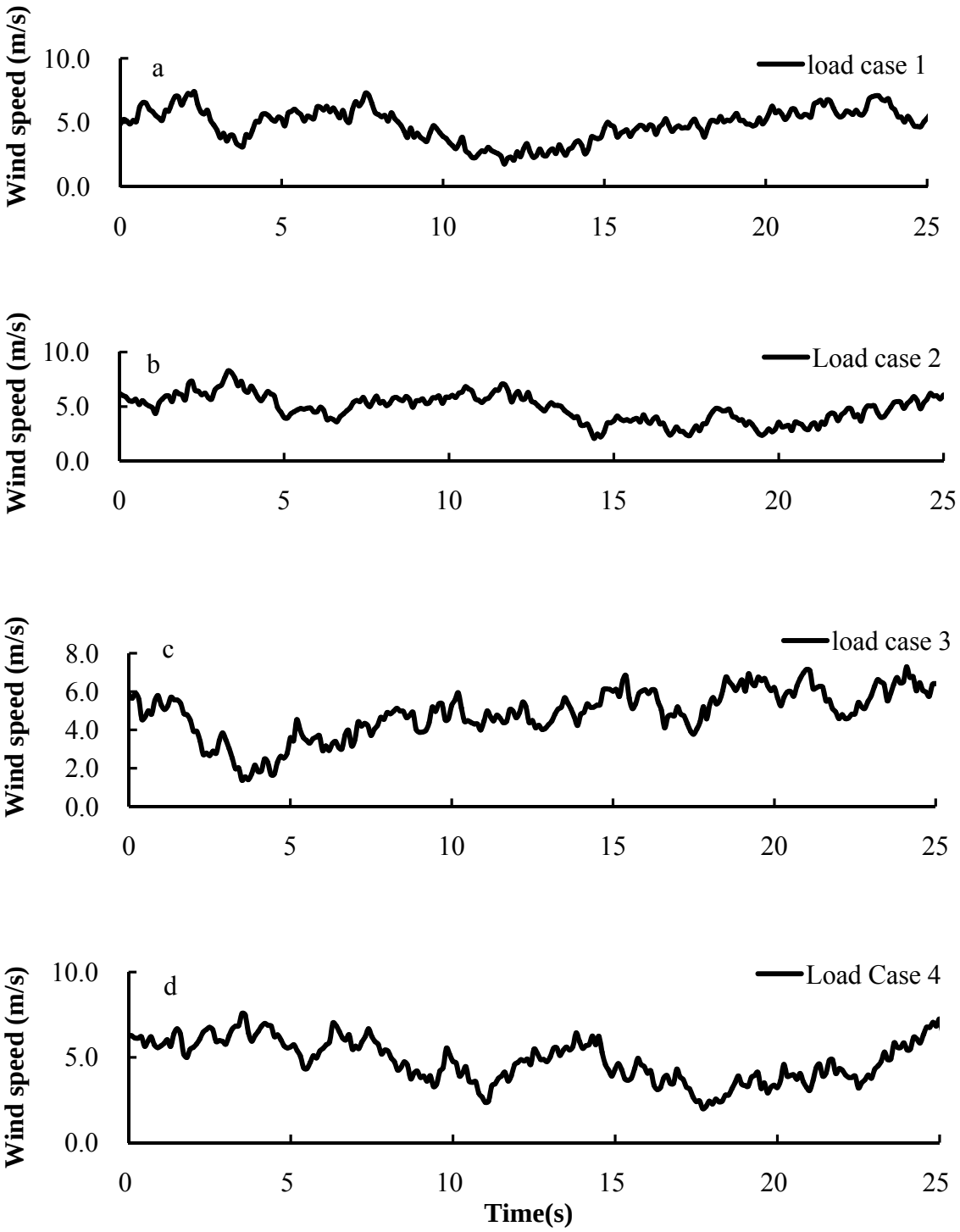

Figure 5.7 Simulated wind speed data against the time at the mean wind speed of 5m/s, a) Load Case 1; b) Load Case 2; c) Load Case 3; d) Load Case 4

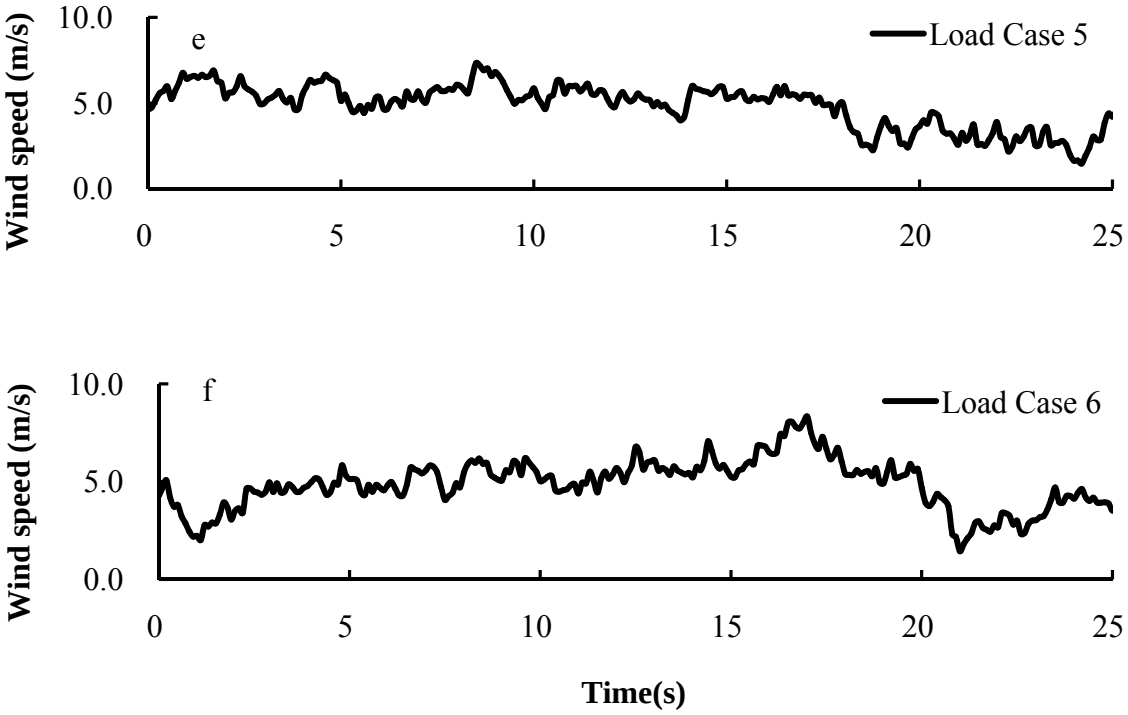

Figure 5.8 Simulated wind speed data against the time at the mean wind speed of 5m/s, e) Load Case 5; f) Load Case 6.

The robustness of the wind loads is then examined by calculating the standard deviation of the wind fluctuations shown in Figure 5.9. The abscissa represents the standard deviation of wind fluctuations, and the y-axis presents the number of cases included.

The standard deviation is calculated using the average of the sum of the wind fluctuations over the number of case studies. It is found that an increase in the number of case studies causes the standard deviations of the average of the sum of these wind load cases to asymptotically reach a fixed value. Agreement on this finding at different mean wind speeds shows that wind database is robust.

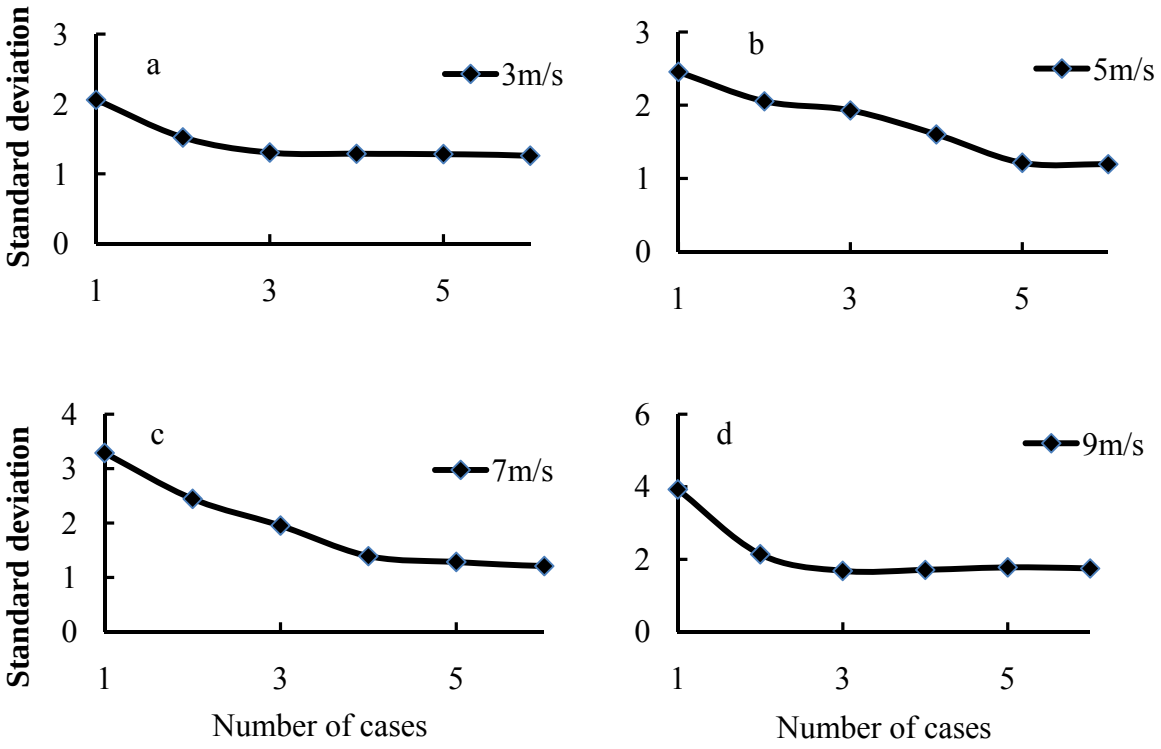

Figure 5.9 The robustness of the wind loads database at the mean wind speeds of a) 3m/s, b) 5m/s, c) 7m/s, d) 9m/s

Second, the isolated oat model is described. In keeping with the previous work, the oat plant at maturity (see Figure 3.4b, Chapter 4) is generated using the ABAQUS software.

The parameters of the oat plant are listed in Table 4.3 and Table 4.4, with an assumption that the stem is a uniform beam because the maximum bending moment of a uniform beam is larger than other tapered beams acted on the same loading (Saunderson *et al.*, 1997). Considering the actual wind force that is relative to the motion of the plant,

the dashpots are adopted to represent the aerodynamic damping. The drag force $F(x, y, z, t)$ acting on the plants is given by：

$$F(x, y, z, t) = 0.5\rho_a A(z) C_D u_r^2(x, y, z, t) \tag{5.3}$$

Where the (x, y, z) are the Cartesian coordinates, ρ_a is the density of air, A(z) is the projected area at height z, C_{D} is the drag coefficient and $u_r(x, y, z, t)$ is the velocity of the plant relative to the wind, which is given by:

$$u_r(x, y, z, t) = u(x, y, z, t) - dx(x, y, z, t)/dt \tag{5.4}$$

where $u(x, y, z, t)$, including the mean wind speed and the turbulent wind, is the longitudinal wind speed at the height z; $dx(\mathrm{x, y, z, t})/\mathrm{dt}$ is the velocity of the oat plant.

5.4.1 The bending moment of an isolated plant

As stated in Chapter 2, the maximum bending moment is our target to evaluate the oat lodging. This section discusses the bending moment of the plants along the plant at different times.

The bending moment of the plant according to different times at the mean wind speed of 5m/s (load case 1) is shown in Figure 5.10 and Figure 5.11. The abscissa represents the distance along the non-dimensional oat plant height, and the y-axis presents the bending moment.

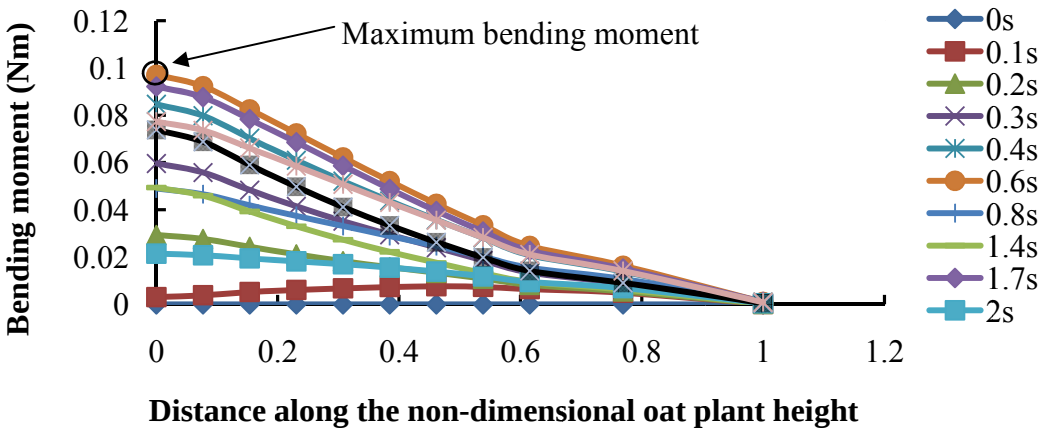

Figure 5.10 Bending moment along the plant at different times when the mean wind speed is 5 m/s

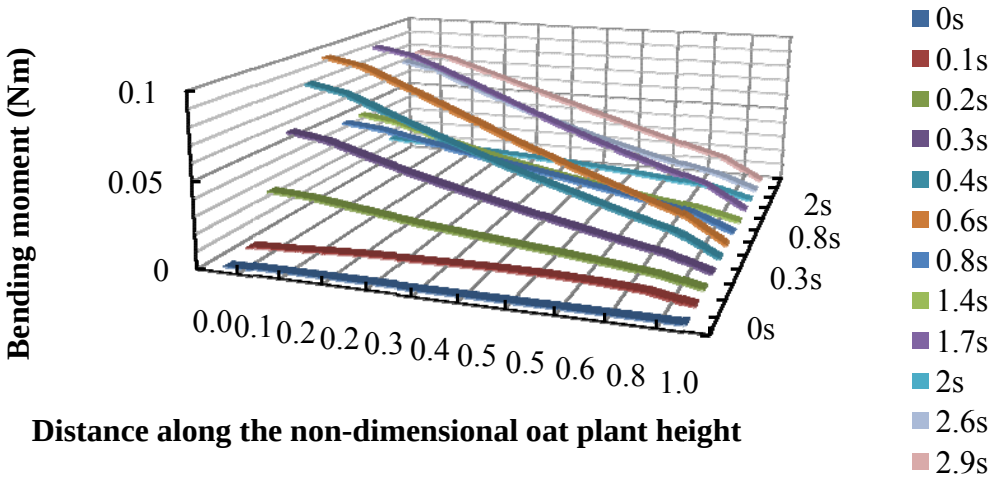

Figure 5.11 3-D plot of bending moment along the non-dimensional plant height at different time when the mean wind speed is 5m/s

The figures show that the bending moment of the plant varies in time and oscillates in a range, between its maximum to its minimum value. The global maximum bending moment occurs at the base of the plant. Because only the maximum bending moments is the target to assess the lodging in oats, the following figures neglect the time information. The results of the bending moment at the mean wind speeds of 7m/s and 9m/s are shown in Figure 5.12. Still, the abscissa represents the distance along the non-dimensional plant height, and the y-axis presents the bending moment.

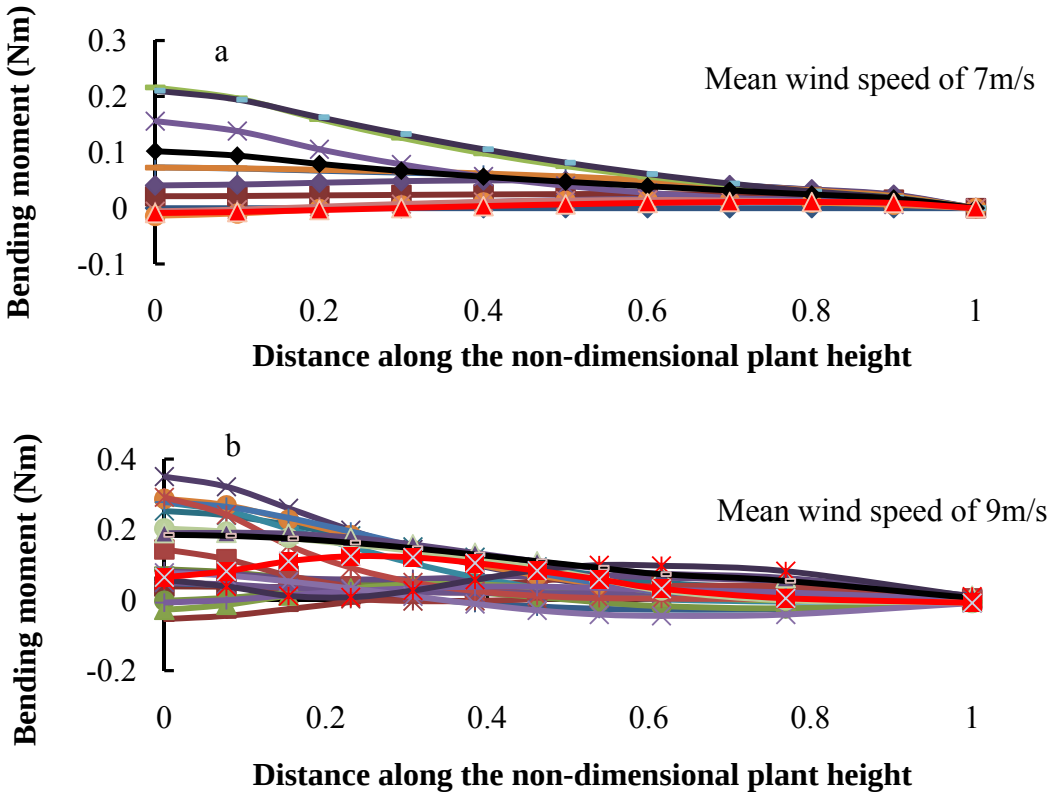

Figure 5.12 Bending moment along the plant, a) at the mean wind speed of 7m/s, b) at the mean wind speed of 9m/s

According to Figure 5.12, it is found that an increase in the mean wind speed increases the maximum bending moment.

Considering the random characteristic, the envelopes of maximum bending moments along the plant according to different mean wind speeds of 3m/s, 5m/s, 7m/s and 11m/s are shown in Figure 5.13. The maximum bending moment are calculated from the average of six load cases for each mean wind speed. The error bar refers to the standard deviation of envelope of maximum bending moment for each of the six load cases.

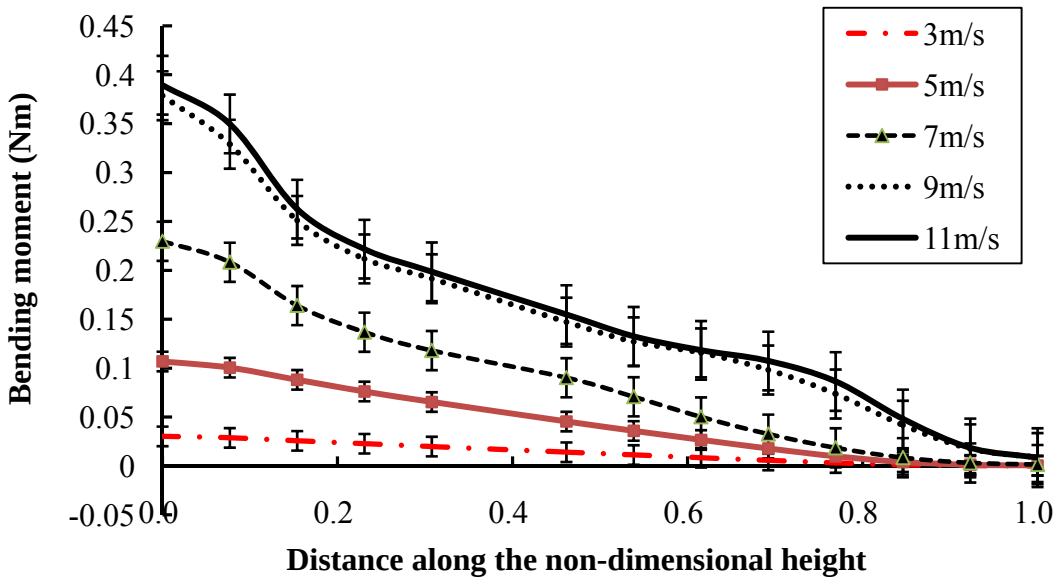

Figure 5.13 The maximum bending moment of the oat plant along the plant according to different mean wind speeds of 3m/s, 5m/s, 7m/s and 11m/s. The error bar refers to the standard deviation.

From Figure 5.13, it can be seen that no matter what the wind speed is, the highest value

of the bending moment appears at the base of the plant. An increase in the wind speed when it is less than 7m/s increases the maximum bending moment; however, beyond 7m/s, the maximum bending moment does not increase much further due to the effect of geometric non-linearity. Please note that an increase in wind speed will lead to an increase in the standard deviation of the bending moment. This is because the results shown in this chapter indicate that an increase in wind speed increase the bending moment, whilst the standard deviation of the wind speed equals to the mean wind speed divided by turbulence intensity (Equation 2.11). If the turbulence intensity is a constant (see Chapter 3, all the simulated wind uses a constant turbulence intensity value of 0.4), an increase in the mean wind speed increases the stand deviation of the wind speed, and the standard deviation of the bending moment also increases.

In summary, this section examined the temporal and spatial distribution of the bending moment of an isolated oat plant subjected to realistic wind loading. The envelopes of maximum bending moments along the plant according to different mean wind speeds were provided, and a nonlinear relationship between the square of the wind speed and the maximum bending moment when the mean wind speed was higher than 7m/s was found.

5.4.2 The deflection of the isolated plant

This section examines the deflection of the plants along the plant at different times. The purpose of this study is to compare the numerical predictions with the wind tunnel

test results and to give a visual representation of the plant's motion.

The deflection along the stem of the plant at various times for the mean wind speed of 3m/s (load case 1) is shown in Figure 5.14.

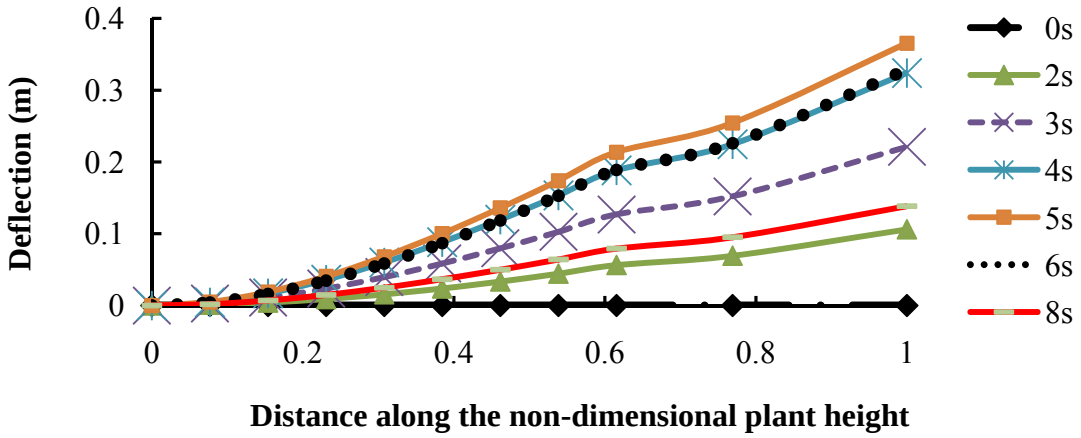

Figure 5.14 Deflection along the plant at various times when the mean wind speed is 3m/s

From the figure it can be seen that the shape of the plant deflection is approximately the same as the first mode shape of the beam. This also shows that the oat plant mainly oscillates its first mode when it is subjected to natural wind. In addition, the deflection of the plant varies with time and oscillates between its maximum deflections to its minimum value. At every time interval, an increase in the distance along the height increases the deflection. The maximum deflection occurs at the top of the plant is identified.

In order to identify the location of the global maximum deflection, the next figure

shown in Figure 5.15 only offers the envelopes of the deflections along the plant according to different wind speeds and neglects the time information.

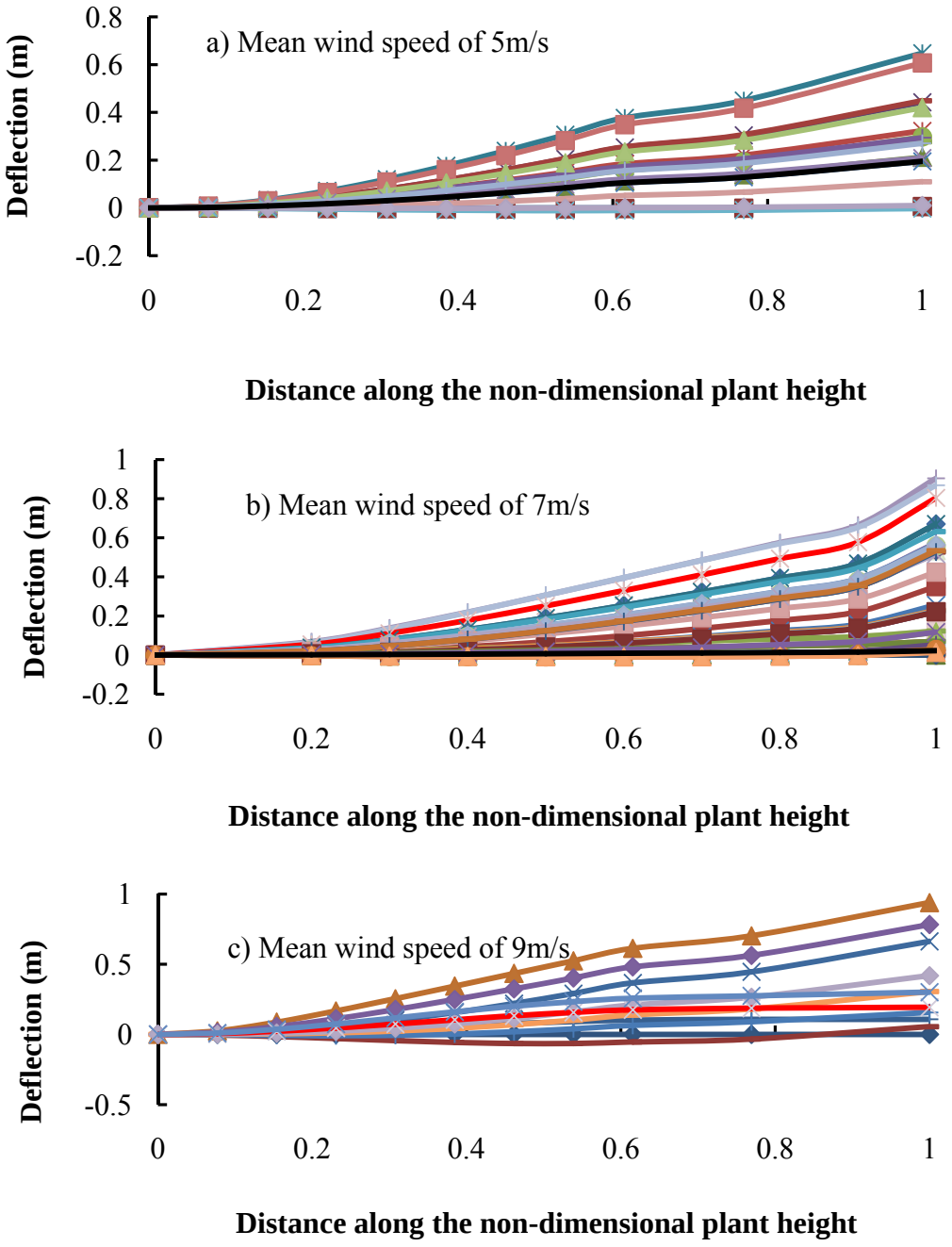

Figure 5.15 Deflections along the plant, a) at the mean wind speed of 5m/s, b) at the mean wind speed of 7m/s, c) at the mean wind speed of 9m/s

It is found that an increase in the mean wind speed increases the maximum deflection of the plant. Also, whatever the wind speed is, the highest value of the deflection appears at the top of the plant.

Second, in order to compare with the wind tunnel test, the mean values of the top deflections are plotted against the non-dimensional square of the wind speed shown in Figure 5.16. The mean values of the top deflection are calculated from the average of six load cases for each mean wind speed. The error bar refers to the standard deviation of top deflection for each of the six load cases.

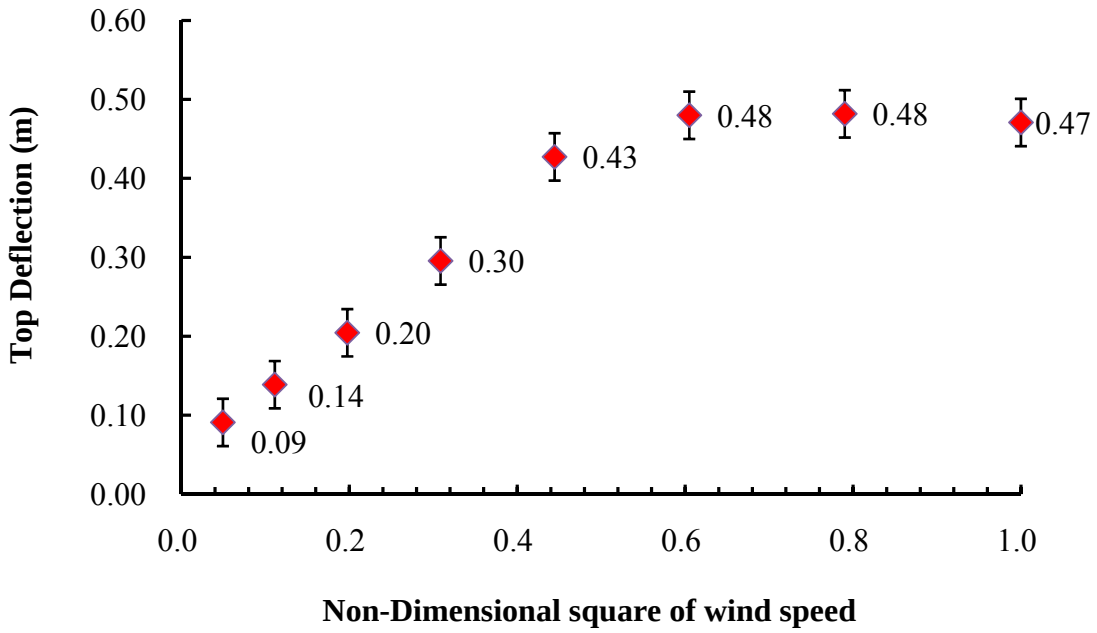

Figure 5.16 The mean values of the top deflections against non-dimensional the square of the wind speed ranging from 2m/s to 9m/s with an interval of 1m/s. The error bar refers to standard deviation of top deflection for each of the six load cases.

Figure 5.16 shows that an increase in the top deflection for the wind speed of less than 6m/s and there is a linear relationship between the square of the wind speed and mean values of the top deflection. However, beyond 6m/s, the top deflections do not increase much further. This illustrates that the relationship between the square of the wind speed and the top deflection is non-linear during the high winds; i.e., the mean wind speed is higher than 6m/s.

In summary, the temporal and spatial distribution of the deflection of an isolated oat plant in real wind conditions has been discussed in this section. It was found that the deflection of the plant varied with time and oscillated between its maximum deflections to its minimum value. Deflection increased along the height and the global maximum deflection occurred at the top of the plant. Also, an increase in the mean wind speed led to an increase in the maximum deflection when the mean wind speed was less than 6m/s, and a linear relationship between the square of the wind speed and the maximum deflection was found. However, the relationship was non-linear when the mean wind speed was higher than 6m/s.

5.4.3 Correlation between the base bending moment and the top deflection

Although the deflection and the bending moment were examined separately in the previous sections, the relationship between them both still needs to be explored. As the global maximum bending appears at the bottom of the oat plant, whilst the global

maximum deflection occurs at the top of the plant, this section examines the correlation between the base bending moment and its corresponding top deflection.

The top deflection and base bending moment at the wind speed of 3m/s are shown in Figure 5.19, whist the corresponding wind speed is shown in Figure 5.20.

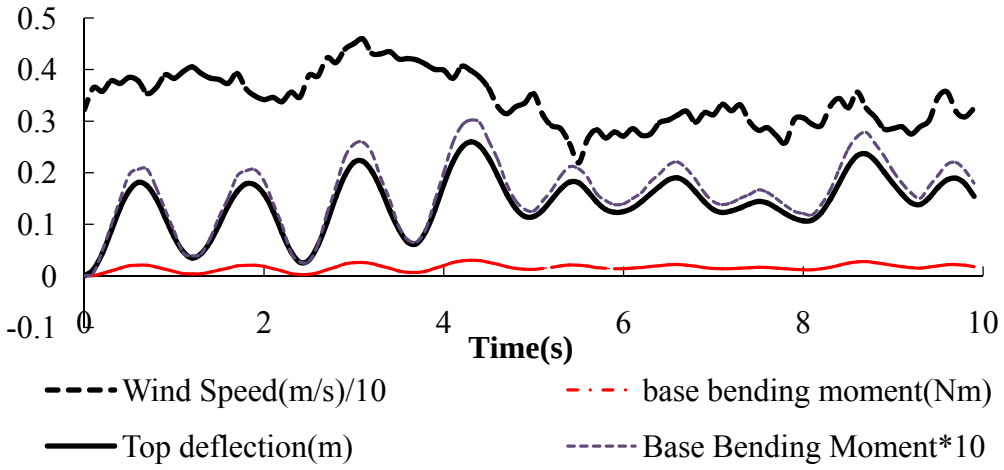

Figure 5.17 Comparison between the base bending moment, the top deflection and the corresponding wind speed

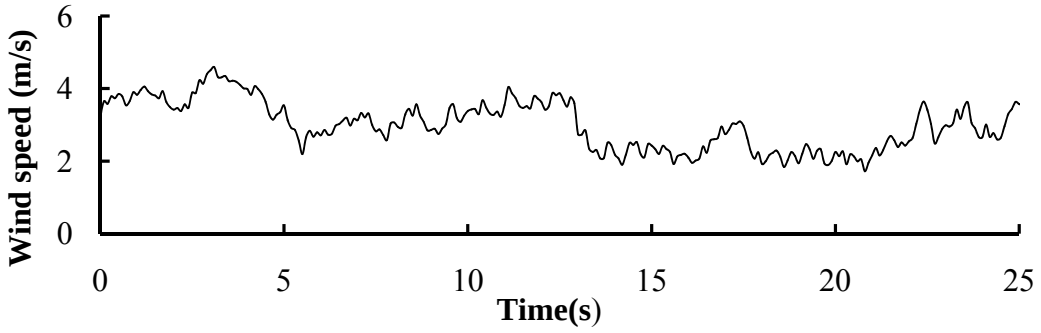

Figure 5.18 The corresponding wind fluctuation at a mean value of 3m/s

From Figure 5.19, it is found that the correlation factor of the top deflection and the bottom bending moment are almost +100%. This indicates that global maximum bending moment synchronously occurs with the appearance of the global maximum deflection. Thus, if either of the two is confirmed, the new proposed lodging model is validated.

5.5 Comparison with the wind tunnel test

In order to validate the model, a wind tunnel experiment was undertaken in the School of Civil Engineering, University of Birmingham in July 2012 (Baker *et al.*, 2012). The introduction to this test is briefly outlined as follows.

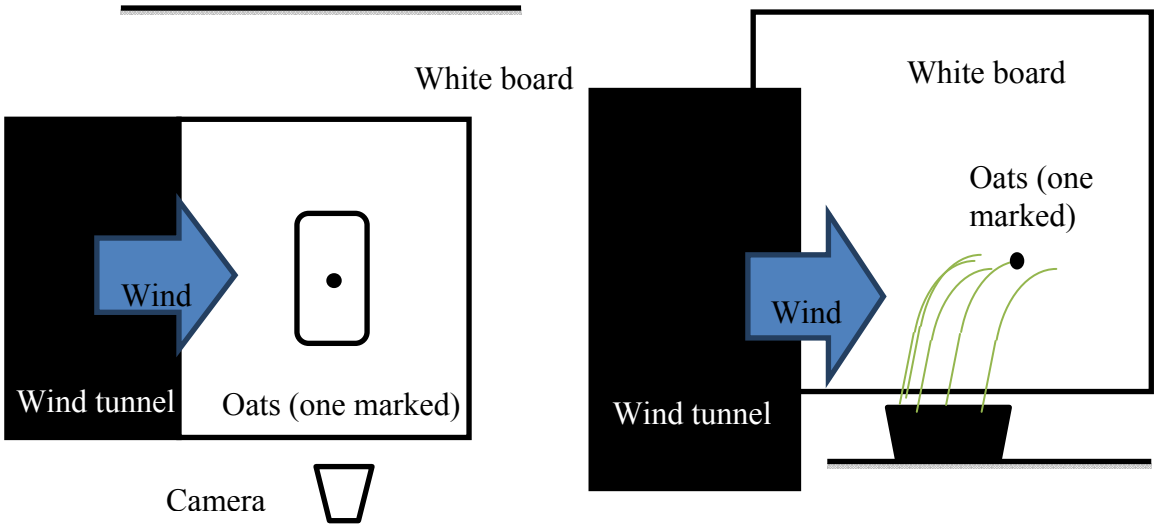

Figure 5.19 Setup for oat testing experiment (Baker et al 2012)

In the test a selection of (potted) oat plants was placed in the wind tunnel. These

plants were put in front of a white board, and a black marker was attached to a high oat plant. A digital camera was positioned in front of the oats, ensuring the plane of the plant motion and wind direction was perpendicular to the camera axis. The setup for the oat testing experiment under the wind force is shown in **Figure 5.19**. The oats were dragged by the wind force and the movement of the target was recorded by a digital video. The videos were edited in order to track the motion of the particle (marked), which was initially at rest, and the mean displacements in both directions were recorded.

Two tests were undertaken. In the first test, the tray of oats laid parallel to the end of the wind tunnel, in the second it laid parallel to the direction of the wind. In both cases, the target oat was near the centre of a 0.25m by 1m tray of oats. The plot of displacement against U^2 (U being wind speed) of both tests is shown in Figure 5.20.

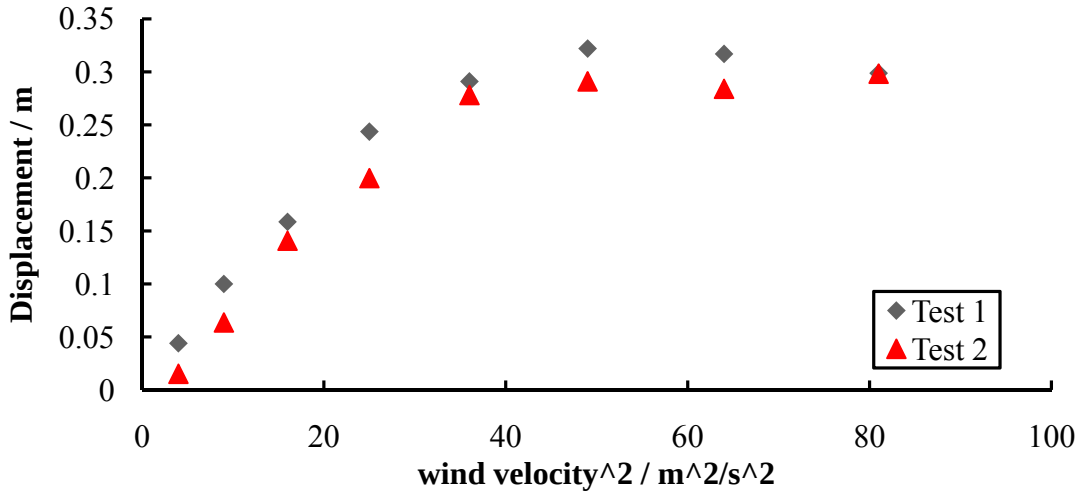

Figure 5.20 Canopy displacements against the square of wind speed for both tests (Baker *et al.*, 2012).

Figure 5.20 shows that at less than approximately 6 metres/second, a linear relationship between the square of windspeed and canopy displacement is found as expected. Beyond this, the deflection of the plant does not increase much further. It is possible that the effects of non-linear characteristics tend to increase with an increase in wind speed, and these effects are significant after 6 metres/second.

To validate the numerical result as well as to determine whether the geometric non-linearity plays a role in governing the motion of the plant by comparing the numerical data to the wind tunnel test result, the non-dimensional mean value of the top deflection against the non-dimensional square of the wind speed compared with the wind tunnel test data is shown in Figure 5.23.

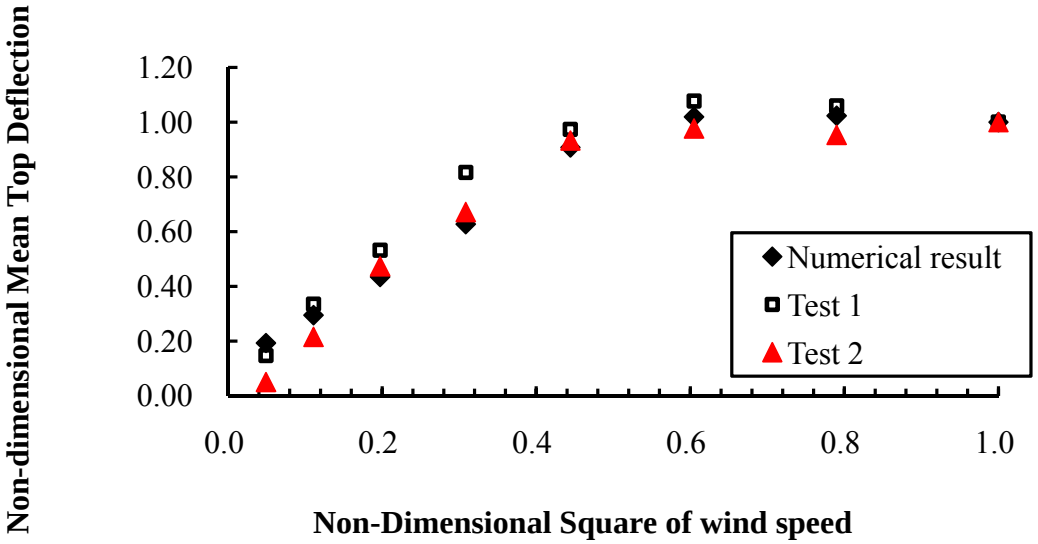

Figure 5.21 The non-dimensional mean value of top deflection against the non-dimensional square of the wind speed compared the numerical results with the test data

The numerical result is calculated using Implicit Dynamics analysis with geometric non-linearity. The RMS difference between the numerical result and the experimental data is calculated using the equation below.

$$\sqrt{\sum_{i=1}^{N}(Simulation_{(i)} - Experiment_{(i)})^2 / N} = \sqrt{\sum_{i=1}^{12}(Simulation_{(i)} - Experiment_{(i)})^2 / 12} = 0.03 \quad (5.5)$$

The agreement (the difference is less than 5%) between the numerical simulations and the wind tunnel test data shows the model is reasonable. It also proves that the influence of the geometric non-linearity of an oat plant is significant after mean wind speed of 6m/s. Thus, the time domain analysis considering the geometric non-linearity is more accurate than previous methods used to assess the motion of the plants as stated in section 5.4.

5.6 Prediction of the failure wind speed

In the previous sections, the dynamic behaviour of an oat plant subjected to realistic wind loading was examined and validated. The maximum bending moments along the oat plant under different wind speeds have been obtained. In this section, the failure wind speed will be estimated.

5.6.1 Measurement of the oat failure moment

The measurements of the oat failure moment are briefly introduced in this section.

The length of the internode was measured from its adjacent nodes, whilst the failure force was measured using a three-point bending test, which supported the two nodes of the internode and applied a force at its mid-point using a digital spring balance pulled at a steady rate. The breaking strength was recorded just before the internode buckled (Berry, et al., 2000). The stem strength (B_S) is calculated from:

$$B_S = \frac{F_S L_{in}}{4} \tag{5.6}$$

Where F_S is the failure force recorded by the digital spring balance, L_{in} is the length of the internode measured by the digital calliper.

A close view of the buckled internode is given in Figure 5.22. The measurement data of the stem strength is shown in Table 5.1.

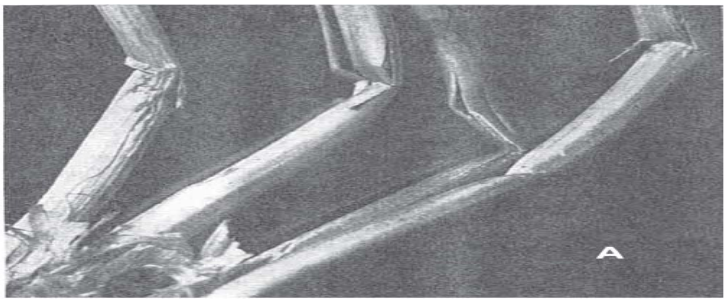

Figure 5.22 A close view of the buckled internodes

Variety	Stem strength of Internode 1 (Nm)	Stem strength of Internode 2 (Nm)	Average Stem strength between Internode 1 and Internode2
00-61	0.43	0.45	0.44
00-61	0.44	0.46	0.45
00-61	0.43	0.43	0.43
Balado	0.48	0.52	0.50
Balado	0.50	0.48	0.49
Balado	0.40	0.42	0.41
Brochan	0.40	0.38	0.39
Brochan	0.32	0.31	0.32
Fusion	0.36	0.39	0.38
Fusion	0.45	0.52	0.49

Fusion	0.41	0.41	0.41
Gerald	0.29	0.25	0.27
Gerald	0.30	0.32	0.31
Gerald	0.24	0.24	0.24
Tardis	0.36	0.32	0.34
Tardis	0.44	0.36	0.40
Tardis	0.25	0.34	0.30
Average	**0.38**	**0.39**	**0.39**
S.D.	**0.08**	**0.08**	**0.08**

Table 5.1 The measurement data of the stem strength. S.D. is the standard deviation.

The anchorage strength was measured on 10 plants per plot. Each individual plant was dug up and the roots were retrieved to a depth of 10cm. The roots were washed and the root plate spread and the depth were measured. The anchorage strength (B_R) is calcu-

lated as:

$$B_R = k_5 s d^3 \tag{5.7}$$

in which k_5 is the coefficient assumed to be a constant. A theoretical value of 3.5, which is given by Crook and Ennos (1993), is used here. *s* is the soil shear strength, and *d* is the root plate spread. The measurement data of the anchorage strength is shown in Table 5.2. The soil shear strength depends on the clay content of the soil (0.25), the water content of the soil (the value of the water content at field capacity is 0.27, and the value of the water content at permanent wilting point is 0.15), the daily rainfall (0.006m), the root depth(62mm) and the visual score (5) for the structure (Baker *et al.*, 1998).

Variety	Anchorage Strength coefficient	Shear strength (Pa)	Root plate spread (mm)	Anchorage Strength (Nm)
00-61	3.5	24985	40.55	0.58
00-61	3.5	24985	42.85	0.69
00-61	3.5	24985	41.2	0.61
Balado	3.5	24985	37.55	0.46
Balado	3.5	24985	43.1	0.70
Balado	3.5	24985	41.35	0.62

Brochan	3.5	24985	40.25	0.57
Brochan	3.5	24985	42.7	0.68
Fusion	3.5	24985	40.8	0.59
Fusion	3.5	24985	38.75	0.51
Fusion	3.5	24985	36.95	0.44
Gerald	3.5	24985	41.35	0.62
Gerald	3.5	24985	51.55	1.20
Gerald	3.5	24985	43.6	0.72
Tardis	3.5	24985	36.75	0.43
Tardis	3.5	24985	37.7	0.47
Tardis	3.5	24985	37.65	0.47
Average	3.5	**24985**	**40.86**	**0.61**
S.D.	**0**	**0**	**3.56**	**0.18**

Table 5.2 The measured data of the anchorage strength. S.D. is the standard deviation.

Considering the shoot (stem) numbers of an oat plant, the critical failure moment of each stem is calculated. The results are shown in Table 5.3. Please note that root lodging occurs on a per plant basis, but stem lodging on a per stem (shoot) basis.

Parameters	Mean Value ± S.D.
Stem failure moment per shoot B_s (Nm)	0.38 ± 0.08
Root failure moment per plant B_R (Nm)	0.61 ± 0.18
Shoot number N	3 ± 0
Critical stem failure moment per shoot B_{Sc} (Nm)	0.38 ± 0.08
Critical anchorage failure per shoot B_{Rc} (Nm)	0.20 ± 0.06

Table 5.3 Critical failure moment of each shoot.

A details about the shoot number N will be listed in Table 5.5.

5.6.2 The failure wind speed predicted by Baker's (1995) model

This section predicts the failure wind speed using the Baker model (see Equation 2.12 in section 2.7, Chapter 2). The failure wind speed can be determined by following the assumption of Baker *et al.* (1998), which is briefly summarised as follows.

- When the bending along the plant per shoot (B) exceeds the critical strength of the stem (B_{Sc}), the stem lodging is expected,

- When the ground cannot hold the oat root during the stem bends ($NB > NB_{Rc} = B_R$, where N is an integer number of average shoots per plant), the root failure occurs.

The measured parameters of the oat plants related to Baker's (1995) model are shown in Table 5.4, and the parameters of the wind properties are shown in Table 4.2. The acceleration due to gravity (g) is assumed to be 9.81 m/s^2, and the plant damping ratio (δ) is 0.081 according to the free vibration test (Section 4.3.4).

Variety	X_{hcg} (mm)	n (Hz)	N
00-61	476.00	0.85	3
00-61	402.70	0.80	3
00-61	471.30	0.90	3
Balado	392.20	1.05	3
Balado	462.40	0.90	2
Balado	430.80	1.02	3
Brochan	490.10	0.77	3
Brochan	576.60	0.82	3
Fusion	361.80	1.07	3
Fusion	389.70	1.08	3
Fusion	437.00	1.12	3
Gerald	552.20	0.71	3

Gerald	544.40	0.71	3
Gerald	584.50	0.70	3
Tardis	529.20	0.80	3
Tardis	491.30	0.79	3
Tardis	555.20	0.73	4
Mean	**479.26**	**0.87**	**3**
S.D.	**69.99**	**0.14**	**0.41**

Table 5.4 The parameters of the oat plants related to the Baker's (1995) model; S.D. is the standard deviation; X_{hcg} is the main shoot's height at the centre of gravity; n is the natural frequency; N is the shoot number, which is a integer.

The stem and root failure wind speeds with regard to different oat varieties predicted by the Baker's model are shown in Table 5.5. Because the root failure wind speed is less than the stem one, the failure mode will be the uprooting failure assuming 6 mm of rain falls every day. The global failure wind speed predicted by Baker's (1995) model is 7.5 $\pm$ 1.3m/s.

Variety	FS1 (m/s)	FS2 (m/s)	FR (m/s)
00-61	10.6	11.8	7.3
00-61	10.9	12.4	7.6
00-61	10.9	11.5	7.5
Balado	12.9	14.5	8.1
Balado	11.7	12.5	9.7
Balado	11.4	12.4	8.6
Brochan	9.8	10.3	6.3
Brochan	8.5	9.0	6.9
Fusion	11.6	13.1	9.5
Fusion	12.6	14.6	8.4
Fusion	11.8	12.5	7.1

Gerald	7.7	7.6	6.8
Gerald	7.9	8.5	9.7
Gerald	6.9	7.2	6.9
Tardis	9.2	9.3	5.9
Tardis	10.4	10.3	6.8
Tardis	7.3	8.8	5.1
Mean	**10.1**	**11.0**	**7.5**
S.D.	**1.9**	**2.3**	**1.3**

Table 5.5 The failure wind speed predicted by the Baker's (1995) model.

FS1, FS2, and FR are the failure wind speed predicted in accordance with the stem strength of the internode 1, the stem strength of the internode 2, and the anchorage strength. S.D. is the standard deviation.

5.6.3 The failure wind speed predicted by the new model

This section predicts the failure wind speed using the new model proposed in Chapter 4.

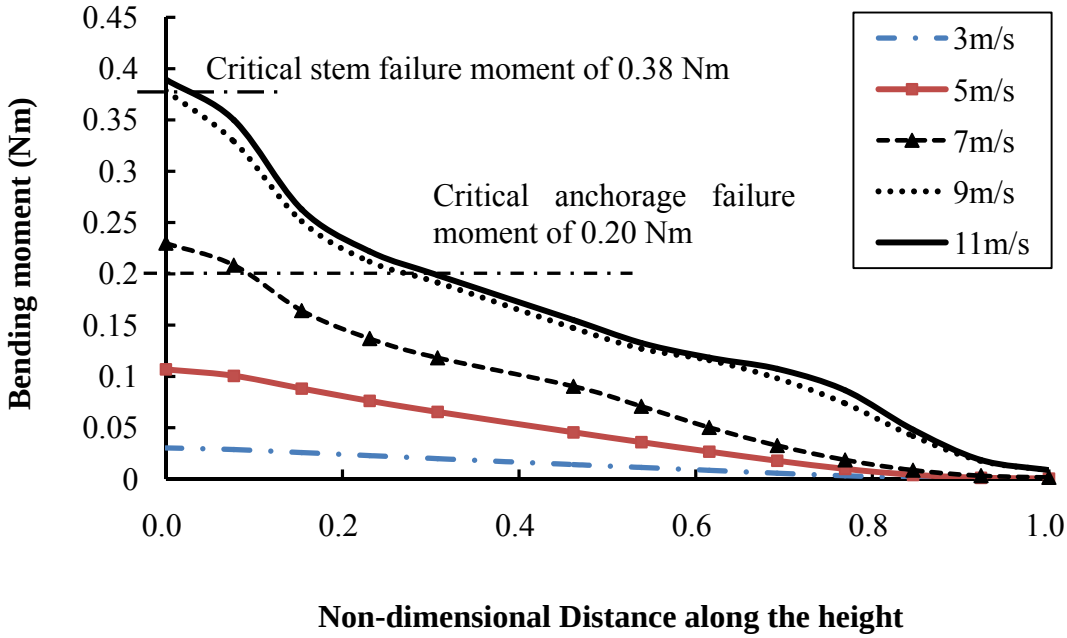

Figure 5.23 The envelope of the maximum bending moment corresponds to different wind speeds of 3m/s, 5m/s, 7m/s, 9m/s and 11m/s, respectively

According to the envelope of the maximum bending moment corresponding to the different wind speeds shown in Figure 5.23 and the critical stem failure moment (0.38Nm) outlined in Table 5.3, the stem failure wind speed is predicted to be between 9m/s and 11m/s. This matches the prediction of the Baker model as it gives the failure wind speeds of 10.1m/s and 11m/s (see Table 5.5).

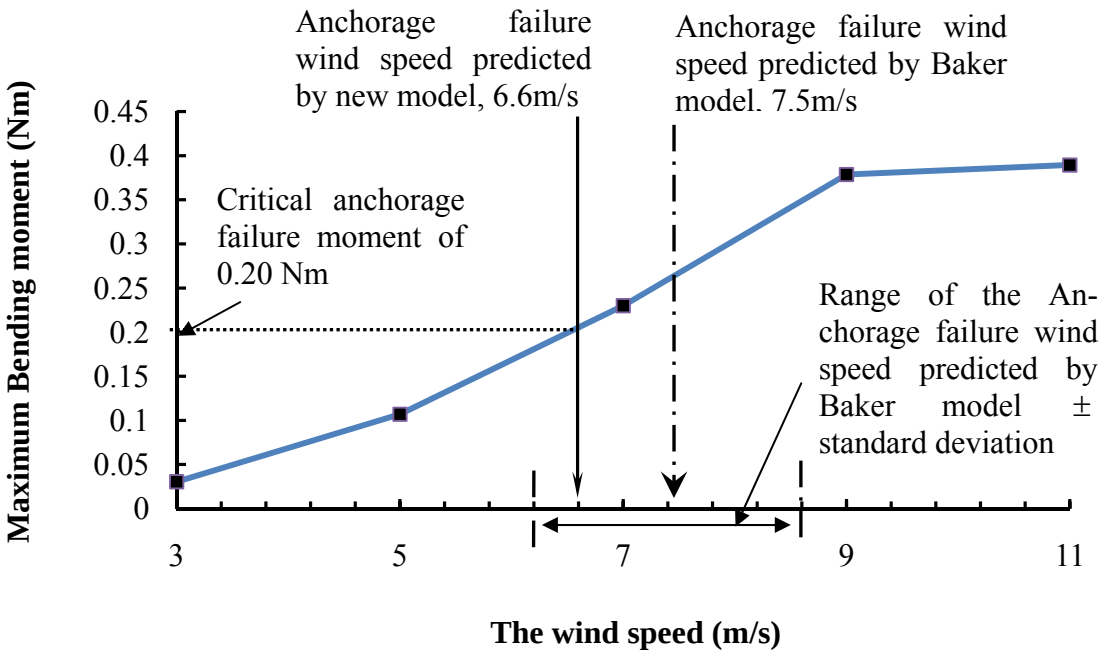

Figure 5.24 The maximum bending moment against the wind speed (m/s)

Figure 5.25 shows the anchorage failure wind speed predicted by the new model. This value is 6.6m/s, which is located in the range of the anchorage failure wind speed predicted by the Baker's (1995) model ± standard deviation. The difference between the anchorage failure wind predicted by the new model and the Baker's (1995) model is -0.9m/s. Because the root failure wind speed is less than the stem failure wind speed, the failure wind speed of the new model is 6.6m/s and the failure mode will be the root lodging. In addition, this failure wind speed is located in the range of the failure wind speed predicted by the Baker model ± standard deviation. This finding matches the prediction of the Baker's model with difference less than 1m/s.

5.7 Parametric analysis

This section explores the sensitivity of the plant response to changes in parameters of the wind and of the plant itself in order to find how wind or plant properties changes influence the plant response. A parametric analysis is undertaken using Implicit Dynamics analysis with geometric non-linearity. The key parameters involved in terms of the wind properties (e.g., the drag coefficient, the projected area, the damping) are listed in Table 5.6, whilst plant parameters involved are outlined in Table 5.7.

Parameter	**Value**	**Sources**
Damping ratio ζ	0.081	MA
Drag coefficient C_D	0.51	WTTEST
Projected area A_{pj} (m^2)	0.009	ADAS

Table 5.6 The wind parameters of an isolated oat plant in winds.

Key to sources: WTTEST, wind tunnel test (Baker *et al.*, 2012); ADAS, data from ADAS Company; MA, data measured by author using free vibration test (Section 4.3.4)

Parameter	Value
Plant height H (m)	1.1
Radius of section at base R_0 (m)	3.5×10^{-3}
Wall width t_w (m)	1×10^{-3}
Tapered parameter β	0.1
Density ρ (Kg/m^3)	600
Young's Modulus E (MPa)	800
Grain weight per node m_g (g)	1

Table 5.7 The plant parameters of an isolated oat plant in winds.

The wind loads are the same series of 6 load cases at the mean wind speed of 5m/s. Each key parameter has been varied by 10% and the results are shown in Table 5.8 and Table 5.9. The RMS values of the top deflection and base bending moment are calculated for each case. Then, the average of these six values is calculated and is compared

to the unchanged corresponding values.

Parameter	Bottom Bending Moment B_b (Nm)		Top Deflection X_t (m)	
	% change in B_b for 10% decrease in parameter	% change in B_b for 10% increase in parameter	% change in X_t for 10% decrease in parameter	% change in X_t for 10% increase in parameter
Drag coefficient C_D	-9	+8	-4	+3
Projected area A_{pj}	-9	+8	-3	+3
Damping ratio ζ	+0.7	-0.7	+0.08	-0.05

Table 5.8 Sensitivity of the response of an isolated oat to changes in wind parameters

The effects of change in the drag coefficient, the projected area and the damping, respectively, are shown in Table 5.8. An increase in the drag coefficient and the projected area increases the value of the bottom bending moment and the top deflection, whilst the damping ratio also influences the value of plant's responses, but its effect is not signifi-

cant.

From table 5.8, it is also found that the effects of the drag coefficient and the projected area are nearly the same. This is because they both are related to the wind force given in Equation (5.19). If they change at the same rate, the change of the wind force is the same. As the plant's response is a function of the wind force identified in the section 4.2.2, the drag coefficient or the projected area play a similar role in the plant motion subjected to wind loading. Furthermore, an increase in damping ratio reduces the amplitude of oscillations and decreases the damping frequency (given by the equation (5.8)). However, 10% increase in the damping cannot significantly change the damping frequency (the change is less than 1%) and the RMS amplitude of plant response.

$$\omega_{dr} = \omega_{nr}\sqrt{1-\zeta_r^2}, \tag{5.8}$$

In which, ω_{dr} is the damped circular frequency; ω_{nr} is the circular frequency; and ζ_r is the damping ratio.

Table 5.9 shows the effect of varying the height, the radius of cross section and the wall width, respectively. A decrease in plant height decreases the value of the top deflection and the bottom bending moment. However, a decrease in the sectional radius increases the top deflection and bottom bending moment. The variation in plant height is most significant, whilst variations in the section radius also produce a large change in the plant motion. Whereas, the wall width and the tapered parameter has insignificant effects on the response of the oat plant subjected to wind.

Parameter	B_b (Nm)		X_t (m)	
	% change in B_b for 10% de-crease in parameter	% change in B_b for 10% in-crease in parameter	% change in X_t for 10% de-crease in parameter	% change in X_t for 10% in-crease in parameter
Plant height H (m)	-35	+31	-33	+29
Radius of section at base R_0 (m)	+10	-10	+12	-13
Wall width t_w (m)	+0.7	-0.7	-0.08	+0.05
Taped parameter β	-0.8	+0.9	-0.1	+0.2
Density ρ (Kg/m^3)	-0.1	-2	-0.1	+0.1
Young's Modulus E (MPa)	-5	+3	+4	-3
Grain weight per node m_g (g)	-0.2	-3	-0.3	+0.3

Table 5.9 Sensitivity of the response of an isolated oat to changes in plant parameters

Table 5.9 also shows the effect of varying density, Young's modulus, and grain weight, respectively. The effects of Young's modulus, density and grain weight are found to have no statistically significant effect (less than 5%) on the motion of an oat plant compared to the plant height and the radius of the section.

5.8 Summary

The current chapter addresses the third objective of the research, that is, to explore the features of an isolated oat plant's response in real wind. The dynamic behavior of an isolated oat plant subjected to natural wind was provided, in terms of both frequency and the time domain. This analysis was realistic and reasonable because the non-dimensional top deflection of an oat plant against the square of the wind speed matched the corresponding measured values from the wind tunnel test. This agreement indicated that this modelling method was suitable to study the interaction of an oat plant with wind.

Other findings of this Chapter could be summarised as follow.

In the frequency domain, it was indicated that the branches would increase the wind loading on an oat plant. Whether the plant has branches or not, and what the wind speed was, it has been identified that the oat plant was most likely to lodge when forced to oscillate at its natural frequency and the plant's base was most susceptible to failure. In addition, the wind energy transference to the oat plant was very little above 3Hz due to the cut-off effect of the aerodynamic admittance function.

In the time domain, it was found that the motion of an isolated oat plant oscillated between its maximum to its minimum value. An increase in wind speed increased the motion of this oat plant when the mean wind speed was less than 7m/s, where a linear relationship between the square of the wind speed and the response of an isolated oat plant was found. However, the relationship between this square of the wind speed and plant response was non-linear during the high winds, i.e., the mean wind speed was higher than 6m/s, where failure wind speed occurred. This implied that the new analysis method, namely the time domain analysis considering the geometric non-linearity, would be more accurate than the previous ones based on the linear assumption. The failure wind speed (6.6m/s) and failure mode (root failure) were predicted using the new method, and the predictions agreed with the Baker's model (Baker, 1995). This new approach also could provide more information regarding the correlation between the instantaneous wind loading and the transient plant's response, so that it could study the important effects that the previous model could not, the fatigue or the dynamic effects on soils for instance.

A parametric investigation into the sensitivity of the plant's response to changes in key parameters was undertaken, which showed that an increase in the drag coefficient and the projected area increased the plant's responses, whilst the effect of the damping was not significant compared to the drag coefficient and the projected area. However, a decrease in plant height decreased the value of the top deflection and the bottom bending moment, and a decrease in the section radius increased the top deflection and bottom bending moment. The variation in plant height is most significant, whilst variations in the section radius also produce a large change in the plant motion. Whereas,

wall width, the density, Young's modulus, tapered parameter and grain weight have insignificant effects (less than 5%) on the response of the oat plant subjected to wind compared to the plant height and the radius of section at plant base.

6 THE DYNAMIC BEHAVIOUR OF A GROUP OF INTERACTING OATS IN REALISTIC WIND LOADING

6.1 Introduction

This chapter outlines a new model that is capable of simulating the interaction of a group of oats to achieve the fourth objective of the research. In this model, a new method that accounts for the dynamic interaction of two nearby plants is proposed. The layout of this chapter is arranged as follows. The introduction to this chapter is provided in Section 6.1. The interaction between the plants is examined in Section 6.2. The percentage of oat lodging in the field is predicted in Section 6.3, which is followed by the summary in Section 6.4.

6.2 The interaction between oat plants

When an oat plant matures and the grains become heavier, the motion of an individual plant will affect its neighbours. In this section, the influence of this interaction between

neighbouring plants on the dynamics of the crop canopy is described to provide a deeper insight into this phenomenon.

The mechanical model of a group of oat plants is proposed in Section 6.2.1. The generation of a model for a group of synthetic oat plants using the ABAQUS software is introduced in Section 6.2.2. Next, the interference damping between the oat crops and connecting nonlinear springs are examined in order to identify the interacting effect. A case study of the dynamic behaviour of the five oat plants in a line is investigated and compared to its corresponding isolated case. Finally, the numerical result is compared with the wind tunnel test results.

6.2.1 The mechanical model of a group of oat plants including plant-plant interaction

This section explains the proposed mechanical model of a group of oat plants. Because the individual oat model has been well established and validated in the previous chapters, this section only focuses on the modelling of the plant-plant interaction.

There have been very few attempts to study this effect (Doare et al, 2004). Doare et al. (2004) was perhaps one of the first to propose linear springs with a gap to model the interaction between two cereal crops, such as alfalfa. The behaviour predicted by his model agreed with the experimental data, which indicated that his model was reasonable. Developed from Doare's work and considered the unique feature of the oat plants, i.e., the two adjacent oat stems connect by the panicles and there is no gap between them, the

nonlinear springs are applied here to model the interaction between two plants. These nonlinear springs are of zero tension and there is a constant compression stiffness when deviating from their equilibrium (Figure 6.1), i.e., when two plants are moving closely, they will push each other, and when the two plants are moving away from each other, there is no interaction between them. The interference damping between oat crops will also be taken into account.

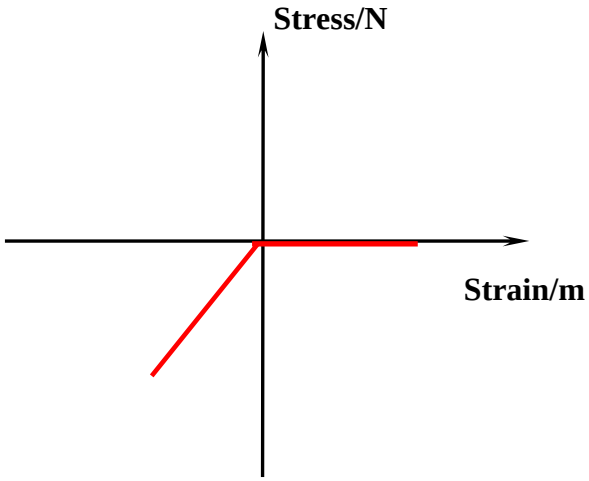

Figure 6.1 The relationship between the strain and stress of the non-linear connecting spring

Considering the simplest situation, i.e., the canopy is viewed as a group of stems in a line along the wind's direction, the individual oat plants, which are spaced at an interval *d* in a line, are connected to their adjacent oats by these springs (see Figure 6.2). According to the oat model at maturity (see Figure 4.3b), two springs are used to model the interac-

tion effect caused by the branches and one spring is adopted to model the interaction at the top of the stem. Thus, three springs are located at the heights of *H*, *H*-*b*/2, and *H*-*b*, where *H* is the height of the oat plant and *b* is the length of the panicle. This is because the branches spread from two whorls located at *H*-*b*/2 and *H*-*b*, which are in accordance with the oat model at maturity (Figure 4.3b). Instead of a rigid rod which is used by Doare (2004) to represent the plant stem, a flexible beam, considering the effect of the geometric nonlinearity, which proved to be significant for lodging, is applied here.

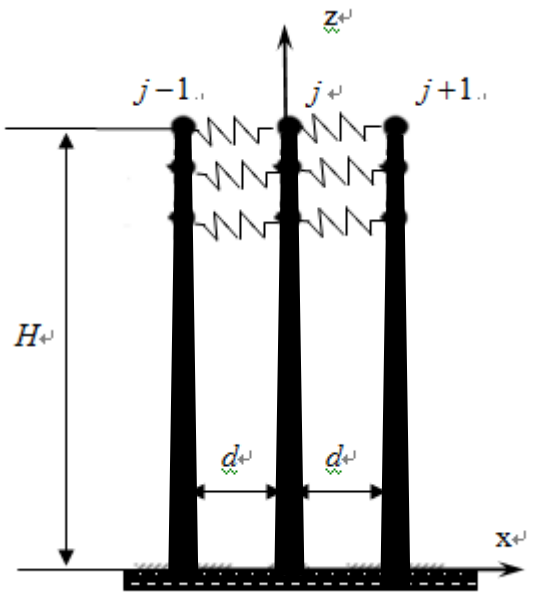

Figure 6.2 A side view of an oat plant connecting with its neighbours in the field

6.2.2 Construction of a group of oat plants

Following the proposed mechanical model of a group of oat plants in the previous section, an example of five interacting oat plants in a row is generated to examine the

effect of the plant-plant interaction. The geometry of the five plants in a line is shown in Figure 6.3.

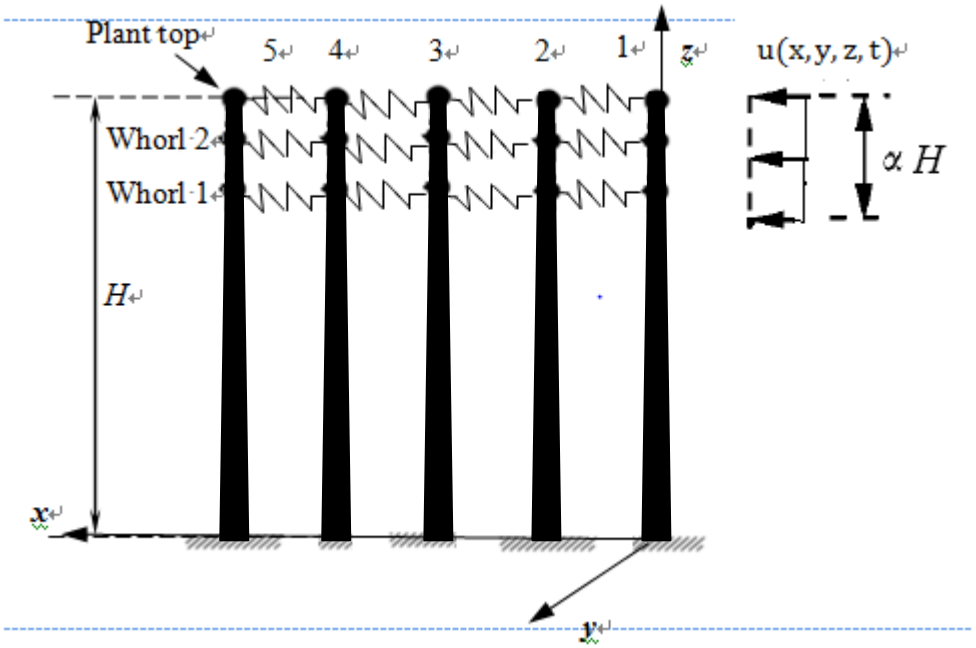

Figure 6.3 The geometry of five plants in line

With the aid of ABAQUS software, beam elements, inertia point masses, non-linear springs and dashpots are adopted to describe the stems, grains, plant-plant interactions and damping, respectively. The main stem is fixed at its base and is divided into 10 elements. The inertia mass is attached to the top of the main beam and to the whorls (see Figure 6.3). The springs are located at the heights of *H*, *H*-*b*/2, and *H*-*b*, where *H* is the height of the oat plant and *b* is the length of the panicle (Figure 6.3).

Parameter	Standard value		
	Case 1	**Case 2**	**Case 3**
Damping ratio	0.08	0.08	0.12
Spring stiffness-closing (N/m)	0	10	10
Spring stiffness-departing (N/m)		0	
Distance between two plants (m)		0.10	

Table 6.1 The standard parameters of five oat plants in line

Case 1: non-interaction; Case 2: Only consider the interaction of the nonlinear springs; Case 3 considers the interaction of the nonlinear springs and interference damping between oat crops.

The dashpots are attached to the nodes where the wind forces act on. The wind direction is parallel to the x axis and the z axis is in a vertical direction (Figure 6.3). Chapter 5 has proved the influence of the geometric non-linearity exists in the motion of an oat plant. Thus, this chapter only examines the dynamic behaviour of oat plants in the time domain and takes the geometric non-linearity into account.

In keeping with the work of the previous chapters, the wind fluctuations were calculated using the WAWS method, ranging from 5m/s to 11m/s with 2m/s intervals. A series of 6 load cases for each mean speed were taken into account because of the random characteristic of the wind loading. Examples of the wind loadings were shown in Section 5.4.

The parameters of the individual oat plant are given in Table 4.3, whilst the distance between two plants and the parameters of plant-plant interaction are shown in Table 6.1, where the parameters are estimated by the measurement. Three case studies are undertaken in order to examine the effect of the plant-plant interaction. Note that, although in reality the interaction between two individual plants may be different, in these cases, the interaction between two plants is assumed to be the same in order to identify the interacting effect.

6.2.3 Interacting effect 1-interference damping between oat crops

In this section, the effect of interference damping between oat crops is examined. The responses of the five oat plants were calculated using Implicit Dynamic analysis with geometric non-linearity. The motions of the five plants in a line of case 2 and case 3 are shown in Figure 6.4 and Figure 6.5, respectively. The corresponding wind fluctuation at the mean speed of 5m/s is shown in Figure 6.6. The abscissa represents the time and the y-axis presents the top deflection.

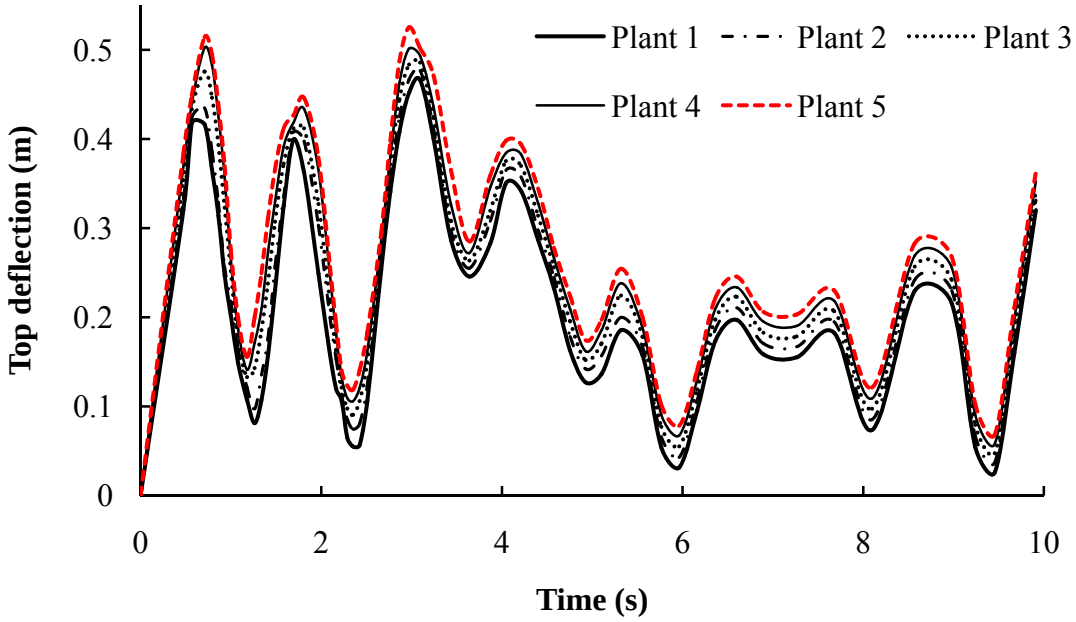

Figure 6.4 The top deflections of the oat plants in a line subjected to wind loading at 5 m/s. The spring stiffness (closing) is 10N/m, and the damping ratio is 0.08.

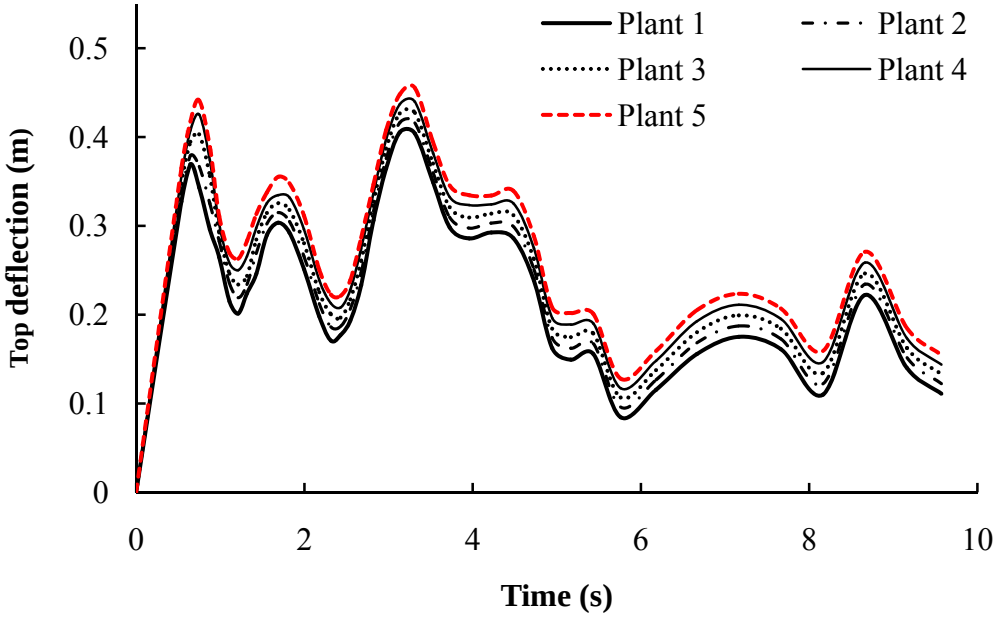

Figure 6.5 The top deflections of the oat plants in a line subjected to wind load at 5 m/s. The spring stiffness (closing) is 10N/m, and the damping ratio is 0.12.

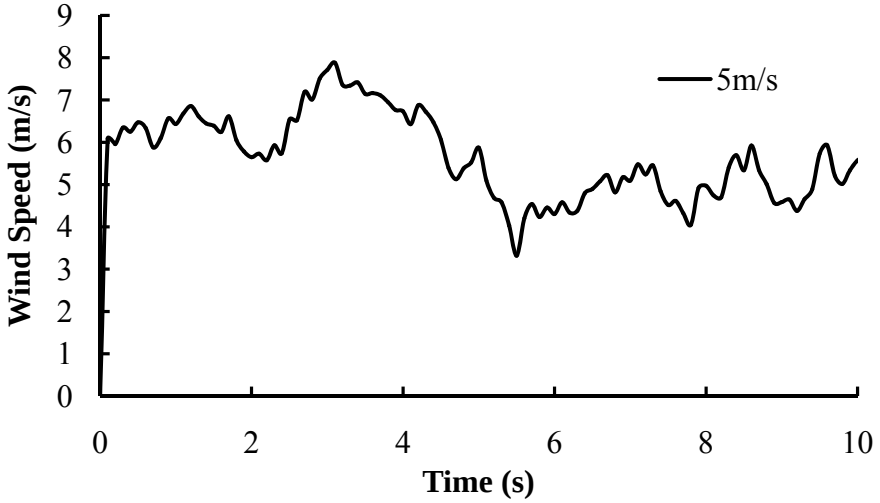

Figure 6.6 The wind fluctuation at a mean value of 5m/s applied to the plants

From Figure 6.4 and Figure 6.5, it is found that the top deflections of the plants increases as there is an increase in the plant order, i.e., the top deflection of the fifth plant is higher than the other plants in a line. This may be because all other plants support the first plant, but apply additional loading to the last plant (the fifth plant in this case). From Figures 6.4 and 6.5 it is also observed that the motions of the five plants are correlated.

In Figure 6.4 the correlation factor of the first plant with the second, the third, the fourth and the fifth plant are 0.998, 0.988, 0.977 and 0.970, respectively. This finding matches the fact that the nearby wind is correlated, where the correlated factor between two wind monitoring stations decreases as the distance between them increases.

Comparing Figure 6.4 to Figure 6.5, it is found that an increase in the damping ratio

decreases the top deflection, and the top deflections of the oat plants in a line tend to follow the wind fluctuation shown in Figure 6.6. The correlation factors between the wind fluctuation and the top deflection of the first oat plant of case 2 and case 3 are 0.56 and 0.64, respectively. An increase in the damping ratio (from 0.08 to 0.12) increases this correlation (from 0.56 to 0.64). Moreover, an increase in the damping ratio also decreases the maximum and mean values of the top deflection (for the first plant, the maximum and mean value of the top deflection decreases from 0.42 to 0.4 and 0.24 to 0.23, respectively), i.e., when the damping ratio is increased by 50%, the maximum and mean value of the top deflection decrease by 4.7% and 2.5%, respectively. Furthermore, comparing Figure 6.4 and Figure 6.5 with Figure 6.6, it is found that an increase in the instantaneous wind speed increases the transient top deflection.

6.2.4 Interacting effect 2-effect of connecting nonlinear springs

The effect of interference damping between oat crops was examined in the last section. This section will identify the nonlinear spring effect. The top deflection of the first plant and its corresponding isolated case are our targets, as it is easy to examine the effect of the nonlinear spring, i.e., the first plant in a row is only influenced by the motion of one nearby plant. The top deflection of the first plant and the corresponding motion of the isolated oat plant are shown in Figure 6.7. These results were calculated using Implicit Dynamics analysis with geometric non-linearity. The corresponding wind fluc-

tuation at the mean speed of 5m/s was given in Figure 6.6.

In Figure 6.7, compared to the values of an isolated plant, a decrease in the top deflection of the first plant is found. The mean deflection decreased from 0.30m to 0.24m. This implies that the connecting springs are likely to decrease the lodging risk in oat plants.

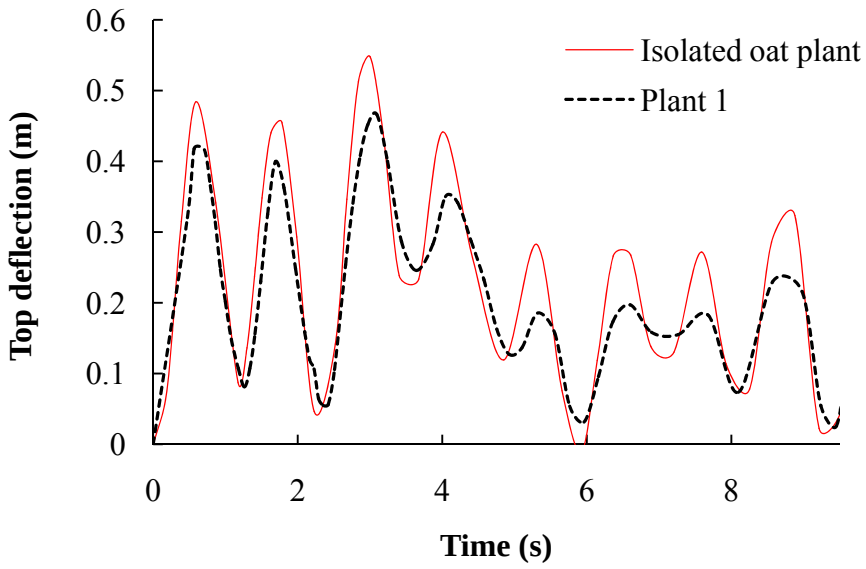

Figure 6.7 The top deflection of the first oat plant in a line and its corresponding isolated plant subjected to wind loading at 5 m/s. The stiffness of spring (closing) is 10N/m, and the damping ratio is 0.08.

To further explore how the values of the stiffness of connecting springs influence the motion of the oat plants, four case studies for the stiffness values of 10N/m, 20N/m,

30N/m and 40N/m, were undertaken. The mean value of the top deflection of the first plant against the square of the wind speeds of 3m/s, 5m/s, 7m/s and 9m/s are shown in Figure 6.8, which shows that an increase in the connecting spring stiffness decreases the top deflection of the first plant. However this change is not significant. The reason for this may be that the properties of the five oat plant models are the same and the correlated wind acting on these nearby oat plants is also approximately the same (Figure 6.9), which means the relative displacement between the two adjacent plants is small and causes a small increase in the interacting force.

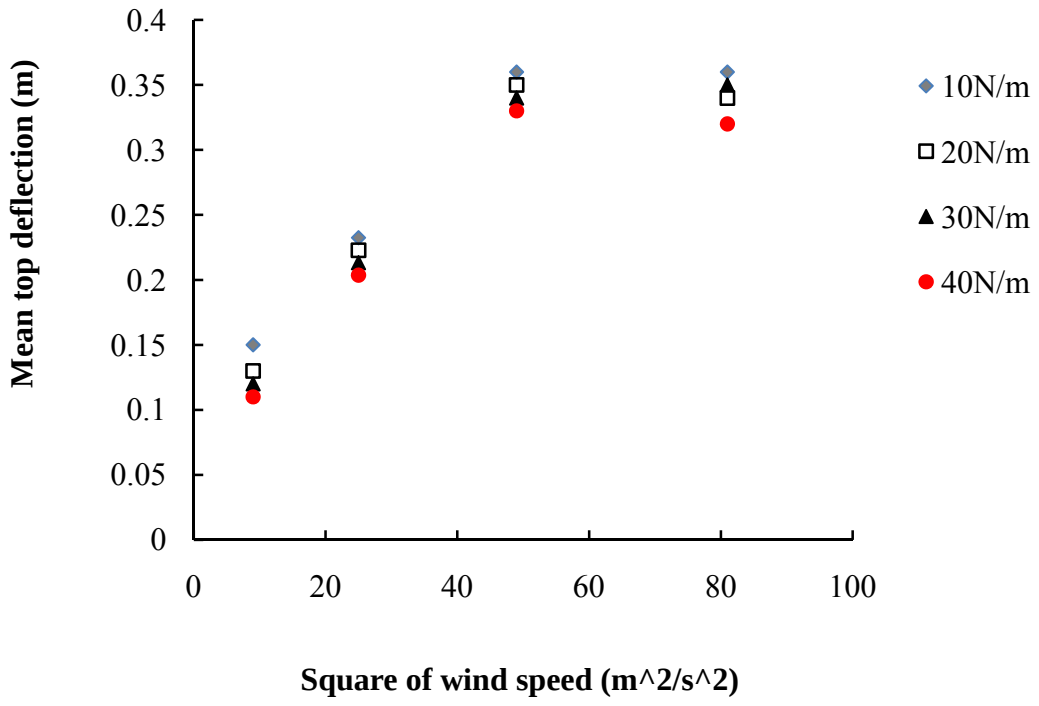

Figure 6.8 The mean top deflection of the first plant against the square of wind speed

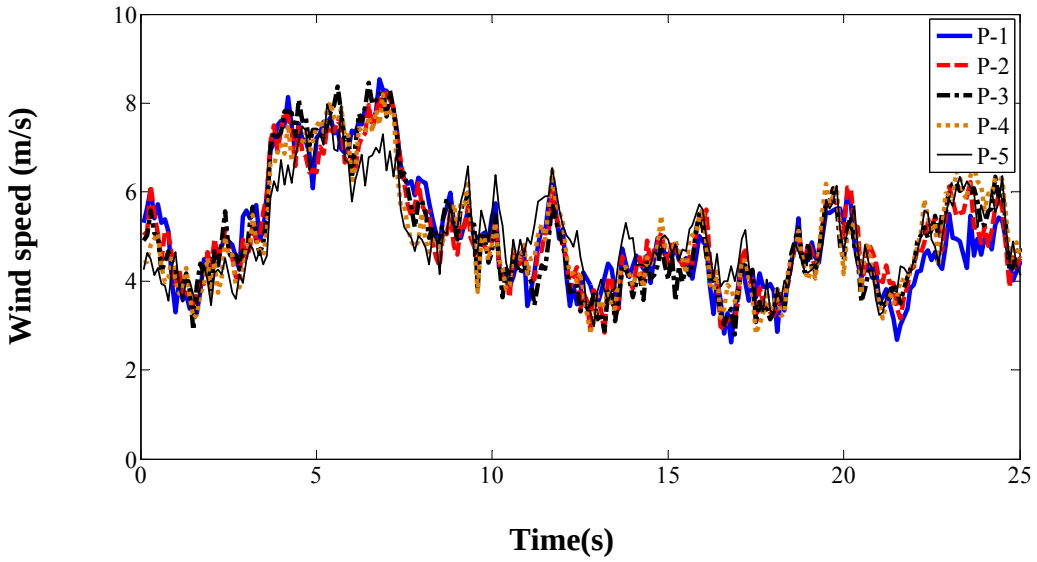

Figure 6.9 Simulated longitudinal wind at $\overline{U}$=5m/s; five monitoring stations are located in a line with an interval of 0.1m in accordance with the distribution of the five oat plants.

6.2.5 Comparison with the wind tunnel test

In the previous sections the interacting effect of an individual plant with its neighbours was examined. In this section the numerical results are compared with the wind tunnel test in order to validate the model of five oat plants in a row. The wind tunnel test was briefly introduced in Section 5.5. Considering stiffness of the connecting springs did not influence the result very much, the model of five oat plants in a line was calibrated by the interference damping between oat crops. The free vibration test of five oat plants in a line gave the damping ratio of 0.12 (Baker *et al.*, 2012). This value was

adopted here. The motion of this model at the wind speed of 5m/s is shown in Figure 6.5.

Compared to the wind tunnel test data, the mean value of the top deflection of the central oat plant (third plant) against the square of the wind speed is plotted in Figure 6.10. This is because the central oat plant was examined in the wind tunnel test.

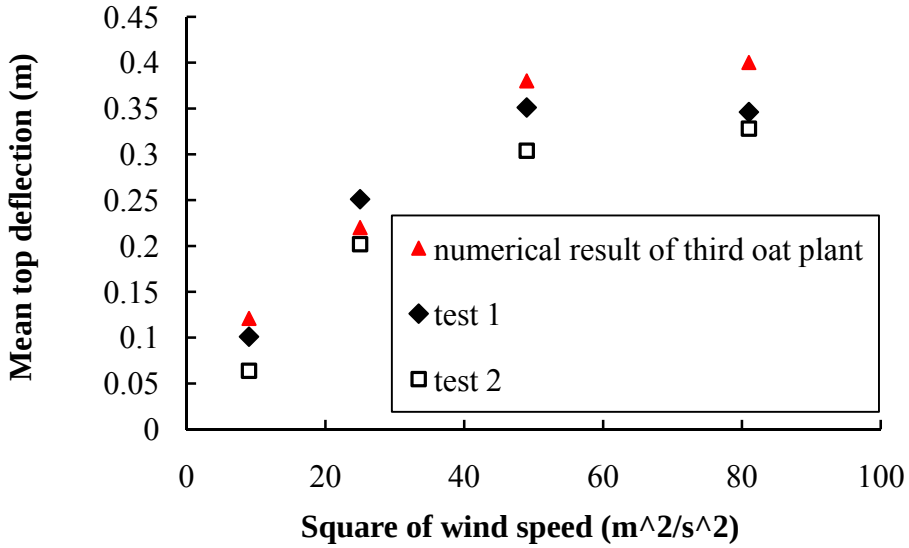

Figure 6.10 The mean value of the top deflection of the third oat plant against the square of the wind speed with a comparison of the wind tunnel test data

The value of the average of the squares of the difference is：

$$\sigma = \sqrt{\sum_{i=1}^{4} (Calculation_{(i)} - Experiment_{(i)})^2} \,/\, 4 = 1.7\% \tag{6.1}$$

The difference between the calculation and the wind tunnel measurement is less than

5% which is within the range of experimental error. This shows the calibrated model is reasonable.

In summary, plant-plant interaction, whose effects include interference damping between oat crops and elastic collisions, was examined in this section. These two types of interaction could decrease the motion of the oat plant. In addition, the motions between the individual plant and its nearby neighbours were correlated in realistic wind loading. It was also found that the motion of an oat plant tended to follow the wind fluctuation, which matched the work of Py, Dupont and their colleagues (Py *et al.*, 2006, Dupont *et al.*, 2010), which showed the movement of a plant and its coherently passing wind flow was correlated. An increase in damping increased the correlation factor between the motion of the plant and the passage of wind was also found.

6.3 The lodging on a large scale

In the previous section, the effect of the plant-plant interaction was examined. Considering this effect, this section assesses the percentage of oat lodging in the field. Before proceeding further, instantaneous images of the wind–plant interactions are provided in Figure 6.11 to allow a qualitative view of the structures of an oat canopy with the passage of coherent wind flow.

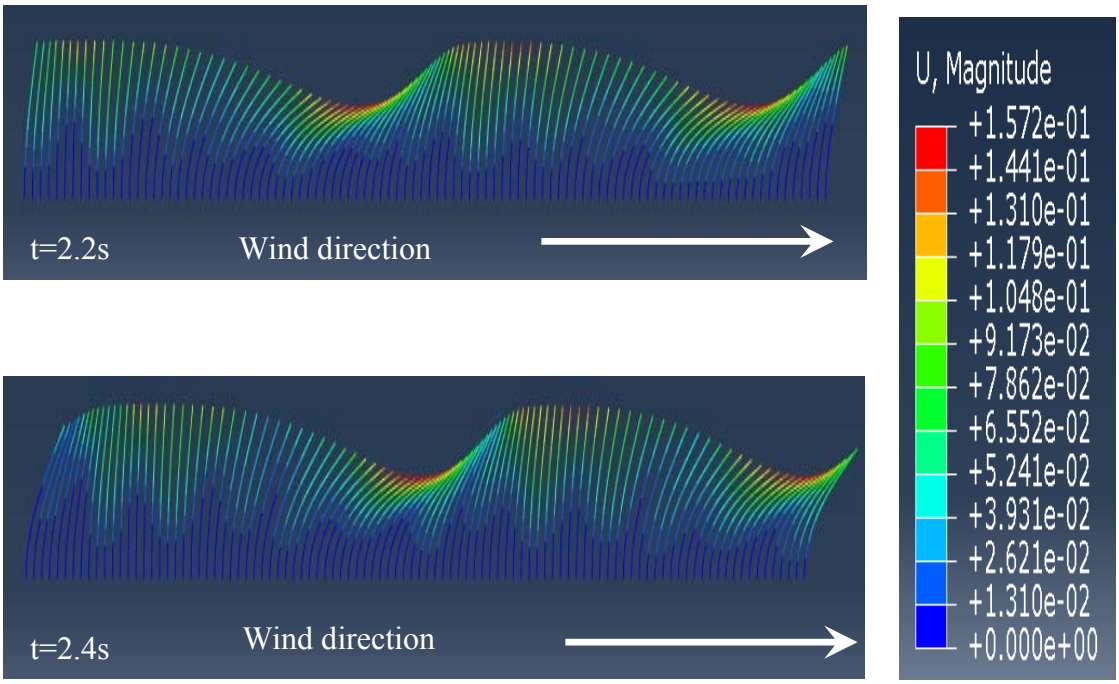

Figure 6.11A qualitative look at the structures of an oat canopy with the passage of coherent gusts. The colour means the deflections of the oat canopy, minimum in blue and maximum in red.

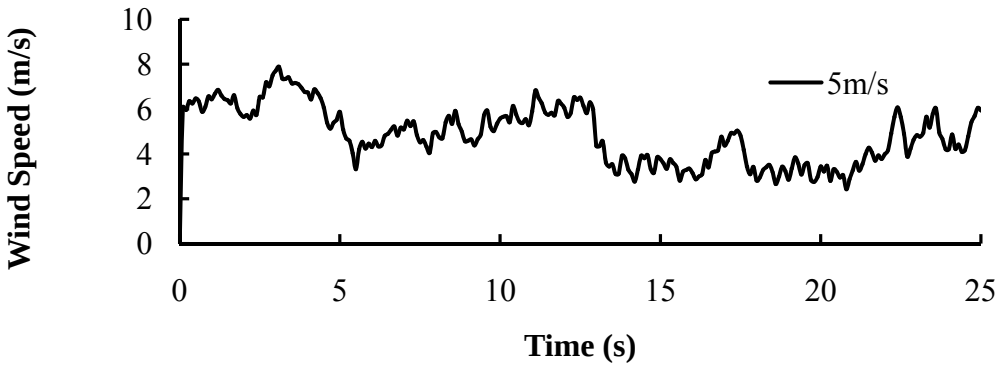

Figure 6.12 The corresponding coherent gusts

Figure 6.11 provides a side view of the structures of an oat canopy (100 oat plants in a

line) over 0.2s. The white arrows show the wind direction and the green stems present the plants' canopy. The corresponding wind gusts at a mean speed of 5m/s was given in Figure 6.12. The coherent structures of an oat canopy with the passage of gusts were observed.

Next a correlated wind field having the appropriate spectral properties was simulated over a 98.01 m^2 area, where 10,000 oat plants were assumed to be uniform distribution (see Figure 6.13). The wind field was generated using the WAWS method, which was detailed in Chapter 3. A hundred series of the time history of spatial correlated wind speeds were calculated using a MATLAB program by the author. These series are located in a horizontal grid of 10×10 stations (i.e. nodes, denoted as $P-l-r$, $l,\ r = 1,\ 2, \ldots,\ 10$). This grid is spaced at 1m intervals within an area of 98.01 m^2 ($d = 1m$, see Figure 6.13) at the height of H. Each wind speed has two components, i.e., longitudinal and lateral winds. The wind direction is parallel to the $\mathbf{x}$ axis (Figure 6.13), while the $\mathbf{y}$ axis is in the lateral direction. The typical results of simulated winds have been examined and discussed in Chapter 3.

Two case studies of the mean wind speeds ranging from 5m/s to 11m/s with an interval of 2m/s were undertaken. At each mean speed, six load series have been taken into account due to the random characteristics of wind fluctuations discussed in Chapter 5.

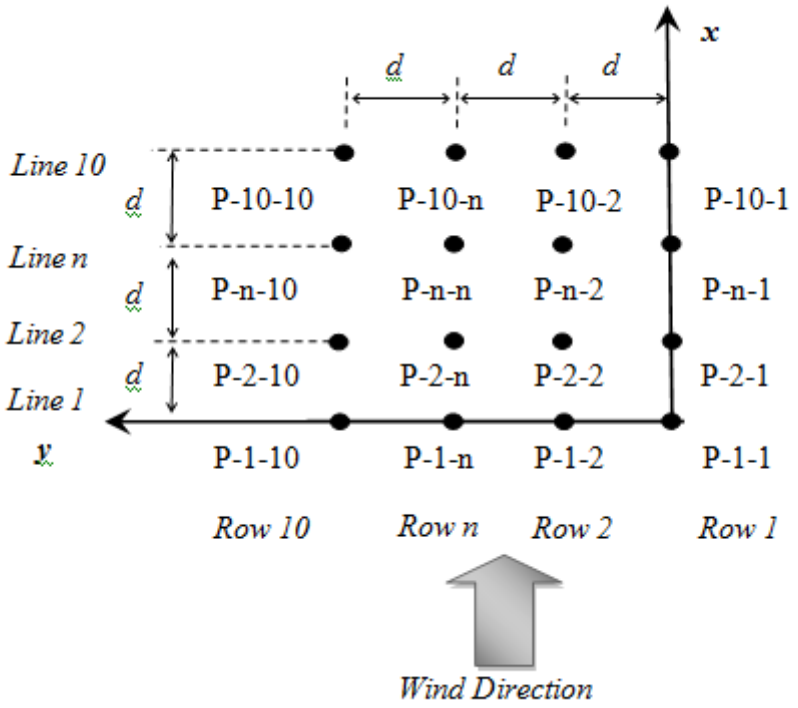

Figure 6.13 Distribution of the wind stations

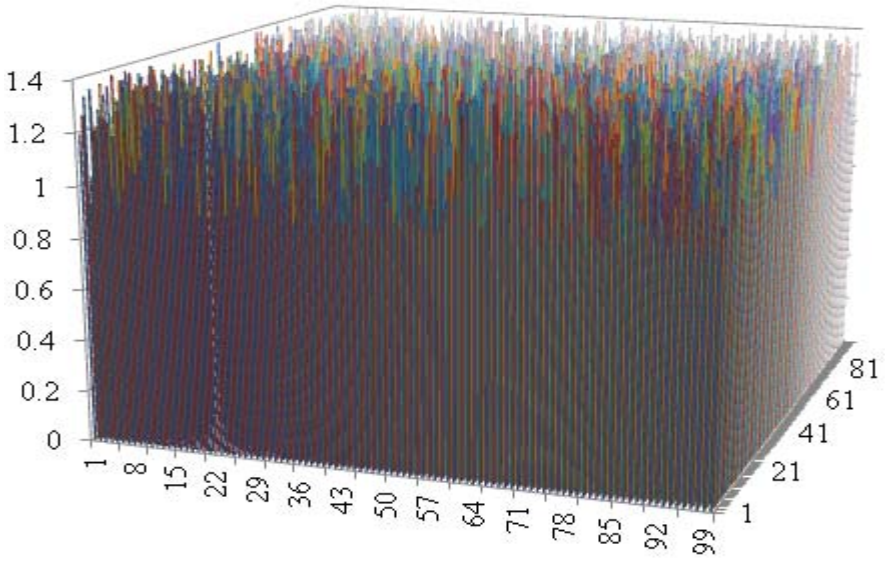

Figure 6.14 Distribution of the oat plants in the field

The oat plant was assumed to act as a cantilever beam with three concentrated masses attached (Figure 6.3). The beam is connected with its surrounding neighbours by non-linear springs, as shown in Figure 6.15. An artificial 100×100 plants located in a horizontal grid of 100×100 points spaced at an interval of 0.1m (Figure 6.14) was generated using the software ABAQUS followed by the work of Martinez-Vazquez and Sterling (2011). Still, the beam elements (B31) and the inertia point masses, and dashpots are adopted to describe the stems, grains and damping. The height of these oat plants was artificially produced using the mean and coefficient of variation shown in Table 4.10, assuming the database is Gaussian distribution. Other parameters of these plants were the standard value shown in Table 4.3. This is because the height was the leading parameter related to oat lodging found in chapter 5.

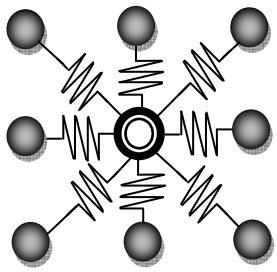

Figure 6.15 An overview of an oat plant connecting with its neighbours in the field

The parameters related to the wind loading are shown in Table 4.2, and the wind force and the movement of the oat plant was coupled via dashpots representing the aerodynamic damping. The resistance of the plant to failure was estimated via comparing root

failure moment and stem failure moment shown in Chapter 5 with the instantaneous bending moment as a result of the motion of the plants subjected to realistic wind loading. The percentage of failures on a large scale determined in this investigation is shown in Table 6.2.

Wind speed	**Percentage of failures**	
	Case 1	Case 2
5 m/s	0%	0%
7 m/s	11%	2%
9 m/s	89%	37%
11 m/s	100%	81%
13 m/s	100%	98%

Table 6.2 The percentage of failures on a large scale; Case 1: Stiffness of the connecting spring is 0N/m, damping ratio is 0.08; Case 2: Stiffness of the connecting spring is 10N/m, damping ratio is 0.12

It was found that the interacting effect decreased the lodging risk of the oat plants. At the wind mean speed of 9m/s, 52% of plants were prevented from damage, when com-

pared to isolated cases.

6.4 Summary

This chapter has completed the final objective of the research. Plant-plant interaction, whose effects include interference damping between oat crops and elastic collisions, was examined. These two types of interaction could decrease the motion of the oat plant, and would prevent the individual oat plant from damage.

In addition, the mean top deflection of third oat plant in a line was examined. These mean values against the square of the wind speed matched the corresponding measured values from the wind tunnel test, which validated the constructed interacting model.

The correlation between the movement of oat plants and the passage of coherent wind gusts was also influenced by plant-plant interaction, and the motions between the individual plant and its nearby neighbours were correlated in real wind.

7 CONCLUSIONS AND FUTURE WORK

This thesis aims to give a better understanding of the interaction of wind with oat plants, ranging from the causes of the vibrations of oat plants to the contribution to lodging in oats, which can reduce yields by up to 40% (Fischer & Quail, 1990). This problem is regarded as a complicated case, involving fluid- structure coupling and nonlinearity characteristics. The weighted amplitude wave superposition method (WAWS) and Finite Element (FE) technique were adopted in accordance with the literature review to study these dynamic behaviours of oat plants under natural wind conditions.

Using the WAWS method, a MATLAB computer programme was written to perform the simulation of a correlated turbulent wind field, i.e., longitudinal and lateral wind fields possessed the spectral characteristics, which achieved the first objective of the research. The work on this aspect was discussed in Chapter 3, where the simulated wind fluctuations agreed with the theoretical (Von Karman) power spectrum, theoretical correlations, and recording wind data above the oat canopy, which guaranteed the simulation could capture and reproduce the effect of the transient natural wind over an oat canopy. This was a major breakthrough in the prediction on the crop lodging because the natural wind is neither constant nor sinusoidal, as was previously assumed (Deodatis, 1996). At the same time, some important effects, for example, the fatigue or the dynamic

effects on soils, that the previous model could not study, could be examined. However, there were still some limitations of the wind field simulations. The experiments showed that there was a vertical transport associated with longitudinal vorticities (Boldes, et al., 2006), which were not considered in the current study. This was because previous attempts proved that lateral flow and longitudinal vorticities were more important to assess the plant failure induced by winds (Raupach et al., 1996; Finnigan, 2000). In addition, lacking in experimental information on the vertical dynamics of the turbulence within the oat canopy, it was hard to supply an adequate vertical turbulence within the oat canopy. As a result, in this thesis, the wind field was simply defined as a 2-D dimension horizontal flow.

Next, in Chapter 4, the second objective of the study was attained**.** Two three-dimensional models corresponding to an isolated oat plant at an early growth stage and at maturity were originally constructed. With the aid of ABAQUS software, the dynamic movements of an isolated oat plant were validated by measured data via free vibration test and analytical predications. These models could consider the variant oat properties (Niklas, 2002); more complex oat morphology and overcome the limitations of the previous model (Baker, 1995; Sterling *et al*., 2003; Berry *et al*., 2003). Compared with the isolated oat model at an early growth stage, oat plants were more likely to lodge when they matured. In addition, the morphology of the isolated oat plant was examined. It was found that the asymmetrical distribution of the panicle did not significantly change the fundamental natural frequency. The effect of the branches and grains was a decrease of the fundamental natural frequency by adding the additional mass. Furthermore, the underlying mechanism of an isolated oat subjected to dynamic loading was explored:

- It was found that the bending moment of the plant was a function of time, natural frequency, damping, external wind loading and position along the plant. The natural frequencies, especially the fundamental natural frequency, played a key role in the plant's damage.

- A parametric investigation into the fundamental natural frequency to changes in the properties of an isolated oat plant, i.e., the height of plant, the radius of cross section, the wall width, the tapered parameter of the stem, the material density, the Young's Modulus, the Poisson's ratio, the parameters of oat branches, and the total grain weight, was undertaken. The analyses showed that the natural frequency was most sensitive to variations in the plant height and the cross sectional radius of the stem, which agreed with the field measurements, and the grain weight, the material density and the Young's Modulus also produced a change in the natural frequency. Whereas, the effects of section wall width, tapered parameter of the stem, Poisson's ratio and parameters of oat branches, i.e. branch numbers, branch length, branch Young's Modulus and radius of branch section were found to have no significant effect on the natural frequency.

- An analytically modified formula regarding the predication of the natural frequency was produced for industrial use. A good agreement between the analytical formula, the numerical result and the field measurement indicated that the formula was promising for application in industry.

In this thesis, an assumption was made that the material of the oat was isotropic (the properties are not dependent on the direction) and homogeneous (the material properties

are the same at each point). This assumption matched our aim to build up a realistic but simple model for use in industry. However, this is not true in reality (Jin, et al., 2009). In order to exploit how heterogeneous or even anisotropic materials influence the motion of the oat plants in wind, the model based on heterogeneous or even anisotropic material properties is worthy of study in the future with a comparison of current material assumption.

Moreover, the third objective of the research, which was to examine the behaviour of oats in winds and model the likelihood of lodging, was achieved in Chapter 5. The dynamic behavior of an isolated oat plant subjected to natural wind was examined in the frequency and in the time domain. In the time domain, the dashpots were originally used to represent the aerodynamic damping that is the wind and oat plant coupling. The results were calculated and were then validated against the data from the wind tunnel test. Next, the likelihood of lodging was also modelled. The failure wind speed was predicted using this model and agreed with Baker's model (Baker, 1995). These two agreements indicated that the modelling method used to study the interaction of an oat plant with wind was suitable. At the same time, the features of the responses of an isolated oat plant in natural wind were explored and can be summarised as follows.

- The branches would increase the wind loading on an oat plant. Whether the plant had branches or not, and what the wind speed was, the highest value of the wind energy transference to the isolated oat crop appeared at the oat plant's fundamental natural frequency. In addition, above 3Hz, the wind energy transference to the oat plant was very little.

- When the mean wind speed was less than 6m/s, the relationship between the square of the wind speed and the response of an isolated oat plant was linear. Thus, an increase in wind speed increased the motion of this oat plant. However, during the high winds, i.e., the mean wind speed was beyond 6m/s, where the failure wind speed was located, the influence of the geometric non-linearity of an oat plant was significant. These results implied this new analysis method, namely the time domain analysis considering the geometric non-linearity, was more accurate than previous ones which are based on the linear assumption.

- A parametric investigation showed that the variation in the plant height was most significant, whilst variations in the drag coefficient, the projected area, and the section radius also produced a large change in the plant motion: An increase in the drag coefficient and the projected area, the plant height increased the value of the top deflection and the bottom bending moment, whilst an increase in the radius of the cross section decreased the top deflection and bottom bending moment.

- It was found that the wind force acting on the oat plant, and the failure moment of the oat crop, including the stem failure moment and root failure moment, were also important parameters for oat lodging.

The main contribution of this Chapter was the consideration of the wind and oat plant coupling and geometric nonlinearity characteristics, which overcame the limitation of the previous models based on the linear assumption. However, although the prediction of the failure wind speed using the new model agreed with Baker's model (Baker, 1995),

there was no experimental data regarding the wind speed and movements of the oat plants at winds which is near to the failure wind speed. Therefore, further work is needed to collect more data on a series of oats at high wind speeds in order to extend the range of results and confirm how oats respond under extreme wind conditions.

Finally, the fourth objective of the research was completed. A new model that was capable of simulating the dynamic interaction of two nearby plants was proposed. The top deflections of five oat crops were examined. These crops were uniformly distributed in a line. The mean values of the top deflections against the square of the wind speed matched the corresponding measured values from the wind tunnel test, which validated the constructed interacting model. The key findings of this chapter could be listed as follows.

- Plant-plant interaction, whose effects include interference damping between oat crops and elastic collisions, could prevent the individual oat plant from damage.

- The correlation between the movement of oat plants and the passage of a coherent wind gust was also influenced by plant-plant interaction, and the motions between the individual plant and its nearby neighbours were correlated in real wind.

One of the limitations at this stage was the oat plants were assumed to be uniformly distributed in the field in order to take the simplest situation into account. However, in reality, the oat plants are randomly distributed. Therefore, based on the current model, one of the possibilities for further work is to exam how a random distribution of oat plants

affects the lodging of oats.

In summary, the main contribution of this project was to present a new approach which forecasts lodging in oats. It was found that the natural frequency, which was most sensitive to variations in the plant height, had a key influence on lodging in oats, whilst the drag coefficient and the projected area also largely affected the movement of an oat plant. The motion of an oat plant was correlated with its neighbours, and influenced by the effect of the geometric non-linearity. This led to a new analysis method, which was more accurate (roughly 10%) than previous alternatives based on the linear assumption. However, this research is an early attempt to explore the interaction between the oat plants and real wind conditions. Based on this research, future work has been identified to give a deeper understanding of this interesting phenomenon, namely the dynamic behaviours of oats in natural wind. The future work linking to the objectives can be briefly summarised as follows.

1) Future field experiments are needed to supply an adequate vertical turbulent field within the oat canopy in order to update understanding about the three-dimensional turbulent flow pattern in and above the plant canopy.

2) Future work also includes the comparison of heterogeneous or even anisotropic material properties with the current material assumption, namely heterogeneous and isotropic material.

3) Further work is needed to collect a series of oats' motions at high wind speeds in order to extend the range of results and to confirm how oats respond

under extreme wind conditions.

4) Based on the current model, it is worth studying how the random distribution of oat plants affects lodging in the future in order to give a more realistic view.

5) It is need to test model in field conditions in order to provide a more realistic view that how this model can use in industry.

Through this study, the **oat plant breeders** will benefit through the development of new oat varieties. Oat varieties with lower height and larger stem radius should be bred in order to increase the lodging resistance. The **farmers** will benefit by ensuring the commercial sustainability of the appropriate oat varieties that will allow them to reduce economic losses. The **plant growth regulator manufacturers** will benefit from reduced environmental impact of production and enable the industries to better avoid the requirements of lodging in oats.

The method developed was not limited to oat crops but could be extended to other plants subjected to wind such as trees and other cereal crops.

8 REFERENCE LIST

Agriculture, forestry & fisheries (online) (2010) Oats Production guideline. [online]. Available from http://www.nda.agric.za/docs/Brochures/Oats.pdf [Accessed 19 Jan. 2013].

Azad, R.S. (1993) **The Atmospheric Boundary Layer for Engineers**, Dordrecht; Boston; London: Kluwer Academic Publishers.

Baines, G.B.K. (1972) Turbulence in a wheat crop. **Agricultural Meteorology**, 10: 93-105.

Baker C.J. (1995) The development of a theoretical model for the windthrow of plants. **Journal of Theoretical Biology**, 175: 355-372.

Baker, C.J., Berry P.M., Spink , J.H., Sylvester-Bradley, R., Griffin J., Scott R.K. and Clare R. (1998) A method for the assessment of the risk of wheat lodging. **Journal of Theoretical Biology**, 194: 587-603.

Belcher, S.E. and Hunt, J.C.R. (1998) Turbulent flow over hills and waves. **Annual Review of Fluid Mechanics**, 30: 507-538.

Berry, P.M., Griffin, J.M., Sylvester-Bradley, R., Scott, R.K., Spink, J.H., Baker, C.J., and Clare, R.W. (2000) Controlling plant form through husbandry to minimise lodging in wheat. **Field Crops Research**, 67: 59-81.

Berry, P.M., Sterling, M., Baker, C.J., Spink, J.H. and Sparkes, D.L.(2003) A calibrated model of wheat lodging compared with field measurements. **Agricultural and Forest Meteorology**, 119: 167-180.

Berry, P.M., Sterling, M., Spink, J.H., Baker, C.J., Sylvester-Bradley, R., Mooney, S.J., et al. (2004) Understanding the reducing lodging in cereals. **Advances in Agronomy**, 84: 217-271.

Berry, P.M., Berry, S.T. and Spink, J.H. (2008). Identification of genetic markers for lodging resistance in wheat. Final report for LINK Project LK0958. Defra, London, 184.

Berthier, S., Stokes, A. (2005) Phototropic response induced by wind loading in maritime pine seedlings (Pinus pinaster Aït). **Journal of Experimental Botany**, 56 (413): 851-856.

Blackburn, P., Miller, K.F., Petty J.A. (1998) An assessment of the static and dynamic factors involved in windthrow. **Forestry**, 61: 29-43.

Böhm, M., Finnigan, J.J. and Raupach, M.R. (2000) Dispersive fluxes and canopy flows: Just how important are they? In: **Proc 24th AMS (American Meteorological Society) conf. On Agricultural and Forest Met**. 14-18 August 2000, University of California, Davis, CA, pp, 106-107

Byers, H.R. (1959) **General Meteorology**, 3rd ed., N.Y. : Magraw-Hill.

Carassale, L. and Solari, G. (2006) Monte Carlo simulation of wind velocity fields on complex structures. **Journal of Wind Engineering and Industrial Aerodynamics**, 94: 323-339.

Carlson, G.E. (1998) Spectra of discrete-time signals. **Signal and Linear System Analysis**, 2nd Ed., New York: John Wiley&Sons.

Cionco, R.M. (1972) A wind-profile index for canopy flow. **Boundary Layer Meteorology**, 3 (2): 255-263.

Cilas, C., Costes, E., Milet, J., Legnate, H., Gnagne, M., and Clement-Demange, A. (2004) Characterization of branching in two Hevea brasiliensis clones. **Journal of Experimental Botany,** 55(399): 1045-1051.

Clough, R.W., Penzien J. (1995) **Dynamics of Structures**. 3rd ed., New York: McGraw Hill Inc.

Cook, N.J. (1985) **The Designer's Guide to Wind Loading of Building Structures**, Part 1: Static Structures. London: Butterworths.

Coutts, M.P. (1986) Components of tree stability in Sitka spruce on peaty gley soil. **Forestry**, 59(2): 173-195.

Craig, R.R. (1981) **Structural Dynamics**. New York: John Wiley & Sons Inc.

Csanady, G.T. (1973) **Turbulent Diffusion in the Environment**, Kluwer Academic Publishers.

Cushman-Roisin, B. (2005) Kelvin-Helmholtz instability as a boundary-value problem. **Environmental Fluid Mechanics**, 5: 507-525.

De Langre, E. (2008) Effects of Wind on Plants. **Annual Review of Fluid Mechanics**, 40: 141-168.

Denmead, O.T. and Bradley, E.F. (1973) Heat, Mass and Momentum Transfer in a Wheat Crop. **First Australasian Conference on Heat and Mass Transfer**, Melb., Aust.

Den Hartog, J.P. (1985) **Mechanical Vibrations**, 4th ed. New York: Dover Publications Inc.

Doare, O., Moulia, B., de Langre, E. (2004) Effect of plant interaction on wind-induced crop motion. **Transactions of the ASME： Journal of Biomechanical Engineering**, 126 (2): 146–151.

Dupont, S., Gosselin, F., Py, C., de Langre, E., Hemon, P., and Brunet, Y. (2010) Modelling waving crops using large-eddy simulation: comparison with experiments and a linear stability analysis. **Journal of Fluid Mechanics**, 652: 5-44.

Dyrbye, C. and Hansen, S. O. (1996) **Wind Loads on Structures**. UK: Wiley.

Engineering Sciences Data Unit: ESDU (2000) Characteristics of atmospheric turbulence near the ground, Item 85020.

Farquhar, T. and Eggleton, C.D. (2000) Pulsatile flow heightens vertical moment exchanges in a wheat canopy. In **Proceedings of the 3rd Plant Biomechanics Conference**, Freiburg.

Farquhar, T., Zhou, J. and Haslach, H. (2003) A possible mechanism for sensing crop canopy ventilation. **Chp 15 in Sensors and Sensing in Biology and Engineering**,

Barth, F.G., Humprey, J.A.C., Secomb, T. (Eds.), New York: Springer Press.

Finnigan J.J. and Mulheran P.J. (1978) Modelling waving crops in a wind tunnel. **Boundary-Layer Meteorology**, 14: 253-277.

Finnigan, J.J. (1979) Turbulence in waving wheat. I. Mean statistics and honami. **Boundary-Layer Meteorology**, 16: 181-211.

Finnigan J.J. and Brunet Y. (1995) Turbulent airflow in forests on flat and hilly terrain, In: Coutts, M.P. and Grace, J. (eds.) **Wind and Trees**. Cambridge: Cambridge University Press. pp. 3-40.

Finnigan, J.J. (2000) Turbulence in plant canopies. **Annual Review of Fluid Mechanics**, 32: 519-571.

Fischer, R.A. and Quail, K.J. (1990) The effect of major dwarfing genes on yield potential in spring wheat. **Euphytica**, 46: 51-56.

Garratt, J.R. (1992) **The Atmospheric Boundary Layer**, Cambridge: Cambridge University Press.

Gardiner, B.A. (1995) The interactions of wind and tree movement in forest canopies. In: Coutts, M.P. and Grace, J. (eds.) **Wind and Trees**, 41-59, Cambridge: Cambridge University Press.

Gardiner, B.A. (1994) Wind and wind forces in a plantation spruce forest. **Boundary-Layer Meteorology**, 55: 161-186.

Gardiner, B.A., Peltola, H., Kellomäki, S. (2000) Comparison of two models for predicting the critical wind speeds required to damage coniferous trees. **Ecological Modelling**, 129 (1): 1-23.

Gardiner, B.A. and Quine, C.P. (2000) Management of forests to reduce the risk of abiotic damage-a review with particular reference to the effects of strong winds. **Forest Ecology and Management**, 135 (1): 261-277.

Godin, C. and Caraglio Y. (1998) A multi-scale model of plant topological structures.

Journal of Theoretical Biology, 191: 1-46.

Godin, C., Costes, E., Caraglio, Y. (1997) Exploring plant topological structure with the AMAPmod software: an outline. **Silva Fennica**, 31 (3): 357-368.

Gosselin, F. and de Langre, E. (2009) Destabilising effects of plant flexibility in air and aquatic vegetation canopy flows. **European Journal of Mechanics B-fluids**, 28: 271-282.

Guitard, D.G.E. and Castera, P. (1995) Experimental analysis and mechanical modelling of wind-induced tree sways. In: Coutts, M.P. and Grace, J. (eds.) **Wind and Trees**, 182-194, Cambridge: Cambridge University Press.

Gurley, K.R. and Kareem, A. (1998) A conditional simulation of non-normal velocity pressure fields. **Journal of Wind Engineering& Industrial Aerodynamics**, (77&78): 39-51.

Hadley, G. (1735) On the cause of the general trade winds. **The Philosophical Transactions of the Royal Society**, , 34: 58-62.

Hangan, H., Kopp, G.A., Vernet, A., Marinuzzi, R. (2001) A wavelet pattern recognition technique for identifying flow structures in cylinder generated wakes. **Journal of Wind engineering and Industrial aerodynamics**, 89: 1001-1005.

Holmes, J.D. (2001) **Wind Loading of Structures**. London: Spon Press.

Holton, J.R. (2004) **An Introduction to Dynamic Meteorology**, 4th edition, Burlington, MA, US: Elsevier Academic Press.

Hu, Z. (2011) Wind-Induced Vibration Analysis in Time Domain, In **Proceedings of Fourth International Conference on Information and Computing**, Phuket Island, Thailand: 294-297.

Ingver, A., Tamm, I., Tamm, Ü., Kangor, T. and Koppel R. (2010) The characteristics of spring cereals in changing weather in Estonia. **Agronomy Research**, 8 (Special Issue III): 553-562.

Inoue, R. (1955) Studies of the phenomena of waving plant (‘honami’) caused by wind.part 1: Mechanism and characteristics of waving plant phenomena. **Agricultural and Forest Meteorology**, (Japan) 11:71-82.

Jaffe, M.J. (1973) Thigmomorphogenesis: the response of plant growth and development to mechanical stimulation. **Planta (Berl.)**, 114: 143-157.

Jaffe, M.J. (1980) Morphogenetic responses of plants to mechanical stimuli or stress. **Bioscience**, 30 (4): 239-243.

James, K.R. (2003) Dynamic loading of trees. **Journal of Arboriculture**29 (3): 165-171.

James, K.R., Haritos, N., Ades, P.K. (2006) Mechanical stability of trees under dynamic loads. **American Journal of Botany**, 93 (10): 1522-1530.

Jin, X., Fourcaud, T., Li, B., Guo, Y. (2009) "Towards modeling and analyzing stem lodging for two contrasting rice cultivars." In **Proc. of 3rd International Symposium on Plant Growth Modeling, Simulation, Visualization and Applications**, **PMA09, November 9, 2009 - November 13**, **2009**, IEEE Computer Society, 253-260.

Kaimal, J.C. and Finnigan, J.J. (1994) **Atmospheric Boundary Layer Flows: Their Structure and Measurement**. New York: Oxford University Press.

Kolmogorov, A.N. (1941) **Dissipation of Energy in Locally Isotropic tTrbulence**. Dokl. Akad. Nauk SSSR, 32, 19-21 [in Russian].

Long, R.R. (1997) Homogeneous isotropic turbulence and its collapse in stratified and rotating fluids. **Dynamics of Atmospheres and Oceans**, 27: 471-483.

Long, J.N. and Smith, F.W. (1992) Volume increment in Pinus contorta var. latifolia: the influence of stand development and crown dynamics. **Forest Ecology and Management**, 53 (1-4): 53-64.

Lohou, F., Lopez, A., Druilhet, A., Brunet, Y., Irvine, M., Lamaud, E. (2003) The VENFOR Project: response of a homogeneous forest canopy to wind stress through the analysis of accelerometer measurements. In **Proceedings of the wind effects on trees**, University of Karlsruhe, Germany: 109-116.

Mahrer, Y. (1984) An improved numerical approximation of the horizontal gradients in a terrain following coordinate system. **Monthly Weather Review**112: 918-922.

Mahrt, L., Lee, X., Black, A., Neumann, H., Staebler, R.M., (2000) Nocturnal mixing in a forest subcanopy. **Agricultural and Forest Meteorology**101 (1): 67-78.

Mallat, S. (1999) **A Wavelet Tour of Signal Processing**, 2nd edn. Academic Press.

Martinez-Vazquez, P. and Rodriguez-Cuevas, N. (2007) Wind field reproduction using neural networks and conditional simulation. **Engineering Structures**, 29 (7):1442-1449.

Martinez-Vazquez, P. and Sterling, M. (2011). Predicting wheat lodging at large scales. **Biosystems Engineering**, 109 (4): 326-337.

Mayer, H. (1987) Wind-induced tree sways. **Trees**, 1: 195-206.

Mellor, G.L. and Yamada, T. (1982) Development of a turbulence closure model for

geophysical fluid problems. **Reviews of Geophysics and Space Physics**, 20: 851-875.

Meirovitch, L. (1975), **Elements of Vibration Analysis**. New York: McGraw-Hill Inc.

Miller, L. (2005) Structural dynamics and resonance in plants with nonlinear stiffness. **Journal of Theoretical Biology**, 234: 511-524.

Milne, R. (1991) Dynamics of swaying Picea sitchensis. **Tree Physiology**, 9: 383-399.

Moore, J.R. (2002) **Mechanical Behavior of Coniferous Trees Subjected to Wind Loading**. PhD thesis, Oregon State University, USA.

Moore, J.R. and Maguire, D.A. (2004) Natural sway frequencies and damping ratios of trees: concepts, review and synthesis of previous studies. **Trees-Structure and Function**, 18 (2): 195-203.

Neenan, M. and Spencer-Smith, J.L. (1975) An analysis of the problem of lodging with particular reference to wheat and barley. **The Journal of Agricultural Science**, 85:

495-507.

Newmark, N. M. (1959) A method of computation for structural dynamics. **Journal of Engineering Mechanics**, 85, 67-94.

Oliver, H.R. and Mayhead, G.J. (1974) Wind measurements in a pine forest during a destructive gale. **Forestry**, 47: 185-194.

Panofsky, H.A. and Dutton, J.A. (1984) **Atmospheric Turbulence**. New York: John Wiley.

Papesch A. (1974) A simplified theoretical analysis of the factors that influence wind-throw of trees. In **Proceedings of the 5th Australasian Conference on Hydraulics and Fluid Dynamics**, 235-242.

Papesch, A. (1984) **Wind and Its Effects on (Canterbury) Forests**. Ph.D. Thesis, University of Canterbury, New Zealand.

Pinthus, M.J. (1973) Lodging in wheat, barley and oats: the phenomenon, its causes and preventative measures. **Advances in Agronomy**, 25: 209-263.

Peltola, H., Kellomaki, S., Hassinen, A., Lemettinen, M., Aho, J. (1993) Swaying of trees as caused by wind: analysis of field measurements. **Silva Fennica**, 27: 113-126.

Peltola, H., Kellomaki, S., Vaisanen, H., Ikonen, V.P. (1999) A mechanistic model for assessing the risk of wind and snow damage to single trees and stands of Scots pine, Norway spruce, and birch. **Canadian Journal of Forest Research**, 29: 647-661.

Peterson, C.J. and Pickett, S.T.A. (1995) Forest reorganization: a case study in an old growth forest catastrophic blow down. **Ecology**, 76 (3): 763-774.

Pope, S.B. (2000) **Turbulent Flows**, Cambridge: Cambridge University Press.

Py, C., de Langre, E., Moulia, B. (2004) The mix**ing** layer instability of wind over a flexible crop canopy. **Comptes Rendus Mecanique**, 332 (8): 613-618.

Py, C., de Langre, E., Moulia, B. (2006) A frequency lock-in mechanism in the interaction between wind and crop canopies. **Journal of Fluid Mechanics**, 568: 425-449.

Py, C., de Langre, E., Moulia, B., Hemon, P. (2005) Measurement of wind-induced motion of crop canopies from digital video images. **Agricultural and Forest Meteorology**, 130 (3-4): 223-236.

Raupach, M.R. and Thom, A.S. (1980) Turbulence in and above plant canopies. **Annual Review of Fluid Mechanics**, 13: 97-129.

Raupach M.R. (1988) Canopy transport process. In: Steffen, W.L. and Denmead, O.T (eds) **Flow and transport in the natural environment: advances and application**, Springer-Verlag Berlin Heidelberg, 95-127.

Rodriguez, M., Ploquin, S., Moulia, B (2012) The Multimodal Dynamics of a Walnut Tree: Experiments and Models. **Journal of Applied Mechanics**, 79: 044505 1-5

Rudnicki, M., Meyer, T.H., Lieffers, V.J., Silins, U., and Webb, V.A. (2008) The periodic motion of lodge pole pine trees as affected by collisions with neighbours. **Trees**,

22: 475-482.

Rudnicki, M., Lieffers, V.J., and Silins, U. (2003) Stand structure governs the crown collisions of lodge pole pine. **Canadian Journal of Forest Research**, 33 (7): 1238-1244.

Rudnicki, M., Silins, U., Lieffers, V.J., and Josi, G. (2001) Measure of simultaneous tree sways and estimation of crown interactions among a group of trees. **Trees-Structure and Function**, 15 (2): 83-90.

Saddoughi, S.G., and Veeravalli. S.V. (1994) Local isotropy in turbulent boundary layers at high Reynolds number. **Journal of Fluid Mechanics**, 268: 333-372.

Saunderson, S.E.T., Baker, C.J., and England, A. (1999) A dynamic model of the behaviour of Sitka Spruce in high winds. **Journal of Theoretical Biology**, 200: 249-259.

Saunderson, S.E.T., Baker, C.J., and England, A. (2000) A dynamic analysis of the wind throw of trees. **Forestry**, 73 (3): 225-237.

Scannell, B. (1984) **Quantification of the Interactive Motions of the Atmospheric Surface Layer and a Conifer Canopy**. PhD thesis, Cranfield Institute of Technology, Bedford.

Sellier, D., Fourcaud, T., and Lac, P. (2006) A finite element model for investigating effects of aerial architecture on tree oscillations. **Tree Physiology**, 26 (6): 799.

Sellier, D., Brunet, Y., and Fourcaud, T., (2008) A numerical model of tree aerodynamic response to a turbulent airflow. **Forestry**, 81 (3): 279-297.

Shaw, R.H., Hartog, G., Neumann, H.H. (1988) Influence of foliar density and thermal stability on profiles of Reynolds stress and turbulence intensity in a deciduous forest. **Boundary-Layer Meteorology**, 45 (4): 391-409.

Sinoquet, H., Rivet, P., and Godin, C. (1997) Assessment of the three dimensional architecture of walnut trees using digitizing. **Silva Fennica**, 31: 265-273.

Silins, U., Lieffers, V.J., Bach, L. (2000) The effect of temperature on mechanical properties of standing lodge pole pine trees. **Trees-Structure and Function**，14 (8): 424-428.

Simiu, E. and Scanlan, R.H. (1986) **Wind Effects on Structures**. New York: John Wiley & Sons.

Skatter, S. and Kucera, B. (2000) Tree breakage from torsional wind loading due to crown asymmetry. **Forest Ecology and Management**, 135: 97-103.

Skinner, D.P. (1976) Pruning the decimation in-time FFT algorithm. IEEE Transactions on **Acoustics, Speech, and Signal Processing**, 24(2): 193-194.

Spatz, H.C. and Speck, O. (2002) Oscillations frequencies of tapered plant stems. **American Journal of Botany**, 89: 1-11.

Sterling, M., Berry, P.M., Baker, C.J., & Wade, A. (2003) An experimental investigation of the lodging of wheat. **Agricultural and Forest Meteorology**, 119: 149-165.

Sterling, M., Berry, P.M., Baker, C.J., and Wade, A. (2003) Wind induced forces on wheat crops. **Agricultural Forestry Meteorology**, 119: 149–165.

Sterling, M., Baker, C.J., Richards, P.J., Hoxey, R.P. and Quinn, A.D. (2006) An investigation of the wind statictics and extreme gust events at a rural site. **Wind and Structures**, 9 (3): 193-216.

Stull, R.B. (1988) **An Introduction to Boundary Layer Meteorology**. Boston: Kluwer Academic Publishers.

Sugden M.J. (1962) Tree sway period: a possible new parameter for crown classification and stand competition. **Forestry Chronicle**, 38(3): 336-344.

Temam, R. (2001) Navier–Stokes Equations. **Theory and Numerical Analysis**, AMS Chelsea, 107-111.

Tennekes, H. and Lumley, J. L. (1972) **A First Course in Turbulence**, Cambridge, Massachusetts, and London, England: MIT Press.

Thorpe, S. A. (1971) Experiments on the instability of stratified shear flows: miscible fluids. **Journal of Fluid Mechanics**, 46: 299-319.

Vanmarcke, E., Heredia-Zavoni, E., and Fenton, G. (1993) Conditional simulation of spatially correlated ground motion. **Journal of Engineering Mechanics**, 119 (11): 2333-2352.

Webb, V.A. and Rudnicki, M. (2009) A linear analysis of the interaction between the atmosphere and an underlying compliant plant canopy. **Boundary-Layer Meteorology**, 133 (1): 93-111.

Wilson, J.D., Ward, D.P., Thurtell, G.W., and Kidd, G.E. (1982) Statistics of Atmospheric Turbulence Within and Above a Corn Canopy. **Boundary Layer Meteorology**, 24: 495-519.

White, E.M. (1991) Response of winter barley culivars to nitrogen and a plant growth regulator in relation to lodging. **The Journal of Agricultural Science**, 116: 191-200.

Wood, C. J. (1995) Understanding wind forces on trees. In: Coutts MP, Grace J, eds, **Wind and Trees**, Cambridge University Press, 133-164.

Wright, J. L. (1965) **Evaluating Turbulent Transfer Aerodynamically within the Microclimate of a Cornfield**. PhD Thesis, Cornell University, Ithaca, New York.

Zadok J.C., Chang T.T., Konzak F.C. (1974) A decimal code for growth stages of cereals. **Weed Research**, 14: 415-421.

Zhuang, Y. and Amiro, B.D. (1994) Pressure fluctuations during coherent motions and their effects on the budgets of turbulent kinetic energy and momentum flux within a forest canopy. **Journal of Applied Meteorology .**, 33: 704-711.